

Exciton-driven quantum phase transitions in holographyE. Gubankova,^{1,*} M. Čubrović,^{2,†} and J. Zaanen^{2,‡}¹*Instituut Lorentz, Leiden University, Niels Bohrweg 2, 2300 RA Leiden, Netherlands*²*Institute for Theoretical Physics, J. W. Goethe-University, D-60438 Frankfurt am Main, Germany*

(Received 11 April 2015; published 28 October 2015)

We study phase transitions driven by fermionic double-trace deformations in gauge-gravity duality. Both the strength of the double-trace deformation and the infrared conformal dimension/self-energy scaling of the quasiparticle can be used to decrease the critical temperature to zero, leading to a line of quantum critical points. The self-energy scaling is controlled indirectly through an applied magnetic field and the quantum phase transition naturally involves the condensation of a fermion bilinear which models the spin density wave in an antiferromagnetic state. The nature of the quantum critical points depends on the parameters and we find either a Berezinsky-Kosterlitz-Touless-type transition or one of two distinct second-order transitions with non-mean-field exponents. One of these is an anomalous branch where the order parameter of constituent non-Fermi liquid quasiparticles is enhanced by the magnetic field. Stabilization of ordered non-Fermi liquids by a strong magnetic field is observed in experiments with highly oriented pyrolytic graphite.

DOI: [10.1103/PhysRevD.92.086004](https://doi.org/10.1103/PhysRevD.92.086004)

PACS numbers: 11.25.Tq, 71.27.+a

I. INTRODUCTION

The anti-de Sitter/conformal field theory correspondence (AdS/CFT) or gauge/gravity duality is a new proving ground to describe strongly correlated systems, and its application to unresolved questions in condensed matter is an exciting new direction. It is especially compelling, as conventional methods, such as large- N [1] and $(4 - \epsilon)$ -type [2] expansions fail to describe quantum critical behavior in $2 + 1$ -dimensional systems. The primary examples of such are the strange metal states in the high- T_c cuprates and heavy fermion systems. Both systems are characterized by anomalous behavior of transport and thermodynamic quantities. In heavy fermions, the Sommerfeld coefficient grows as the temperature is lowered, meaning that the effective mass of the electrons on the Fermi surface diverges or the Fermi energy of the electrons vanishes [3]. In the strange metal phase of the high- T_c superconductors as well as in heavy fermions near a quantum phase transition, the resistivity is linear with temperature $\rho \sim T$. These anomalous behaviors are partly explained by the phenomenological marginal Fermi liquid model [4], and it is an early success of AdS/CFT that the marginal Fermi liquid can be seen to emerge as the low-energy dynamics of a consistent theory.

A particularly simple gravity description for strongly interacting finite-density matter is the planar AdS-Reissner-Nordström (AdS-RN) black hole (BH), which is dual to a system at finite chemical potential. While the AdS-RN black hole is a natural starting point to study the universal

aspects of finite charge density systems, the universality of a black hole makes it difficult to explain experiments that are keen on the nature of the charge carriers, such as transport properties (e.g. conductivity). In particular the dominance of Pauli blocking for observed physics, requires that at the minimum one needs to add free Dirac fermions to the AdS-RN background. A self-consistent treatment shows that this system is unstable to a quasi-Lifshitz geometry in the bulk [5–7], that encodes for a deconfined Fermi liquid system [8–11]. Here we shall initiate the study of instabilities in the unstable metallic AdS-RN phase that are driven by Fermi bilinears.

The essential low-energy property of the metallic system dual to the AdS-RN black hole background is the emergence of Fermi surfaces [12,13] where the notion of a quasiparticle need not be well defined, i.e. stable [14]. In Ref. [15], we used the magnetic field as an external probe to change the characteristics of the Fermi surface excitations and as a consequence the transport properties of the system. It strongly suggested that a quantum phase transition should occur when the underlying quasiparticle becomes (un)stable as a function of the magnetic field. The study in this article of the influence on stability of Fermi bilinears allows us to show that there is a phase transition between the two regimes and that for a specific set of parameters the critical temperature vanishes. Our work is therefore also a fermionic companion to Ref. [16].

Continuing the connection of AdS models to actual observations, the results we find resemble other experimental findings in quantum critical systems. At low temperatures and in high magnetic fields, the resistance of single-layer graphene at the Dirac point undergoes a thousandfold increase within a narrow interval of field strengths [17]. The abruptness of the increase suggests that

* Also at ITEP, Moscow, Russia.
elena1@mit.edu

† cubrovic@lorentz.leidenuniv.nl

‡ jan@lorentz.leidenuniv.nl

a transition to a field-induced insulating, ordered state occurs at the critical field h_c [18]. In bilayer graphene, measurements taken at the filling factor $\nu = 0$ point show that, similar to single-layer graphene, the bilayer becomes insulating at strong magnetic field [19]. In these systems, the divergent resistivity in strong magnetic fields was analyzed in terms of Kosterlitz-Thouless localization [18] and the gap opening in the zeroth Landau level [20]. However, it remains a theoretical challenge to explain a highly unusual approach to the insulating state. Despite the steep divergence of resistivity, the profile of ρ vs T at fixed h saturates to a T -independent value at low temperatures, which is consistent with gapless charge-carrying excitations [18]. Moreover, in highly oriented pyrolytic graphite in the magnetic field, the temperature of the metal-insulator phase transition $T_c(h)$ increases with increasing field strength, contrary to the $T_c(h)$ dependence in the classical low-field limit [21]. The anomalous $T_c(h)$ behavior has been successfully modeled within a dynamical gap picture [22]. The available data suggest that by tuning the magnetic field graphene approaches a quantum critical point, beyond which a new insulating phase develops with anomalous behavior $T_c(h)$. This picture is in agreement with expectations of quantum critical behavior, where e.g. in heavy fermion metal a new magnetically ordered state (antiferromagnet) emerges when tuned through the quantum critical point [3].

We shall see that the same qualitative physics emerges with our use of the the magnetic field as a knob to tune to the IR fixed point to gain some insight into the quantum critical behavior driven by fermion bilinears. In our gauge/gravity dual prescription, the unusual properties characteristic for quantum criticality can be understood as being controlled by the scaling dimension of the fermion operator in the emergent IR fixed point. The novel insight of AdS/CFT is that the low-energy behavior of a strongly coupled quantum critical system is governed by a nontrivial unstable fixed point which exhibits nonanalytic scaling behavior in the temporal direction only (the retarded Green's function of the IR CFT is $G_{\text{IR}}^R \sim \omega^{2\nu}$) [14]. This fixed point manifests itself as a near-horizon region of the black hole with AdS₂ geometry which is (presumably) dual to a one-dimensional IR CFT. Building on the semilocal description of the quasiparticle characteristics by simple Dyson summation in a Fermi gas coupled to this 1 + 1-dimensional IR CFT [23] an appealing picture arises that quantum critical fermionic fluctuations in the IR CFT generate relevant order parameter perturbations of the Fermi liquid theory. Whether this is truly what is driving the physics is an open question. Regardless, quantum critical matter is universal in the sense that no information about the microscopic nature of the material enters. Qualitatively our study should apply to any bilinear instability in the strange metal phase of unconventional superconductors, heavy fermions as well as for a critical

point in graphene. Universality makes applications of AdS/CFT to quantum critical phenomena justifiable and appealing.

The paper is organized as follows. In Sec. II, we review the AdS-RN black hole solution in AdS-Einstein-Maxwell gravity coupled to charged fermions and the dual interpretation as a quantum critical fermion system at finite density. In Sec. III we use the bilinear formalism put forward in Ref. [6] to explore an instability of a quantum system towards a quantum phase transition using the AdS dual description. We study a quantum phase transition to an insulating phase as a function of the magnetic field. For completeness we test the various phases by a spectral analysis in Sec. IV. We conclude by discussing a phase space in (h, T) variables for a quantum critical matter at nonzero temperatures.

II. HOLOGRAPHIC FERMIONS IN THE BACKGROUND OF A DYONIC BLACK HOLE

The gravity dual to a 2 + 1-dimensional CFT at finite density in the presence of a magnetic field starts with the Einstein-Maxwell action describing an asymptotically AdS₄ geometry:

$$S_g = \frac{1}{2\kappa^2} \int d^4x \sqrt{-g} \left(\mathcal{R} + 6 - \frac{1}{g_F^2} F_{MN} F^{MN} \right). \quad (1)$$

Here A_M is the gauge field, g_F^2 is an effective dimensionless gauge coupling and the curvature radius of AdS₄ is set to unity. The equations of motion following from Eq. (1) are solved by a dyonic AdS black hole, having both electric and magnetic charge

$$ds^2 = \frac{1}{(1-z)^2} \left(-f dt^2 + dx^2 + dy^2 + \frac{dz^2}{f} \right) \quad (2)$$

where the redshift factor f and the vector field A_M are given by

$$f = z(3 - 3z + z^2 - (Q^2 + H^2)(1-z)^3), \\ A_t = \mu z, \quad A_y = hx, \quad \text{with } \mu = g_F Q, \quad h = g_F H. \quad (3)$$

The AdS boundary is reached for $z \rightarrow 1$, the black hole horizon is at $z \rightarrow 0$ and the electric and magnetic charge of the black hole Q and H , encoding the chemical potential μ and magnetic field h of the dual CFT, are scaled such that the black hole temperature equals¹

$$T = \frac{1}{4\pi} (3 - (Q^2 + H^2)). \quad (4)$$

¹The independent black hole mass parameter is restored after rescaling $t \rightarrow Mt$, $x \rightarrow Mx$, $y \rightarrow My$ and $h \rightarrow M^{-2}h$.

In these units, the extremal $T = 0$ black hole corresponds to $Q^2 + H^2 = 3$ and in this case the red shift factor develops a double zero at the horizon

$$f = 3z^2(z - z_*)(z - \bar{z}_*), \quad z_* = (4 + i\sqrt{2})/3. \quad (5)$$

To include the bulk fermions, we consider a spinor field ψ in the AdS_4 of charge q and mass m , which is dual to a fermionic operator \mathcal{O} in the boundary CFT_3 of charge q and dimension

$$\Delta_\psi = \frac{3}{2} + m, \quad (6)$$

with $m \geq -\frac{1}{2}$ (in units of the AdS radius). The quadratic action for ψ reads

$$S_\psi = \int d^4x \sqrt{-g} (\bar{\psi} \Gamma^M \mathcal{D}_M \psi - m \bar{\psi} \psi), \quad (7)$$

where $\bar{\psi} = \psi^\dagger i\Gamma^{\hat{t}}$, and

$$\mathcal{D}_M = \partial_M + \frac{1}{4} \omega_{Mab} \Gamma^{ab} - iqA_M, \quad (8)$$

where ω_{Mab} is the spin connection, and $\Gamma^{ab} = \frac{1}{2} [\Gamma^a, \Gamma^b]$. Here, M and a, b denote the bulk space-time and tangent-space indices respectively, while μ, ν are indices along the boundary directions, i.e. $M = (z, \mu)$. The Dirac equation in the dyonic AdS-black hole background becomes

$$\left(\Gamma^{\hat{z}} \sqrt{f} \partial_z + \Gamma^{\hat{z}} \frac{\sqrt{f}}{2(1-z)} \left(3 + \frac{(1-z)f'}{2f} \right) - \Gamma^{\hat{t}} \frac{i(\omega + q\mu z)}{\sqrt{f}} - \frac{1}{(1-z)} m + \Gamma^{\hat{x}} \partial_x + \Gamma^{\hat{y}} i(k_y - qhx) \right) \psi = 0 \quad (9)$$

where ψ is the Fourier transform in the y directions and time. The z and x dependences can be separated as in Refs. [15,24,25]. Define

$$\begin{aligned} P &= \Gamma^{\hat{z}} \sqrt{f} \left(\partial_z + \frac{1}{2(1-z)} \left(3 + \frac{(1-z)f'}{2f} \right) \right) \\ &\quad - \Gamma^{\hat{t}} \frac{i(\omega + q\mu z)}{\sqrt{f}} - \frac{1}{(1-z)} m, \\ Q &= \Gamma^{\hat{x}} \partial_x + \Gamma^{\hat{y}} (ik_y - iqx), \end{aligned} \quad (10)$$

in terms of which the Dirac equation is $(P + Q)\psi = 0$. In order to separate the variables, we can proceed by finding the matrix U such that $UP\psi = -UQ\psi = \lambda\psi$. The idea is that, although P and Q do not commute, we can find U so that $[UP, UQ]$ commute and can be diagonalized simultaneously [15].² To this end, U must satisfy the relations

²Rather the part in P not proportional to the identity *anti-commutes* with Q . This realization shows why the relations in the next sentence are the solution.

$\{U, \Gamma^z\} = 0$, $\{U, \Gamma^t\} = 0$, $[U, \Gamma^x] = 0$, $[U, \Gamma^y] = 0$. A clear solution is $U = [\Gamma^z, \Gamma^t]$.

In a convenient gamma matrix basis (Minkowski signature) [14]

$$\begin{aligned} \Gamma^{\hat{z}} &= \begin{pmatrix} -\sigma^3 & 0 \\ 0 & -\sigma^3 \end{pmatrix}, & \Gamma^{\hat{t}} &= \begin{pmatrix} i\sigma^1 & 0 \\ 0 & i\sigma^1 \end{pmatrix}, \\ \Gamma^{\hat{x}} &= \begin{pmatrix} -\sigma^2 & 0 \\ 0 & \sigma^2 \end{pmatrix}, \\ \Gamma^{\hat{y}} &= \begin{pmatrix} 0 & \sigma^2 \\ \sigma^2 & 0 \end{pmatrix}, & \Gamma^{\hat{s}} &= \begin{pmatrix} 0 & i\sigma^2 \\ -i\sigma^2 & 0 \end{pmatrix} \equiv i\Gamma^{\hat{t}}\Gamma^{\hat{x}}\Gamma^{\hat{y}}\Gamma^{\hat{z}} \end{aligned} \quad (11)$$

the matrix U equals

$$U = \begin{pmatrix} -i\sigma^2 & 0 \\ 0 & -i\sigma^2 \end{pmatrix}. \quad (12)$$

This choice of the basis allows one to obtain $k_y = 0$ spectral functions in a simple way. In the absence of a magnetic field one can use rotational invariance to rotate to a frame where this is so. The gauge choice for the magnetic field obviously breaks the isotropy, but the physical isotropy still ensures that the spectral functions simplify in this basis [15]. The x -dependent part of the Dirac equation can be solved analytically in terms of Gaussian-damped Hermite polynomials $H_n(\sqrt{qh}(x + \frac{k_y}{qh}))$ with eigenvalues $\lambda_n = \sqrt{|qh|}n$ quantized in terms of the Landau index $n = 0, 1, \dots$ [15,24,25]. The Dirac equation $(P - U^{-1}\lambda)\psi = 0$, where λ is a diagonal matrix in terms of λ_n and whose square is proportional to the identity, then reduces to

$$\left(\left(\partial_z + \frac{1}{2(1-z)} \left(3 + \frac{(1-z)f'}{2f} \right) \right) \Gamma^{\hat{z}} - \frac{i(\omega + q\mu z)}{f} \Gamma^{\hat{t}} - \frac{m}{\sqrt{f}(1-z)} - U^{-1} \frac{\lambda_n}{\sqrt{f}} \right) \psi = 0. \quad (13)$$

We introduce now the projectors Π_α that split the four-component bispinors into two two-component spinors $\Psi = (\psi_1, \psi_2)^T$ where the index $\alpha = 1, 2$ is the Dirac index of the boundary theory

$$\Pi_\alpha = \frac{1}{2} \left(1 - (-1)^\alpha \Gamma^{\hat{z}} \Gamma^{\hat{t}} \frac{1}{|\lambda|} Q \right), \quad \alpha = 1, 2,$$

$$\Pi_1 + \Pi_2 = 1. \quad (14)$$

The projectors commute with both P and Q (recall that $Q^2 = \lambda^2 \mathbb{1}$). At zero magnetic field projectors are given by $\Pi_\alpha = \frac{1}{2} (1 - (-1)^\alpha \Gamma^{\hat{z}} \Gamma^{\hat{t}} \hat{k}_i \Gamma^i)$ with unit vector $\hat{k}_i = \vec{k}/|\vec{k}|$. The projections $\psi_\alpha = \Pi_\alpha \psi$ with $\alpha = 1, 2$ therefore decouple from each other and one finds two independent copies of the two-component Dirac equation:

$$\left(\partial_z + \frac{1}{2} \left(\frac{3}{1-z} + \frac{f'}{2f} \right) - \frac{i(\omega + \mu_q z)}{f} \sigma^2 + \frac{m}{\sqrt{f}(1-z)} \sigma^3 + \frac{\lambda_n}{\sqrt{f}} \sigma^1 \right) \psi_{1;2} = 0, \quad (15)$$

where the magnetic momentum $\lambda_n = \sqrt{2|qh|n}$ is Landau quantized with integer values $n = 0, 1, \dots$ and $\mu_q \equiv \mu q$. It is identical to the AdS-Dirac equation for an AdS-RN black hole with zero magnetic charge when the discrete eigenvalue λ is identified with the (size of the) momentum k .

As we have shown in Ref. [15], solving Eq. (15) is equivalent to solving the Dirac equation at zero magnetic field but with a rescaled chemical potential and fermion charge. At $T = 0$ the mapping is given by [15]

$$\begin{aligned} (\mu_q, h, q) &\mapsto (\mu_{q,\text{eff}}, h_{\text{eff}}, q_{\text{eff}}) \\ &= \left(\sqrt{3}q \sqrt{1 - \frac{h^2}{3}}, 0, q \sqrt{1 - \frac{h^2}{3}} \right), \end{aligned} \quad (16)$$

which we will use further.

III. BILINEAR APPROACH TO PARTICLE-HOLE PAIRING

The objective of this paper is to use the magnetic field as a tool to probe our unstable quantum critical system dual to the dyonic AdS-RN geometry. We show that the instability is manifest in the appearance of ordering in the system: the magnetic field acts as a catalyzer for the particle-hole pairing. In particular, we will find an unusual behavior for the critical temperature of the normal to paired phase transition as the dialing of the magnetic field drives the system to a quantum critical point: for a critical magnetic field the critical temperature vanishes indicating a new emergent quantum critical point.

We will identify the bulk quantities in the bilinear approach which are dual to the sought-for quantities on the CFT side. We have given the setup of the bilinear formalism in Ref. [6]. Here, we will first give a concise review with the focus on the transport properties and the influence of magnetic fields, and then derive the bilinear equations relevant for computing the pairing gap.

A. Bulk propagators and currents

A controlled method for calculating the expectation value of some composite operator J with the structure of a fermion bilinear ($J \sim \psi^\dagger \psi$) has been put forward in Ref. [6] and it is based on a relation between the bulk and the boundary propagator in the isotropic single-particle approximation. This allows us to identify the familiar quantities at the boundary by matching the resulting expression to known thermodynamic relations. The crucial object was identified in Ref. [6]

$$J^\mu(E, p, z) = \int d\omega \int d^2k \bar{\psi}(\omega, k, z) \Gamma^\mu \psi(E - \omega, p - k, z) \quad (17)$$

and it is the spatial average of the $U(1)$ current four-vector in the bulk.³ The metric then assumes the form given in the first section by Eq. (2) (so that the horizon is located at $z_H = 0$ and the boundary is at $z_0 \rightarrow 1$). Having defined the radial projection of the bulk Dirac equation in Eq. (14) we can also define the radial projections of the current as

$$J_\alpha^\mu(E, p, z) = \int d\omega \int d^2k \bar{\psi}_\alpha(\omega, k, z) \gamma^\mu \psi_\alpha(E - \omega, p - k, z), \quad (18)$$

where $\alpha = 1, 2$ and γ^μ is a Pauli matrix acting in the boundary frame.

The boundary interpretation of this current is, however, subtler than the simple $U(1)$ conserved current which it is in the bulk [6]: it expresses the Migdal theorem, i.e. the density of quasiparticles in the vicinity of the Fermi surface. To see this, express the bulk spinors $\psi_\alpha(z)$ at an arbitrary value of z through the bulk-to-boundary propagators $\mathcal{G}_\alpha(z, z')$ and the boundary spinors $\psi_\alpha(z_0)$ as

$$\psi_\alpha(z) = \mathcal{G}_\alpha(z_H, z) \mathcal{G}_\alpha^{-1}(z_H, z_0) \psi_\alpha(z_0). \quad (19)$$

The meaning of the above expressions is clear: the spinors evolve from their horizon values toward the values in the bulk at some z , under the action of the bulk-to-boundary propagator $\mathcal{G}_\alpha(z, z')$ acting upon them (normalized by its value at the boundary). To find the relation with the boundary Green's function we need to know the asymptotics of the solutions of the Dirac equation (15) at the boundary; see Eq. (A6) in Appendix A:

$$\begin{aligned} \psi_1 &\sim a_1 (1-z)^{3/2-m} \psi_{0,+}^{\text{in}} + b_1 (1-z)^{3/2+m} \psi_{0,-}^{\text{in}}, \\ \psi_2 &\sim a_2 (1-z)^{5/2-m} \psi_{0,+}^{\text{in}} + b_2 (1-z)^{5/2+m} \psi_{0,-}^{\text{in}}. \end{aligned} \quad (20)$$

On the other hand, the boundary retarded propagator is given by the dictionary entry [26], Eq. (A9), where $\gamma^0 = i\sigma^1$.

The bulk-to-boundary Green's function (in dimensionless units) can be constructed from the solutions to the Dirac equation [27] as in Eq. (A4). Using Eq. (A6) and the expression for the Wronskian, we arrive at the following relation between the boundary asymptotics of the solutions ψ^{in} and ψ^{bdy} :

$$\psi_\alpha^{\text{in}}(z_0) = \left(\frac{(1-z)^{-2m}}{G_\alpha} (-i\gamma^0) + 1 \right) \psi_\alpha^{\text{bdy}}(z_0). \quad (21)$$

³As shown in Ref. [6], even though the current is defined as a spatial average, the only mode that contributes at the leading order (tree level) is the quasinormal mode at $k = k_F$.

Taking into account the dictionary entry for the boundary propagator from Eq. (A9) and the representation (19) for ψ^{in} and ψ^{bdy} , the retarded propagator at the boundary is

$$\begin{aligned} G_\alpha &= \lim_{z_0 \rightarrow 1} (1 - z_0)^{-2m} \psi_\alpha^{\text{bdy}}(z_0) (\psi_\alpha^{\text{in}}(z_0))^{-1} \\ &= \lim_{z_0 \rightarrow 1} \mathcal{G}_\alpha(z_H, z_0) \gamma^0 \mathcal{G}_\alpha(z_H, z_0) \end{aligned} \quad (22)$$

with $z_H = 0$. Using Eq. (22) and the definition for the current in Eq. (18) it can now be shown that the current $J_1^\mu \sim \int \tilde{G}_1 \gamma^\mu G_1$ for an on-shell solution becomes at the boundary [6]

$$J_1^\mu(\omega = 0, k = k_F, z_0 \rightarrow 1) = \frac{1 + 2m}{\mu} \int d\omega \gamma^\mu G_1(\omega, k_F). \quad (23)$$

It is well known [28] that the integral of the propagator is related to the charge density. In particular, for $\gamma^\mu = \gamma^0$ and for the horizon boundary conditions chosen so that $G = G_F$ (Feynman propagator), we obtain

$$J_1^0 \equiv \int d\omega \psi_1^\dagger \psi_1 = \frac{1 + 2m}{\mu} n_F, \quad (24)$$

i.e. the bilinear J^0 directly expresses the charge density $n_F = \text{tr}(i\gamma^0 G)|_{\text{on-shell}} \sim |b_1(k_F)|^2$. Notice that to achieve this we need to set $\omega = k - k_F = 0$, i.e. look at the location of the Fermi surface. By analogy, we can now see that the components $J^{1,2}$ correspond to current densities. In particular, the ratio of the spatial components J_1^i/E^j in the external electric field \mathbf{E} readily gives the expression for the conductivity tensor σ_{ij} . Finally, the formalism outlined above allows us to define an arbitrary bilinear $J^A = \int \tilde{\psi} \hat{A} \psi$ and to compute its expectation value. By choosing the matrix \hat{A} appropriately we are able to model particle-hole, particle-particle or any other current. Notice however that all bilinears J^A are proportional on shell, as can be seen from Eqs. (22)–(23), which hold also for any other matrix \hat{A} sandwiched between the two bulk propagators. The proportionality is at fixed parameters (μ , T , etc.) so the dependences of the form $J^A(\mu)$ and $J^A(T)$ will be different for different choices of \hat{A} .

To introduce another crucial current, we will study the form of the action. (We will define our action to model the quantum phase transition and to define the pairing excitonic gap in Sec. III B.) We pick a gauge, Eq. (3), so that the Maxwell field is $A_\mu = (\Phi(z), 0, h(z)x, 0, 0)$, meaning that the nonzero components of $F^{\mu\nu}$ are $F^{z0} = \partial_z \Phi$, $F^{z2} = x \partial_z h$, $F^{12} = h$ and their antisymmetric pairs. The total action [Eqs. (1) and (7)] is now

$$\begin{aligned} S &= \int dz d^3x \sqrt{-g} \left(\frac{1}{2\kappa^2} \left(\mathcal{R} + 6 - \frac{1}{4g_F^2} F_{MN} F^{MN} \right) \right. \\ &\quad \left. + \bar{\psi} \Gamma^M \mathcal{D}_M \psi - m \bar{\psi} \psi \right) \\ &\quad + \int d^3x \sqrt{-h} \left(\mathcal{R}_{\text{bnd}} A_\mu n_\nu F^{\mu\nu} + \sum_\alpha \bar{\psi}_\alpha (-i\sigma^3) \psi_\alpha \right), \end{aligned} \quad (25)$$

where $\bar{\psi}_\alpha = i\psi_\alpha^\dagger \sigma^1$. The second integral is the boundary term added to regularize the bulk action, for which the fermion part vanishes on shell. Knowing the metric (2) and the form of A^μ , we find that the total action (free energy, from the dictionary) can be expressed as [6]

$$\mathcal{F} = \mathcal{F}_{\text{hor}} - \frac{1}{2}(\mu\rho + h\mathcal{M}) + \frac{3}{2}K \quad (26)$$

where \mathcal{F}_{hor} is the free energy at the horizon, which does not depend on the physical quantities on the boundary as long as the metric is fixed [6] so we can disregard it here. In Eq. (26), μ , ρ and h , \mathcal{M} are the leading and subleading terms in the electric and magnetic field

$$\begin{aligned} \Phi(z \rightarrow z_0) &= \mu, & \partial_z \Phi(z \rightarrow z_0) &= \rho, \\ h(z \rightarrow z_0) &= h, & \partial_z h(z \rightarrow z_0) &= \mathcal{M}, \end{aligned} \quad (27)$$

and the fermionic contribution is proportional to

$$K = \int d\omega \int d^2k \sum_\alpha \bar{\psi}_\alpha(\omega, k, z) \psi_\alpha(E - \omega, p - k, z) \quad (28)$$

which brings us to the second crucial bilinear. Along the lines of the derivation (18)–(23), we see that the fermionic contribution to the boundary action (25) is proportional to

$$K = 2 \sum_\alpha \text{Re} G_\alpha, \quad (29)$$

i.e. it is the real part of the boundary propagator.⁴ The bulk fermionic term does not contribute, being proportional to the equation of motion, while the boundary terms include the holographic factors of the form $(1 - z_0)^n$. In accordance with our earlier conclusion that the on-shell bilinears are all proportional, we can reexpress the free energy in Eq. (26) as

$$\mathcal{F} = \mathcal{F}_{\text{hor}} - \frac{1}{2}(\mu\rho + h\mathcal{M}) + \frac{3}{4m + 2} \mu J_1^0 \quad (30)$$

where the chemical potential reappears in the prefactor and the fermionic term becomes of the form μJ_1^0 , confirming again that J_1^0 can be associated with the number density.

⁴In Ref. [6] this bilinear was denoted by I . In the present paper a different bilinear is called I_\pm .

B. Pairing currents

Now we will put to work our bilinear approach in order to explicitly compute the particle-hole (excitonic) pairing operator. We add a scalar field which interacts with fermions by the Yukawa coupling as done in Ref. [29]. Both scalar and fermion fields are dynamical. The matter action is given by

$$\begin{aligned} S_\psi &= i \int dz d^3x \sqrt{-g} (\bar{\psi} \Gamma^M D_M^\psi \psi - m_\psi \bar{\psi} \psi - \lambda |\phi|^2 \bar{\psi} \psi), \\ S_G &= \int dz d^3x \sqrt{-g} \frac{1}{2} G_{\text{int}} (\phi \bar{\psi} \Gamma \psi + \phi^* \bar{\psi} \bar{\Gamma} \psi), \\ S_\phi &= - \int dz d^3x \sqrt{-g} (|D_M^\phi \phi|^2 + V(|\phi|)) \end{aligned} \quad (31)$$

where the covariant derivatives are $D_M^\psi = \nabla_M + \frac{1}{4} \omega_{Mab} \Gamma^{ab} - i q_\psi A_M$, $D_M^\phi = \nabla_M - i q_\phi A_M$, and $\bar{\psi} = \psi^\dagger i \Gamma^t$. The gamma-matrix structure of the Yukawa interaction is specified further. Matter action is supplemented by the gauge-gravity action

$$S_A = \frac{1}{2\kappa^2} \int dz d^3x \sqrt{-g} \left(R + \frac{6}{L^2} - \frac{1}{4g_F^2} F_{MN} F^{MN} \right). \quad (32)$$

We take the AdS radius $L = 1$ and $g_F = 1$. The gauge field components A_0 and A_2 are responsible for the chemical potential and magnetic field, respectively, in the boundary theory. As in Ref. [29], we assume $\lambda = 0$ and $V(|\phi|) = m_\phi^2 |\phi|^2$ and the scalar is real $\phi^* = \phi$. For the particle-hole sector, the scalar field is neutral $q_\phi = 0$.

The Yukawa coupling G_{int} is allowed to be positive and negative. When the coupling is positive $G_{\text{int}} > 0$, a repulsive interaction makes it harder to form the particle-hole condensate. Therefore it lowers the critical temperature and can be used as a knob to tune to a vanishing critical temperature $T_c = 0$ at a critical value G_{int}^c which defines a quantum critical point. When the coupling is negative $G_{\text{int}} < 0$, an attractive interaction facilitates pairing and helps to form the condensate.

Both situations can be described when the interaction term is viewed as a dynamical mass of either sign due to the fact that it is in the $\bar{\psi} \psi$ channel. For $G_{\text{int}} > 0$, the interaction $G_{\text{int}} \phi$ introduces a new massive pole: the massless free fermion field acquires a mass which makes it harder to condense. For $G_{\text{int}} < 0$, there is a tachyonic instability. The exponentially growing tachyonic mode is resolved by a condensate formation, a new stable ground state. It can be shown that we do not need a nonzero chemical potential to form a condensate in this case. A similar situation was considered in Ref. [16] for the superconducting instability

where the spontaneous symmetry breaking of $U(1)$ was achieved by the boundary double-trace deformation. In our case for the electron-hole pairing, Z_2 symmetry is spontaneously broken by a neutral order parameter. Next we discuss the choice for the gamma-matrix structure Γ of the Yukawa interaction (31) and the corresponding pairing parameter Δ

$$\Delta = G_{\text{int}} \langle \bar{\psi} \Gamma \psi \rangle. \quad (33)$$

Now we explain our choice of the pairing operator and give a rigorous justification for this choice.

In principle, any operator that creates a particle and a hole with the same quantum numbers could be taken to define Δ . This translates into the requirements

$$[\Gamma, \Gamma^t] = 0, \quad \{\Gamma, \Gamma^0\} = 0, \quad [\Gamma, \hat{C}] = 0. \quad (34)$$

(Anti)commutation with (time) space gamma matrices is required for the preservation of homogeneity and isotropy, and the last one is there to preserve the particle-hole symmetry. In the basis we have adopted, Eq. (11), $(\Gamma^t)^* = -\Gamma^t$ and $\Gamma^{z*} = \Gamma^z$, and therefore the charge conjugation is represented as

$$\hat{C}: \psi \rightarrow \Gamma^0 \Gamma^3 \psi^*. \quad (35)$$

We will also consider the parity of the order parameter. As defined in Ref. [30], parity in the presence of the AdS boundary acts as $x^1 \rightarrow -x^1$ with x^2, z unchanged, while the transformation of the spinor is given by

$$\hat{P}: \psi \rightarrow \Gamma^1 \Gamma^5 \psi. \quad (36)$$

We can now expand Γ in the usual basis:

$$\mathbb{B} = \{I, \Gamma^\mu, \Gamma^5, \Gamma^5 \Gamma^\mu, [\Gamma^\mu, \Gamma^\nu]\} \quad (37)$$

where the indices in the commutators $[\Gamma^\mu, \Gamma^\nu]$ run along the six different combinations, and check directly that the conditions (34) can only be satisfied by the matrices $I, \Gamma^5 \Gamma^i$ and $[\Gamma^0, \Gamma^z]$. This gives three candidate bilinears:

- (i) For $\Gamma = I$ we get the bulk current $\bar{\psi} \psi = -(\psi_1^\dagger \sigma^1 \psi_1 + \psi_2^\dagger \sigma^1 \psi_2)$, i.e. the mass operator in the bulk. As noted in this section and in more detail in Ref. [6], it can be identified as proportional to the bulk mass term. As such, it describes the free energy per particle, as can be seen from the expression for the free energy (26). The equation of motion for $K = \langle \bar{\psi} \psi \rangle$ [Eq. (28)] exclusively depends on the $U(1)$ current and thus

cannot encapsulate the density of the neutral particle-hole pairs: indeed, we directly see that the right-hand side equals zero if the total charge current vanishes.

- (ii) For $\Gamma = i\Gamma^y\Gamma^5$, the bulk current is $\bar{\psi}i\Gamma^y\Gamma^5\psi = -(\psi_1^\dagger\sigma^1\psi_1 - \psi_2^\dagger\sigma^1\psi_2)$. The crucial difference with respect to the first case is the relative minus sign. It is due to this sign that the current *couples to itself*, i.e. it is a response to a nonzero parameter G_{int} , as we will see soon.
- (iii) For $\Gamma = \Gamma^z$, the resulting bulk current is $\bar{\psi}\Gamma^z\psi = -i(\psi_1^\dagger\sigma^2\psi_1 + \psi_2^\dagger\sigma^2\psi_2)$. It sources the radial gauge field A_z which is believed to be equal to zero in all meaningful holographic setups, as the radial direction corresponds to the renormalization group (RG) scale. Thus, this operator is again not the response to the attractive pairing interaction.

We are therefore left with one possibility only: $\Gamma = i\Gamma^2\Gamma^5$ which is also consistent with the choice of our gauge at nonzero magnetic field. We will therefore work with the channel

$$\Gamma \equiv i\Gamma^y\Gamma^5 = \begin{pmatrix} 1 & 0 \\ 0 & -1 \end{pmatrix}. \quad (38)$$

As we have discussed earlier, the isotropy in the x - y plane remains unbroken by the radial magnetic field, and hence the expectation value should in fact be ascribed to the current $I^\mu = i\bar{\psi}\Gamma^\mu\Gamma^5\psi$ with $\mu = 1, 2$. We show the equivalence of the $i\Gamma^x\Gamma^5$ and $i\Gamma^y\Gamma^5$ order parameters below. The choice of the y channel is motivated by technical simplicity due to the form of the projection operator and the fermion basis we use, Eq. (14): $\Pi_\alpha = \frac{1}{2}(1 - (-1)^\alpha\Gamma^3\Gamma^0\Gamma^1)$ with $\alpha = 1, 2$, since $\Gamma^3\Gamma^0\Gamma^1 = -i\Gamma^2\Gamma^5$ with $\Gamma^5 = i\Gamma^0\Gamma^1\Gamma^2\Gamma^3$. Finally, we note that the structure of the currents defined in Eqs. (17) and (18) depends on the basis choice and that the currents as such have no physical interpretation in the boundary theory: physical meaning can only be ascribed to the expectation values [6]. It is exactly the expectation values that encode for the condensation (order) on the field theory side [6,30].

The AdS/CFT correspondence does not provide a straightforward way to match a double-trace condensate to a boundary operator, though only single-trace fields are easy to identify with the operators at the boundary. Indeed, in holographic superconductors a superconducting condensate is modeled by a charged scalar field $\langle\Phi\rangle$ (see e.g. Ref. [31]). As in Ref. [30], we argue by matching discrete symmetries on the gravity and field theory sides, that the expectation of the bulk current $\langle\bar{\psi}i\Gamma^2\Gamma^5\psi\rangle$ is the gravity dual of the pairing particle-hole gap. Let us consider properties of the corresponding

condensates with respect to discrete symmetries, parity and charge conjugation, in the AdS four-dimensional space. According to Eq. (36), $\langle\bar{\psi}\psi\rangle$ and $\langle\bar{\psi}\Gamma^3\psi\rangle$ are scalars and parity even, while $\langle\bar{\psi}i\Gamma^2\Gamma^5\psi\rangle$ is a pseudoscalar and parity odd. As for the charge conjugation, we easily find that $\langle\bar{\psi}\psi\rangle$ and $\langle\bar{\psi}i\Gamma^2\Gamma^5\psi\rangle$ commute with \hat{C} , while $\langle\bar{\psi}\Gamma^3\psi\rangle$ anticommutes. Since the latter is the component of a vector current while the former two are (pseudo)scalars, we find that all operators preserve the particle number, as promised. The magnetic field H is odd under both parity and charge conjugation, and therefore it is unaffected by $\hat{C}\hat{P}$. The condensate $\langle\bar{\psi}\psi\rangle$ is also unaffected by $\hat{C}\hat{P}$; however $\langle\bar{\psi}i\Gamma^2\Gamma^5\psi\rangle$ and $\langle\bar{\psi}\Gamma^3\psi\rangle$ spontaneously break the $\hat{C}\hat{P}$ symmetry.

In the three-dimensional boundary theory, gamma matrices can be deduced from the four-dimensional bulk gamma matrices; and the four component Dirac spinor ψ is dual to a two-component spinor operator Ψ . As has been also found in Ref. [30], the three-dimensional condensate $\bar{\Psi}\Psi$ is odd under parity and even under charge conjugation, and therefore it is odd under $\hat{C}\hat{P}$. We summarize the transformation properties of the four- and three-dimensional condensates together with the magnetic field

	$\langle\bar{\psi}\psi\rangle_{4d}$	$\langle\bar{\psi}\Gamma^3\psi\rangle_{4d}$	$\langle\bar{\psi}i\Gamma^2\Gamma^5\psi\rangle_{4d}$	$\langle\bar{\Psi}\Psi\rangle_{3d}$	H
\hat{P}	+	+	-	-	-
\hat{C}	+	-	+	+	-
$\hat{C}\hat{P}$	+	-	-	-	+

(39)

which shows that the symmetry properties are matched between $\langle\bar{\psi}i\Gamma^2\Gamma^5\psi\rangle_{4d}$ and $\langle\bar{\Psi}\Psi\rangle_{3d}$ condensates: they spontaneously break the CP symmetry while the magnetic field leaves it intact. Therefore our AdS/CFT dictionary between the bulk and boundary quantities is $\psi \leftrightarrow \Psi$ and $\langle\bar{\psi}i\Gamma^2\Gamma^5\psi\rangle \leftrightarrow \langle\bar{\Psi}\Psi\rangle$, with the corresponding conformal dimensions of boundary operators given by Eq. (84) and Eq. (83).

The natural bulk extension is now the current

$$I = (-i) \int d\omega \int d^2k \bar{\psi}(\omega, k, z) \Gamma \psi(E - \omega, p - k, z) \quad (40)$$

and it is understood that in nonzero magnetic field the integration over k degenerates into the sum over Landau levels (this holds for all currents in this section). We will soon show that a complete set of bulk equations of motion for the operator (40) requires a set of currents that we label J_\pm , I_\pm and K_\pm . In the representation (11) we introduce the following bilinears of the fermion field:

$$\begin{aligned}
J_{\pm}(E, p, z) &= (-i) \int d\omega \int d^2k (\bar{\psi}_1(\omega, k, z) \sigma^1 \psi_1(E - \omega, p - k, z) \pm \bar{\psi}_2(\omega, k, z) \sigma^1 \psi_2(E - \omega, p - k, z)) \\
&\equiv J_1(E, p, z) \pm J_2(E, p, z), \\
I_{\pm}(E, p, z) &= (-i) \int d\omega \int d^2k (\bar{\psi}_1(\omega, k, z) \psi_1(E - \omega, p - k, z) \pm \bar{\psi}_2(\omega, k, z) \psi_2(E - \omega, p - k, z)) \\
&\equiv I_1(E, p, z) \pm I_2(E, p, z), \\
K_{\pm}(E, p, z) &= - \int d\omega \int d^2k (\bar{\psi}_1(\omega, k, z) \sigma^2 \psi_1(E - \omega, p - k, z) \pm \bar{\psi}_2(\omega, k, z) \sigma^2 \psi_2(E - \omega, p - k, z)) \\
&\equiv K_1(E, p, z) \pm K_2(E, p, z),
\end{aligned} \tag{41}$$

where the pairing parameter $\langle \bar{\psi} \Gamma \psi \rangle$ in Eq. (40) is $I \equiv I_-$, the index 0 for the zeroth component is omitted in J_{\pm} , and $\bar{\psi}_{\alpha} = i\psi_{\alpha}^{\dagger} \sigma^1$.

Let us now study the dynamics of the system. We need to know the evolution equations for the currents and the scalar field and to complement them with the Maxwell equations. We will show that the equations of motion for all currents generically have nonzero solutions. This suggests that, due to the coupling with the UV CFT, the pairing can occur spontaneously, without explicitly adding new terms to the action (there is no need to add an interaction for fermions in the bulk). Nevertheless, we will also analyze the situation with nonzero G_{int} and show what new phenomena it brings as compared to UV CFT-only coupling (i.e. no bulk coupling).

Let us start from the equations of motion. The Dirac and Klein-Gordon equations are to be complemented with the Maxwell equation

$$\begin{aligned}
\nabla^M F_{MN} &= iq_{\phi} (\phi^* (\nabla_N - iq_{\phi} A_N) \phi - \phi (\nabla_N + iq_{\phi} A_N) \phi^*) \\
&\quad - iq_{\psi} \bar{\psi} \Gamma_N \psi
\end{aligned} \tag{42}$$

which is reduced when the scalar is real, $\phi^* = \phi$, to

$$\nabla^M F_{MN} = 2q_{\phi}^2 \phi^2 A_N - iq_{\psi} \bar{\psi} \Gamma_N \psi. \tag{43}$$

In the background of a dyonic black hole with the metric

$$ds^2 = \frac{1}{(1-z)^2} \left(-f dt^2 + \frac{dz^2}{f} + dx^2 + dy^2 \right) \tag{44}$$

the Maxwell equation for the component A_0 is

$$\partial_z^2 A_0 - \frac{2q_{\phi}^2 \phi^2}{(1-z)^2 f} A_0 - \frac{iq_{\psi} J_+}{(1-z)^2 f} = 0 \tag{45}$$

where we have used $\bar{\psi} \Gamma_0 \psi \rightarrow -J_+$.

In our setup we ignore the backreaction to $A_2 = Hx$, treating it as a fixed external field. The justification comes from the physics on the field theory side: we consider a stationary nonmagnetic system with zero

current and magnetization density. In the bulk, this means that the currents sourced by—and backreacting to—the magnetic field arise as corrections of higher order that can be neglected to a good approximation.⁵ Inclusion of the second Maxwell equation for A_2 would likely only lead to a renormalization of the magnetic field $H \mapsto H + \delta H$ without quantitative changes of the physics.

The equations of motion for the matter fields read

$$\begin{aligned}
e_A^M \Gamma^M (\tilde{D}_M^{\psi} - iq_{\psi} A_M) \psi - m_{\psi} \psi - iG_{\text{int}} \phi \Gamma \psi &= 0, \\
-(\partial_M - iq_{\phi} A_M) (\partial^M - iq_{\phi} A^M) \phi + \frac{1}{2} \frac{\phi}{|\phi|} V'(|\phi|) \\
- \frac{1}{2} G_{\text{int}} \bar{\psi} \Gamma \psi &= 0
\end{aligned} \tag{47}$$

where we included the connection to the definition $\tilde{D}_M = \nabla_M + \frac{1}{4} \omega_{Mab} \Gamma^{ab}$. In the dyonic black hole background, the Dirac equation is

$$\begin{aligned}
\left[(\partial_z + \mathcal{A}) \Gamma^z - \frac{i(\omega + qA_0)}{f} \Gamma^t - \frac{m}{\sqrt{f}(1-z)} \right. \\
\left. \mp \frac{iG_{\text{int}} \phi}{\sqrt{f}(1-z)} - U^{-1} \frac{\lambda_n}{\sqrt{f}} \right] \psi = 0
\end{aligned} \tag{48}$$

⁵To see this, consider the corresponding Maxwell equation

$$\partial_z^2 A_2 + \frac{\partial_z f}{f} \partial_z A_2 = \frac{2q_{\phi}^2 \phi^2}{\sqrt{f}(1-z)^3} A_2 + \frac{iq_{\psi}}{\sqrt{f}(1-z)^3} K_+, \tag{46}$$

and insert the ansatz $A_2 = Hx + \delta(z, x)$. The resulting relation for the neutral scalar $q_{\phi} = 0$ $\partial_z (f \partial_z \delta) = -q/(\sqrt{f}(1-z)^3)$ predicts $K \sim \bar{\psi}_{\alpha} \sigma^3 \psi_{\alpha} \sim \delta$, compared to the analogous estimate for the electrostatic backreaction $J \sim \bar{\psi}_{\alpha} \sigma^1 \psi_{\alpha} \sim \mu$. Thus the spatial current is of order of the small correction to the field, δ . The reason obviously lies in the fact that the magnetic monopole sources a z -independent field.

where $q_\psi \equiv q$, the scalar is neutral $q_\phi = 0$, $m_\psi \equiv m$ and

$$\begin{aligned} \mathcal{A} &= \frac{1}{2} \left(\frac{3}{(1-z)} + \frac{f'}{2f} \right), & A_0 &= \mu z, \\ \lambda_n &= \sqrt{2qhn}, & U^{-1} &= \begin{pmatrix} i\sigma^2 & 0 \\ 0 & i\sigma^2 \end{pmatrix} \end{aligned} \quad (49)$$

with $f' \equiv \partial_z f$. In the limit $\omega = 0$ it is written as follows:

$$\begin{aligned} \left(\partial_z + \mathcal{A} - \frac{iqA_0}{f} \sigma^2 + \frac{m}{\sqrt{f}(1-z)} \sigma^3 \right. \\ \left. \pm \frac{iG_{\text{int}}\phi}{\sqrt{f}(1-z)} \sigma^3 + \frac{\lambda_n}{\sqrt{f}} \sigma^1 \right) \psi_{1;2} = 0. \end{aligned} \quad (50)$$

We write the bilinears in short as

$$\begin{aligned} I_\pm &= \psi_1^\dagger \sigma^1 \psi_1 \pm \psi_2^\dagger \sigma^1 \psi_2, \\ J_\pm &= \psi_1^\dagger \psi_1 \pm \psi_2^\dagger \psi_2, \\ K_\pm &= \psi_1^\dagger \sigma^3 \psi_1 \pm \psi_2^\dagger \sigma^3 \psi_2, \end{aligned} \quad (51)$$

with $\bar{\psi}_1 \equiv \psi_1^\dagger i\sigma^1$. Therefore $I_- = (-i)\bar{\psi}\Gamma\psi$ because $\bar{\psi} = \psi^\dagger \Gamma^t$. We rewrite the Dirac equation for the bilinears

$$\begin{aligned} (\partial_z + 2\mathcal{A})J_\pm + \frac{2m}{\sqrt{f}(1-z)}K_\pm + \frac{2\lambda_n}{\sqrt{f}}I_\pm \\ + \frac{2iG_{\text{int}}}{\sqrt{f}(1-z)}\phi K_\mp = 0, \\ (\partial_z + 2\mathcal{A})I_\pm + \frac{2qA_0}{f}K_\pm + \frac{2\lambda_n}{\sqrt{f}}J_\pm = 0, \\ (\partial_z + 2\mathcal{A})K_\pm - \frac{2qA_0}{f}I_\pm + \frac{2m}{\sqrt{f}(1-z)}J_\pm \\ + \frac{2iG_{\text{int}}}{\sqrt{f}(1-z)}\phi J_\mp = 0. \end{aligned} \quad (52)$$

The pairing parameter is obtained by averaging the current I_-

$$\Delta = iG_{\text{int}}\langle I_- \rangle. \quad (53)$$

This system should be accompanied by the equation of motion for the neutral scalar field. In the limit of $\omega = 0$ and $k_i = 0$ it is given by

$$-\frac{1}{\sqrt{-g}}\partial_z \left(\sqrt{-g} \frac{1}{g_{zz}} \partial_z \phi \right) + \frac{1}{2}V'(|\phi|) - \frac{1}{2}G_{\text{int}}\bar{\psi}\Gamma\psi = 0 \quad (54)$$

where $g \equiv \det g_{MN}$. In the dyonic black hole background, the equation of motion for the scalar is

$$\partial_z^2 \phi + \mathcal{B}\partial_z \phi - \frac{m_\phi^2}{f(1-z)^2} \phi + \frac{iG_{\text{int}}}{2f(1-z)^2} I_- = 0 \quad (55)$$

where

$$\mathcal{B} = \frac{2}{(1-z)} + \frac{f'}{f}. \quad (56)$$

The system of equations (52) and (55) is solved, at the lowest Landau level, for the unknown I_\pm, J_\pm, K_\pm and ϕ . We do not consider the backreaction of the spinor and scalar fields to the gauge field, and therefore we omit the Maxwell equation (45).

Since the magnetic field is encapsulated in the parameter mapping (16), we may put $\lambda_n = 0$ and use the rescaled fermion charge; furthermore, the terms proportional to off-shell (discrete) momentum cancel out due to symmetry reasons, as explained in Ref. [6]. Another key property of the magnetic systems is that, at high magnetic fields, the ratio μ_{eff}/T can approach zero at arbitrarily small temperatures (including $T \rightarrow 0$).

Next we set up boundary conditions at the IR and UV for the system of equations (52). It is enough to establish the boundary conditions for the fermion components. At the horizon we choose the incoming wave into the black hole. However, as we consider static solutions $\omega = 0$, it is enough to take a regular solution, not growing to infinity as we approach horizon. We write the Dirac equation at the horizon $z \sim 0$ for the upper component $\psi_1 = (y_1, y_2)$,

$$\begin{aligned} \left(\partial_z + \mathcal{A} - \frac{i\mu q z}{f} \sigma^2 + \frac{m + G_{\text{int}}\phi}{\sqrt{f}(1-z)} \sigma^3 + \frac{\lambda_n}{\sqrt{f}} \sigma^1 \right) \begin{pmatrix} y_1 \\ y_2 \end{pmatrix} = 0, \\ \mathcal{A} = \frac{1}{2} \left(\frac{3}{1-z} + \frac{f'}{2f} \right) \end{aligned} \quad (57)$$

where at $T = 0$ the metric factor is $f = z(3 - 3z + z^2 - 3(1-z)^3)$. Near the horizon it becomes

$$\left(\partial_z + \frac{1}{2z} - \frac{i\mu_q}{6z} \sigma^2 + \frac{m + G\phi}{z\sqrt{6}} \sigma^3 + \frac{\lambda_n}{z\sqrt{6}} \sigma^1 \right) \begin{pmatrix} y_1 \\ y_2 \end{pmatrix} = 0. \quad (58)$$

Explicitly, the system is written as

$$\begin{aligned} \partial_z y_1 + \frac{1}{z} \left(\frac{1}{2} + \frac{m + G_{\text{int}}\phi}{\sqrt{6}} \right) y_1 + \frac{1}{z} \left(\frac{\lambda_n}{\sqrt{6}} - \frac{\mu_q}{6} \right) y_2 = 0, \\ \partial_z y_2 + \frac{1}{z} \left(\frac{1}{2} - \frac{m + G_{\text{int}}\phi}{\sqrt{6}} \right) y_2 + \frac{1}{z} \left(\frac{\lambda_n}{\sqrt{6}} + \frac{\mu_q}{6} \right) y_1 = 0. \end{aligned} \quad (59)$$

The solution reads

$$\begin{aligned} y_1 &= C_1 z^{-\frac{1}{2}-\nu} + C_2 z^{-\frac{1}{2}+\nu}, \\ y_2 &= \frac{1}{\frac{\mu_q}{6} - \frac{\lambda_n}{\sqrt{6}}} \left(C_1 \left(\frac{m + G_{\text{int}}\phi}{\sqrt{6}} - \nu \right) z^{-\frac{1}{2}-\nu} \right. \\ &\quad \left. + C_2 \left(\frac{m + G_{\text{int}}\phi}{\sqrt{6}} + \nu \right) z^{-\frac{1}{2}+\nu} \right) \end{aligned} \quad (60)$$

where C_1, C_2 are constants and

$$\nu = \frac{1}{6} \sqrt{6(m + G_{\text{int}}\phi)^2 + 6\lambda_n^2 - \mu_q^2}. \quad (61)$$

We choose the solution with the regular behavior $y \sim z^{-\frac{1}{2}+\nu}$. The solution for z_i in the lower component $\psi_2 = (z_1, z_2)$ where $\psi = (\psi_1, \psi_2)$ is obtained from y_i by a substitute $G_{\text{int}} \rightarrow -G_{\text{int}}$. We have for the bilinear combinations

$$\begin{aligned} I_{\pm} &= y_1^\dagger y_2 + y_2^\dagger y_1 \pm (y \rightarrow z), \\ J_{\pm} &= y_1^\dagger y_1 + y_2^\dagger y_2 \pm (y \rightarrow z), \\ K_{\pm} &= y_1^\dagger y_1 - y_2^\dagger y_2 \pm (y \rightarrow z), \end{aligned} \quad (62)$$

where $\psi_1 = (y_1, y_2)$ and $\psi_2 = (z_1, z_2)$.

We impose two boundary conditions for Eq. (55): at the horizon $\phi'(z=0) = 0$ and at the AdS boundary $\phi(z=1) = 0$.

At the AdS boundary, the boundary conditions for the currents are known from Ref. [6]: one should extract the normalizable components of J, I, K in order to read off the expectation values. However, a normalizable solution is defined in terms of an absence of a source for the fundamental Dirac field ψ_α rather than the composite fields such as J_{\pm} . The solution is to put the source of the Dirac field to zero and then to read off the desired normalizable solution for J_{\pm} directly. Under the assumption that the electrostatic potential A_0 is regular, from Eq. (20) the composite field densities behave near the AdS boundary $z_0 = 1$ as

$$\begin{aligned} \mathcal{J}_1 &= \psi_1^\dagger \psi_1 \rightarrow a_1^2(1-z)^{3-2m} + b_1^2(1-z)^{3+2m}, \\ \mathcal{I}_1 &= \psi_1^\dagger \sigma^1 \psi_1 \rightarrow a_1 b_1 (1-z)^3, \\ \mathcal{K}_1 &= \psi_1^\dagger \sigma^3 \psi_1 \rightarrow a_1^2(1-z)^{3-2m} - b_1^2(1-z)^{3+2m}, \end{aligned} \quad (63)$$

and

$$\begin{aligned} \mathcal{J}_2 &= \psi_2^\dagger \psi_2 \rightarrow a_2^2(1-z)^{5-2m} + b_2^2(1-z)^{5+2m}, \\ \mathcal{I}_2 &= \psi_2^\dagger \sigma^1 \psi_2 \rightarrow a_2 b_2 (1-z)^5, \\ \mathcal{K}_2 &= \psi_2^\dagger \sigma^3 \psi_2 \rightarrow a_2^2(1-z)^{5-2m} - b_2^2(1-z)^{5+2m}. \end{aligned} \quad (64)$$

The currents we have defined in Eq. (41) are the averaged densities, e.g. $J_1 = \int d\omega d^2k \mathcal{J}_1$. A normalizable solution in $\mathcal{J}_{\pm} = \mathcal{J}_1 \pm \mathcal{J}_2$ is thus defined by the vanishing of both the leading and the subleading term.

In what follows the AdS evolution equations (52) and (55) with appropriate boundary conditions are solved numerically with a shooting method from the horizon. Unlike the recent study in Ref. [30] where only in the presence of the four-Fermi bulk coupling G_{int} one finds a nontrivial solution for the averaged current $\langle I_- \rangle$ with the IR boundary taken at $z=0$, we will generically have a nonzero expectation value even for $G_{\text{int}} = 0$. In Ref. [30], one needed to introduce an IR cutoff, such as the hard wall, positioned at a radial slice $z = z_*$. In our setup, the choice of the boundary conditions in the UV guarantees that the condensate will form irrespectively of the IR geometry, as it specifically picks the quasinormal mode of the fermion.

We repeat the same calculations for the x -component order parameter

$$\tilde{\Gamma} \equiv i\Gamma^x \Gamma^5 = \begin{pmatrix} 0 & 1 \\ 1 & 0 \end{pmatrix}. \quad (65)$$

The pairing current defined as

$$\tilde{I} = (-i) \int d\omega \int d^2k \bar{\psi}(\omega, k, z) \tilde{\Gamma} \psi(E - \omega, p - k, z) \quad (66)$$

requires us to introduce the following currents:

$$\begin{aligned} \tilde{J}_{\pm}(E, p, z) &= (-i) \int d\omega \int d^2k (\bar{\psi}_1(\omega, k, z) \sigma^1 \psi_2(E - \omega, p - k, z) \pm \bar{\psi}_2(\omega, k, z) \sigma^1 \psi_1(E - \omega, p - k, z)) \\ &\equiv \tilde{J}_1(E, p, z) \pm \tilde{J}_2(E, p, z), \\ \tilde{I}_{\pm}(E, p, z) &= (-i) \int d\omega \int d^2k (\bar{\psi}_1(\omega, k, z) \psi_2(E - \omega, p - k, z) \pm \bar{\psi}_2(\omega, k, z) \psi_1(E - \omega, p - k, z)) \\ &\equiv \tilde{I}_1(E, p, z) \pm \tilde{I}_2(E, p, z), \\ \tilde{K}_{\pm}(E, p, z) &= - \int d\omega \int d^2k (\bar{\psi}_1(\omega, k, z) \sigma^2 \psi_2(E - \omega, p - k, z) \pm \bar{\psi}_2(\omega, k, z) \sigma^2 \psi_1(E - \omega, p - k, z)) \\ &\equiv \tilde{K}_1(E, p, z) \pm \tilde{K}_2(E, p, z). \end{aligned} \quad (67)$$

A tilde is used to distinguish the two cases of pairings involving x and y components. Using the Dirac equation at $\omega = 0$

$$\left(\partial_z + \mathcal{A} - \frac{iqA_0}{f} \sigma^2 + \frac{m}{\sqrt{f}(1-z)} \sigma^3 + \frac{\lambda_n}{\sqrt{f}} \sigma^1 \right) \psi_{1;2} + \frac{iG_{\text{int}}\phi}{\sqrt{f}(1-z)} \sigma^3 \psi_{2;1} = 0 \quad (68)$$

where the pairing parameter is obtained by averaging the current \tilde{I}_+

$$\tilde{\Delta} = iG_{\text{int}}\langle\tilde{I}_+\rangle \quad (69)$$

we get the following set of coupled equations for the bilinears defined in Eq. (67):

$$\begin{aligned} (\partial_z + 2\mathcal{A})\tilde{J}_\pm + \frac{2m}{\sqrt{f}(1-z)}\tilde{K}_\pm + \frac{2\lambda_n}{\sqrt{f}}\tilde{I}_\pm \\ + \frac{2iG_{\text{int}}}{\sqrt{f}(1-z)}\phi K_+ = 0, \\ (\partial_z + 2\mathcal{A})\tilde{I}_\pm + \frac{2q\Phi}{f}\tilde{K}_\pm + \frac{2\lambda_n}{\sqrt{f}}\tilde{J}_\pm = 0, \\ (\partial_z + 2\mathcal{A})\tilde{K}_\pm - \frac{2q\Phi}{f}\tilde{I}_\pm + \frac{2m}{\sqrt{f}(1-z)}\tilde{J}_\pm \\ + \frac{2iG_{\text{int}}}{\sqrt{f}(1-z)}\phi J_+ = 0. \end{aligned} \quad (70)$$

There are no minus components for the $G_{\text{int}}\phi$ term in the first and third equations of Eq. (70), and these terms contain currents without tildes defined in Eq. (41). The equation of motion for the scalar is

$$\partial_z^2\phi + \mathcal{B}\partial_z\phi - \frac{m_\phi^2}{f(1-z)^2}\phi + \frac{iG_{\text{int}}}{2f(1-z)^2}\tilde{I}_+ = 0. \quad (71)$$

The system of equations (52), (55) and (70), (71) differ only in the G_{int} term: they are identical without it, though currents are defined differently. Therefore, provided there is no ‘‘source’’ in the equations of motion, i.e. there is no Yukawa interaction $G_{\text{int}} = 0$, the x and y components of gamma matrices produce the vacuum expectation values (VEVs)

$$\langle I_\pm \rangle = \langle \tilde{I}_\pm \rangle \quad (72)$$

and according to the definitions of the pairing parameters

$$\Delta \rightarrow \langle I_- \rangle, \quad \tilde{\Delta} \rightarrow \langle I_+ \rangle \quad (73)$$

where I_\pm is found from Eq. (52). However, the equations for the plus and minus components in Eq. (52) are identical. In particular,

$$\langle I_+ \rangle = \langle I_- \rangle \quad (74)$$

which proves that x - y rotational symmetry is intact and

$$\Delta = \tilde{\Delta}. \quad (75)$$

Further we consider only the y component for simplicity.

C. Quantum criticality in the electron-hole channel

1. Thermodynamic behavior

We will first use the bilinear formalism to inspect the thermodynamics, in particular the phase transition that happens at high magnetic fields and the behavior of the pair density after the phase transition has occurred. To detect the transition, we can simply plot the free energy (26) at a fixed temperature as a function of the magnetic field. The action can be rewritten in terms of the gauge field and currents as

$$S = \int dz d^3x \left(\frac{1}{2} \Phi \partial_{zz} \Phi + \frac{1}{2} H^2 - I_- \Delta \right) \quad (76)$$

and we need to include also the boundary term that fixes the boundary values of the gauge field:

$$S_{\text{bnd}} = \int d^3x \sqrt{-h} A_\mu n_\nu F^{\mu\nu} = \int d^3x \Phi \partial_z \Phi \quad (77)$$

where $n_\mu = (0, 0, 0, 1)$ is the unit normal to the AdS_4 boundary, and h is the induced metric for which $\sqrt{-h} = z_0^{-3}$. Identifying $\Phi(z_0) = \mu$ and $\partial_z \Phi(z_0) = \rho$ and using the Maxwell equation (45), we arrive at the final expression

$$\begin{aligned} \mathcal{F} &= \mathcal{F}_{\text{bulk}} + \mathcal{F}_{\text{bnd}} \\ &= \int d^3x \left(\frac{(1-z_0)^{1+2m}}{2\sqrt{f}} J_+ \Phi + \frac{1}{2} h^2 - I_- \Delta \right) \\ &\quad + \int d^3x \left(\frac{\mu}{2m+1} J_1^0 (1-z_0)^{1+2m} + \frac{1}{2} \mu \rho \right). \end{aligned} \quad (78)$$

In particular, we see that I_- is indeed the response to the bulk order parameter Δ . When the coupling G_{int} is set to zero, the I_- term in the bulk part of Eq. (78) will be absent. Let us first see what happens in that case. The free energy is then unaffected by the pairing, and we can only follow the dependence on the magnetic field (Fig. 1). We see the nonanalyticity in the free energy at the point $h = h_c$. The underlying mechanism can be understood from the mapping (16): it is the disappearance of the coherent quasiparticle due to the lowering of the effective chemical potential μ_{eff} . The pairing arises as a byproduct of the interaction with the boundary CFT and does not influence the transition.

With the contact interaction, corresponding to electron-hole attraction in the infrared, we can further rewrite Eq. (78) observing that generically

$$J_1(z, \omega) = \frac{1}{2} G_R(z, \omega) I_-(z, \omega), \quad (79)$$

which gives the following result for the fermionic free energy:

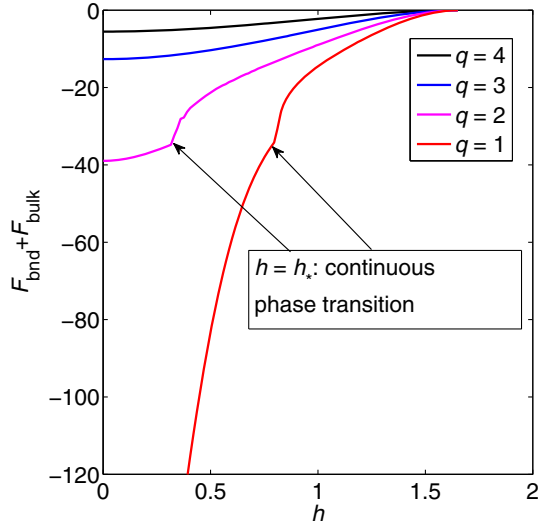


FIG. 1 (color online). Total (bulk plus boundary) free energy of the system $\mathcal{F}(h)$ for increasing values of the charge q . An explicit pairing term $G_{\text{int}} = 2$ has been chosen in order to suppress the stable Fermi surfaces and emphasize the phase transition at $h = h_*$. Still, for higher q values, the $\nu < 1/2$ quasiparticles become subdominant compared to $\nu > 1/2$ ones and the transition is lost. The bulk mass is $m = 0.10$.

$$\mathcal{F}_f = (1 - z_0)^{1+2m} J_1(z_0, \omega = 0) \left(\frac{3\mu}{4m+2} - 2\Delta G_R^{-1}(\omega = 0) \right). \quad (80)$$

The minus sign already makes it obvious that the derivative of the free energy can change sign, signifying a new critical point. To probe the transition point itself, however, we need to rewrite the relation (79) for on-shell values. Then the denominator of G_R vanishes, the current J_1 exactly captures the jump of the particle number on the Fermi surface [6] and Eq. (24) becomes $J_1 = 3\mu/(2m+1) \times Z$, so we need to replace $G_R \mapsto Z$, which gives the equation for the critical point:

$$\mathcal{F}_f = (1 - z_0)^{-2m} J_1(h) \left[\frac{3^{3/2} q}{4(\Delta_\Psi - 1)} \sqrt{1 - \frac{h^2}{3}} - \frac{2G_{\text{int}} I_-(h)}{Z(h)} \right]. \quad (81)$$

We have also used $\Delta_\Psi = 3/2 + m$ in order to write the equation purely in terms of the boundary quantities, and emphasized that Z and J_1 are also complicated functions of h , since h determines the effective chemical potential. Notice that only \mathcal{F}_{bnd} contributes to the fermionic term, while both $\mathcal{F}_{\text{bulk}}$ and \mathcal{F}_{bnd} contribute to the gauge field term. For $G_{\text{int}} = 0$, the second term vanishes and the free energy can only have a nonanalyticity when $J_1(h_c)$ has it. It is a first-order transition already identified in the magnetic case in Ref. [15] and studied from a more general viewpoint in Ref. [6]: the magnetic field depletes the Landau levels of

their quasiparticles and the Fermi surface vanishes. This first-order jump happens at some critical μ_{eff} and we will denote the corresponding value of the magnetic field by h_c . If, however, G_{int} becomes finite, we can see that the first term decreases with h while the second increases, since $Z(h)$ decreases. Thus, the overall free energy $\mathcal{F} = \mathcal{F}_f + \mathcal{F}_{\text{gauge}}$ will have a saddle point ($\mathcal{F}_{\text{gauge}}$ always decreases with h). We can now conclude that the following behavior with respect to G_{int} can take place:

- (i) For $0 \leq G_{\text{int}} < G_{\text{int}}^0$, the second term in Eq. (81) is always negligible and the system only has the first-order transition at $h = h_c$.
- (ii) For $G_{\text{int}}^0 < G_{\text{int}} < G_{\text{int}}^1$, the interplay of the first and the second term in Eq. (81) gives rise to a local stationary point (but not an extremum) at some $h = h_*$. This can potentially be a new critical point. In order to understand it better we will later perform a detailed analysis of the infrared behavior of the currents. It will turn out that it can be either a second-order transition or an infinite-order, Berezinsky-Kosterlitz-Touless (BKT)-type transition.
- (iii) For $G_{\text{int}} > G_{\text{int}}^1$, the Dirac hair cannot be formed and we have $J_1 = 0$ for any magnetic field, including zero. Since in this regime the pairing cannot occur even though G_{int} is large, this means we are in fact outside the applicability of the mean-field approach.

In Fig. 1 we show the second, arguably most interesting case. A second-order nonanalyticity in the free energy is obvious, as long as the stable quasiparticles with $\nu > 1/2$ do not overpower the unstable quasiparticles that govern the transition at $h = h_*$.

The conclusion we wish to emphasize is that order parameter physics is able to stabilize the non-Fermi liquids, while it is known [6,7] that in the absence of additional degrees of freedom a consistent backreaction treatment tends to leave only the stable, Fermi liquid surfaces. The physical nature of the point h_* will be the object of further analysis. The next section will reveal more on the actual pairing phenomenology, showing the new phase to be characterized by an anomalous, growing dependence $\Delta(h)$.

2. Analysis of critical points

Having analyzed the thermodynamics and found the existence of critical points, we will now study the behavior of the order parameter Δ in the most interesting regime, for $G_{\text{int}}^0 < G_{\text{int}} < G_{\text{int}}^1$, where the critical points are expected to appear.

In a nutshell, we will find that the region between G_{int}^0 and G_{int}^1 can be further subdivided into three regions, delimited by the values G_c^* , G_c^{**} and G_c , characterized by one or two second-order transitions or a BKT transition. We will also show that the pairing is favored for high effective chemical potentials when the density is high enough for the gravitational interaction to produce bound states. Finally, at small h values the pairs vanish as $\Delta \propto$

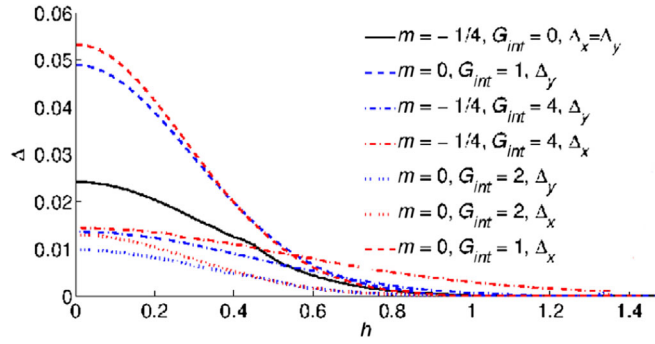


FIG. 2 (color online). Dependence for the x and y components of the pairing order $\Delta_x(h)$ and $\Delta_y(h)$ for $G_{\text{int}} = 0$ (coinciding solid line) and for $G_{\text{int}} = 1, 2, 4$ (dashed, dotted and dash-dotted lines). The coinciding solid line $\Delta_x = \Delta_y$ demonstrates the x - y rotational invariance. For $G_{\text{int}} > 0$, increasing the bare coupling decreases Δ (and lowers T_c) which provides a way to tune to the quantum critical point. Lowering the mass of the bulk fermion enhances pairing and increases Δ as seen for $m = 0$ and $m = -1/4$.

$\exp((T_c - T)^\beta)$ with $0 < \beta < 1$ (presumably $\beta = 1/2$) and finally reach zero density $\Delta = 0$ for $T \leq T_c$, while for higher magnetic fields the trend is reversed and the order parameter starts growing with h .

In order to construct the phase diagram, we will first study $\Delta(h)$ at fixed temperature [Fig. 3(a)]. We see that for $m = -1/4$ (smooth curves) the gap vanishes following a function which is smoother than a power law. Indeed, it turns out that for $h < h_c$ we have the infinite-order BKT scaling behavior

$$\Delta \sim \mu \exp\left(-\frac{C}{2\sqrt{q}(h_c - h)}\right). \quad (82)$$

The scaling (82) will be proven in Sec. IV. Similar behavior has been obtained in Ref. [32] where the scalar mass has been tuned to the quantum phase transition: $\Delta \sim \mu \exp\left(-\frac{C}{2\sqrt{m_c^2 - m^2}}\right)$. Notice also that the value h_c is very high, corresponding to the magnetic length of the order $\sqrt{h\mu_{\text{eff}}^2} \sim 10^2$ (we use $1/\mu_{\text{eff}}$ as the natural unit of length).

The above behavior is characteristic of the normal metal parent materials, i.e. $\nu_{k_F} > 1/2$. At small values of ν_{k_F} (i.e. Δ_Ψ close to $3/2$ or small μ_q), the anomalous growing dependence $\Delta(h)$ appears (found also in the previous section at strong enough magnetic fields) as shown by the dashed curves in Fig. 3(a). The nature of the dependence $\Delta(h)$ is rooted in the unstable Fermi surfaces with $\nu_{k_F} \rightarrow 0$ and can be understood from the analysis of the bilinear equations in the AdS_2 region, which we postpone until the next section.

We study the relation $\Delta(h)$ at different values of the pairing coupling G_{int} . For $G_{\text{int}} > 0$, Δ decreases as we increase G_{int} : repulsive interaction destructs the pairing, as given in Fig. 2. For $G_{\text{int}} < 0$, Δ increases as the absolute value of G_{int} is increased: attractive interaction triggers and enhances the pairing, as given in Fig. 3(b). Combining the two cases, when the sign of G_{int} is taken into account, the dependence Δ versus G_{int} is decaying. Lowering the mass of the bulk fermion enhances pairing as can be seen by comparing cases $m = 0$ and $m = -1/4$ in Fig. 2. As shown in Fig. 2, pairing parameters with the x and y components

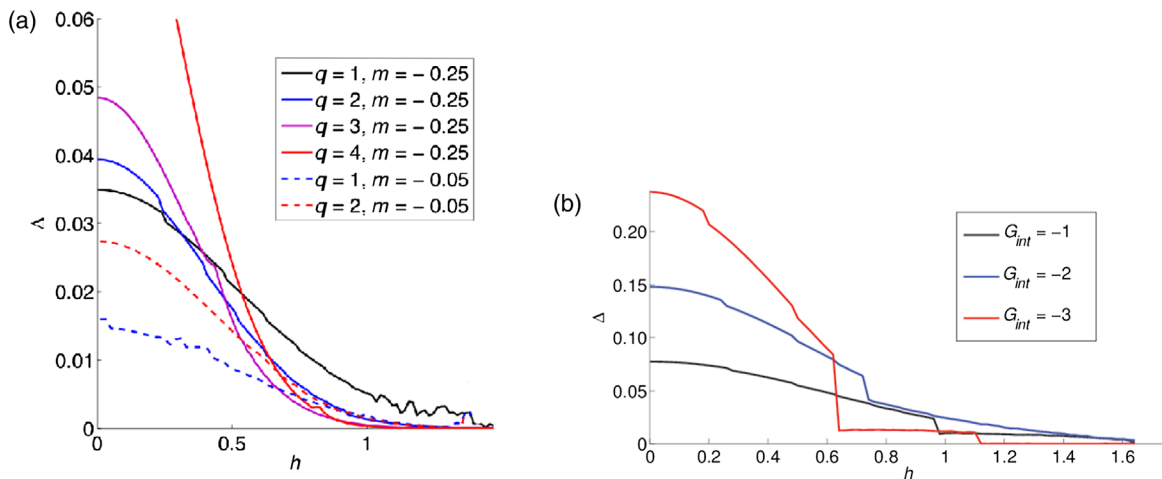


FIG. 3 (color online). (a) Dependence $\Delta(h)$ (in dimensionless units) for $m = -1/4$ (smooth lines) and $m = -1/20$ and for increasing values of the fermion charge. At fixed fermion charge in the Fermi liquid regime ($\nu_{k_F} < 1/2$), the magnetic field reduces the pair density, while small charges reduce the number of pairing particles, thus also reducing $\langle \Delta \rangle$. In the non-Fermi liquid regime ($\nu_{k_F} > 1/2$) for $h > h_c$ we observe an anomalous, power-law growing behavior of the gap. (b) Dependence $\Delta(h)$ for $m = -1/4$ and the negative bulk coupling G_{int} . For increasing absolute values of the bulk coupling G_{int} the pairing order Δ is enhanced. A new value h_* arises where the order parameter drops to zero due to competition between the channel K_1 and the quasiparticle density channel I_1 . For a large absolute value of G_{int} eventually $h_* = 0$ and we are out of the mean-field regime. The temperature is $T = 5.6 \times 10^{-4}$.

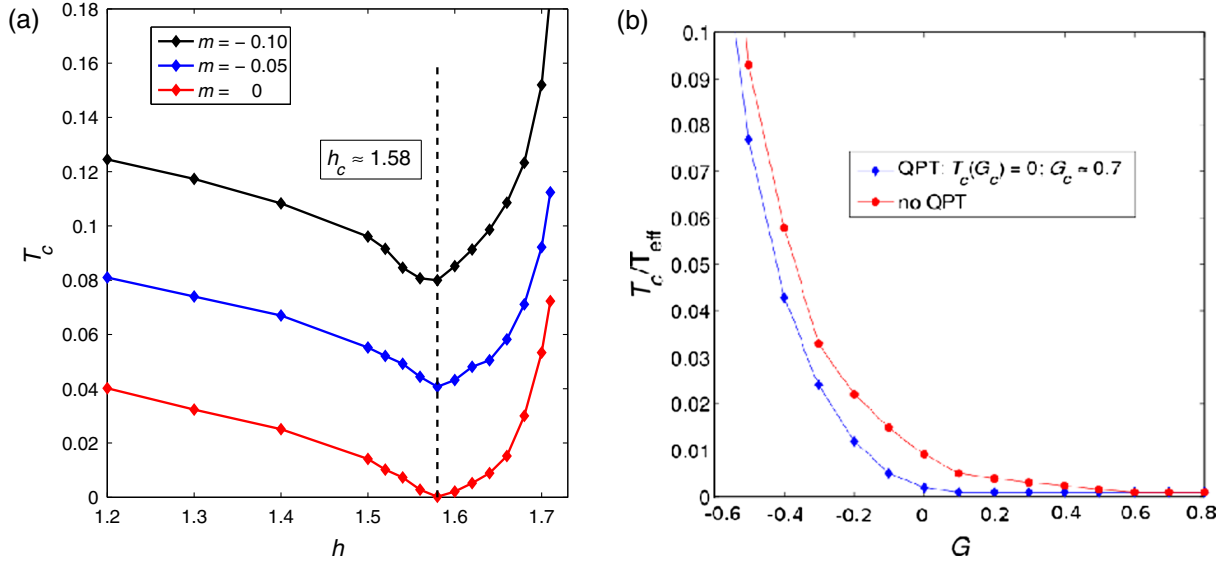


FIG. 4 (color online). Critical temperature T_c vs the magnetic field (a) and the coupling G_{int} (b), for $q = 1$. In (a), we again see the anomalous branch starting at $h_c \approx 1.58$, that signifies the exit from the Landau-Ginzburg regime and the mean field scaling into a new phase. Higher curves do not possess the QCP and arise when the system is always in the condensed phase. The coupling is $G = 0.7$. In (b), we see T_c vanish at the QCP $G_c \approx 1.1$, corresponding to the QPT with a non-mean field exponent $T_c \sim |G_c - G|^\beta$, $\beta > 1$. In the higher curve, T_c remains nonzero for all G_{int} , with no QPT for this set of parameters. The bulk mass is $m = -0.10$.

are identical for $G_{\text{int}} = 0$, which proves that the x - y plane rotational symmetry is intact. As G_{int} is switched on, it disrupts pairing in both channels in a slightly different way causing Δ_x and Δ_y to deviate from each other. An important novel feature distinguishing $G_{\text{int}} > 0$ and $G_{\text{int}} < 0$ is the appearance of the second anomalous branch for $G_{\text{int}} < 0$ as seen in Fig. 3 where the magnetic field enhances pairing: the rising $\Delta(h)$ manifests magnetic catalysis (MC).

The motivation to consider $G_{\text{int}} > 0$ was the ability to reduce the critical temperature to zero and to tune to the quantum critical point. On the other hand, adding $G_{\text{int}} < 0$ increases the critical temperature; however we can tune to vanishing T_c by adjusting other parameters such as the magnetic field. Figures 2 and 3(b) can be used to extract the quantum critical point (QCP) $h = h_c$ when $\Delta = 0$ (or $T_c = 0$) at fixed G_{int} . Upon varying the coupling G_{int} , the QCP becomes the quantum critical line (QCL) $h_c(G_c)$ or $G_c(h_c)$. In Fig. 3(b), for growing G_c , h_c decreases in the normal branch and h_c increases in the anomalous branch. In the normal branch, h depletes the particles from the Fermi surface decreasing the pairing density. Therefore h destroys the condensate. In the anomalous branch though, h enhances the condensation (magnetic catalysis).

The next step toward the phase diagram is the dependence of the critical temperature on the external magnetic field $T_c(h)$. A typical situation is given in Fig. 4(a). We have captured both branches so we see the expected twofold behavior, with the decrease of T_c up to $h = h_c$ and a subsequent increase. A precise tuning of the mass toward zero is necessary to enter the quantum critical regime where $T_c(h_c) = 0$. For reference, we have also

shown the cases $m = -0.10$ and $m = -0.05$, where the approach of the critical point is seen but $T_c(h_c)$ is still a finite minimum.

Figure 4(b) shows the decreasing dependence of the critical temperature T_c vs the coupling strength G_{int} . For the blue curve T_c vanishes at the QCP $G_c \approx 1.1$. It corresponds to the quantum phase transition (QPT) of the second order with a non-mean field exponent $T_c \sim |G_c - G|^\beta$, $\beta > 1$. For the red curve, T_c remains nonzero for all couplings G_{int} . It happens when the system is always in the condensed phase (an extreme RN-AdS black hole is unstable) [33]. As seen from Fig. 4(b), G_{int} is a sensitive “knob” to adjust the critical temperature T_c .

Finally, after studying the influence of the fermion charge q and the bulk mass m on the relation $T_c(h)$, we conclude with Fig. 5, showing the critical temperature vs the magnetic field for different couplings G_{int} . We find *four distinct regimes* located in the interval $G^0 < G < G^1$ (we omit the “int” subscript in G_{int} for now). The delimiting points are denoted by G_c^* , G_c^{**} and G_c , with $G^0 < G_c^* < G_c^{**} < G_c < G^1$.

- (i) For $G < G_c^*$ the critical temperature is nonzero, as demonstrated in Fig. 4(b) and also by the red curve in Fig. 5. There is thus no QCP and the normal and anomalous regimes are separated by a crossover.
- (ii) For $G_c^* < G < G_c^{**}$, there are two second-order phase transitions, one for the normal and one for the anomalous branch. This case is represented by the blue curve in Fig. 5, and can also be seen in Fig. 3(a). The quantum phase transition corresponding to the anomalous branch scales with a non-mean

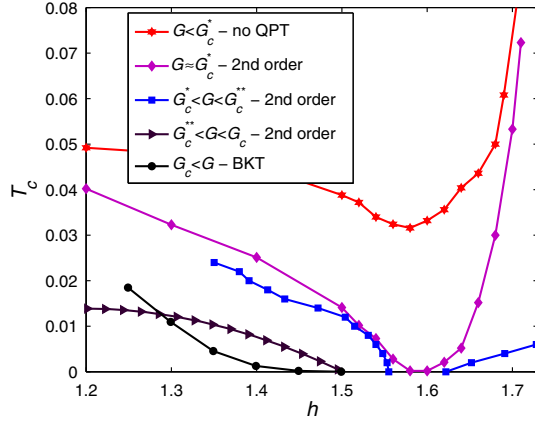


FIG. 5 (color online). Critical temperature T_c vs the magnetic field h for different couplings G_{int} . Depending on the coupling G_{int} , there are the BKT and second-order phase transitions. At $T_c = 0$, the QCP becomes QCL (h_c, G_c) with a decreasing/increasing dependence on h_c as G_c is increased which corresponds to the normal/anomalous branch.

field exponent $T_c \sim |h_c - h|^{\delta'}$, $\delta' > 1$. The limiting case of $G = G_c^*$ is given by the magenta curve, where the two critical points coincide.

- (iii) For $G_c^{**} < G < G_c$, there is the second-order phase transition with the non-mean field exponent $T_c \sim (h_c - h)^\delta$, $\delta < 1$, which describes the normal branch. This is the dark violet curve in Fig. 5, similar to the regime in Fig. 3(b).
- (iv) For $G > G_c$, there is an infinite-order phase transition of the BKT type with the characteristic exponential scaling $T_c \sim \exp(-\frac{C}{\sqrt{h_c - h}})$. This is the black curve in the figure.

Finally, based on the data from Fig. 5 and some additional calculations, we can draw the phase diagram in terms of the magnetic field h and the coupling G_{int} , given in Fig. 6. The QCL (solid line) separates the condensed (ordered) from uncondensed (disordered) phases. The position of the QCL is extracted from the phase transition curve of the critical temperature vs the magnetic field: the QCL where the critical temperature vanishes is given by the relation $G_c(h_c)$. From the dependence $G_c(h)$, one can translate the scaling exponents T_c vs G into T_c vs h : $T_c \sim |G_c - G|^\beta \rightarrow |G_c(h_c) - G|^\beta \rightarrow |h_c - h|^\delta$.

In Fig. 6, increasing the coupling G and the magnetic field h destroy the pairing condensate except in the non-Fermi liquid regime. This twofold behavior manifests itself through a double-valued function $h_c(G_c)$ in some parameter range. Indeed, the region with a condensed non-Fermi liquid is enhanced by the magnetic field, which is a consequence of the magnetic catalysis and the Callan-Rubakov effect discussed in the next section.

A deeper understanding of the phase diagram can be reached by considering the scaling dimensions of the condensate and the fermion field. With some foresight

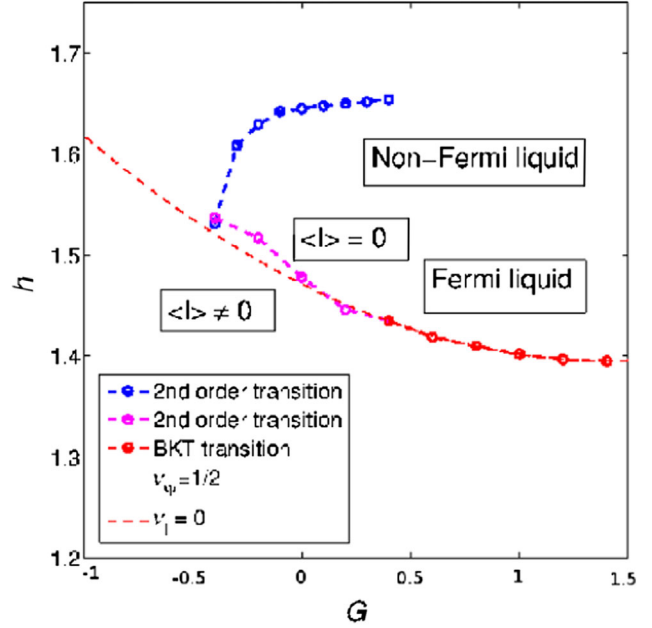


FIG. 6 (color online). Phase diagram h vs G for the condensed/normal (non-)Fermi liquids. G and h destroy the condensate except for the non-Fermi liquid. The ordered non-Fermi liquid is enhanced and stabilized by the strong magnetic field, which is also seen experimentally in pyrolytic graphite.

from the next subsection, we note that the IR conformal dimension of the operator which condenses $\delta_l = 1/2 + \nu_l$, where the bulk pairing current $\tilde{I} = \sqrt{c}I$ is the gravity dual of the excitonic condensate, is given by Eq. (95)

$$\nu_l = \sqrt{\frac{2}{3}} \sqrt{(m + \Delta)^2 + 2qh - \frac{\mu_q^2}{6}}. \quad (83)$$

On the other hand, the IR conformal dimension of the fermion operator $\delta_\psi = 1/2 + \nu_\psi$, where the bulk fermion field ψ is dual to the boundary fermion Ψ , is given by

$$\nu_\psi = \frac{1}{6} \sqrt{m^2 + k_F^2(h) - \frac{\mu_{q,\text{eff}}^2}{6}}, \quad \mu_{q,\text{eff}} = \sqrt{3q} \sqrt{1 - h^2/3}. \quad (84)$$

Importantly, the ratio ν_l/ν_ψ is first a decreasing and then an increasing function of the magnetic field h (see left panel of Fig. 8 in Ref. [15] for ν_ψ). At the dashed line the IR dimension ν_l of the operator with the gravity dual pairing current becomes imaginary, signaling the pairing instability. This is analogous to the instability of a scalar operator, when the Breitenlohner-Freedman (BF) bound in the AdS_2 is violated but the BF bound in the AdS_4 remains unbroken. The dash-dotted line corresponds to the locus of points in the phase diagram where $\nu_\psi = 1/2$, separating the Fermi liquid from the non-Fermi liquid behavior as

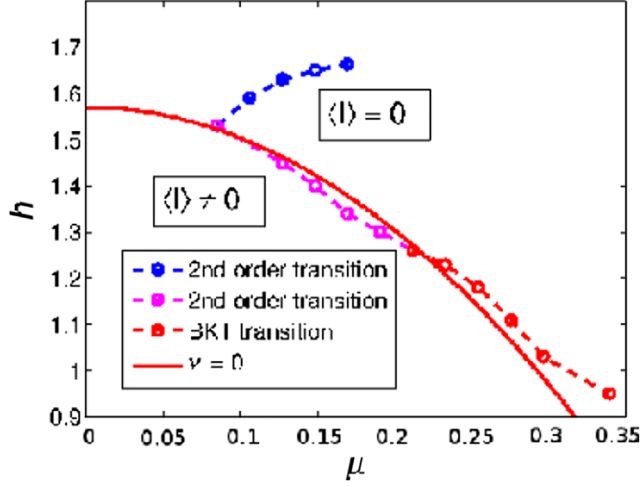


FIG. 7 (color online). Phase diagram h vs q for the condensed/normal (non-)Fermi liquids. Increasing the fermion charge at zero temperature is equivalent to increasing the chemical potential. It stabilizes the condensate in the anomalous regime and then destabilizes it in the normal branch. We can thus qualitatively relate q to G , the coupling constant from the previous figure.

discussed in Ref. [14]. Since $\nu_\psi(h)$ is a monotonically decreasing function, coherent quasiparticles disappear at large magnetic field resulting in the non-Fermi liquid regime at $\nu_\psi \leq \frac{1}{2}$ (upper part of the phase diagram). Notably, there is a similarity between our phase diagram (Fig. 6) and the phase diagram obtained for a scalar field (Fig. 14 in Ref. [16]), which uses the double-trace deformation as the control parameter. This may provide an insight into the mechanism of suppression/enhancement of the ordered phase at small/large magnetic fields.

We can redraw our phase diagram in terms of the magnetic field h vs the chemical potential μ (Fig. 7) to be able to compare our result with the literature [34].

It is worth noting that our phase diagram exhibits the same main features as the analogous phase diagram obtained using the Sakai-Sugimoto model (Fig. 8 in Ref. [34]). Primarily, it also has two regions of weak magnetic field where the condensate is destroyed by the magnetic field (“inverse” magnetic catalysis) and a regime of strong magnetic field which enhances the condensate (magnetic catalysis). Likewise, Fig. 5 shows the same structure as the analogous Fig. 9(b) in Ref. [34]. Thus there are two regimes with opposite dependence $\Delta(h)$ is a robust finding. We will discuss the reasons for it in the next section.

3. Pairing, double-trace deformations and conformal field theory

We will conclude our study of the phase diagram by offering an alternative viewpoint of the observed critical phenomena. Dialing the pairing coupling to drive the system toward QPT can also be understood as dialing the double-trace deformation in the boundary theory [16].

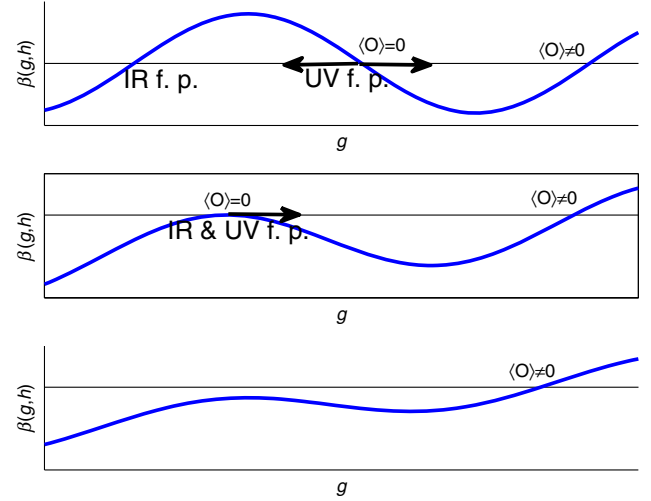


FIG. 8 (color online). Two-loop beta function for the double-trace coupling for decreasing magnetic field values. The disappearance of the original UV and IR fixed points at the critical magnetic field $h = h_c$ leads to conformality loss and the BKT scaling behavior, the middle panel. At $h < h_c$, the bottom panel, the system flows to a new IR fixed point with spontaneous symmetry breaking and nonzero condensate of a scalar field $\langle O \rangle \neq 0$.

For example, in the Gross-Neveu model with vector $SU(N_f)$ symmetry, the four-fermion coupling operator is relevant at the UV fixed point. Hence, as a relevant deformation in UV, it can drive the RG flow of the system to a new IR fixed point with spontaneous symmetry breaking. In holography, the multitrace deformations which are introduced on the boundary and correspond to the multiparticle states in gravity are a powerful knob that can drive the theory either to a free CFT at the IR fixed point or to a CFT with the spontaneously broken symmetry. An RG flow of this kind has been considered in Ref. [35], where the relevant double-trace deformation at the UV fixed point drives the theory toward the asymptotically free IR fixed point. In the gravity dual theory, it corresponds to different boundary conditions imposed at the AdS_4 boundary (alternative/standard quantization), and the UV and IR CFTs are related by a Legendre transform [35].

As an illustration, consider a scalar theory in the bulk as in Ref. [32]. One can hope that this case at least qualitatively captures the behavior of our system as a bilinear fermion combination bosonizes into a scalar field. Figure 8 shows schematically the two-loop beta function for the double-trace coupling for decreasing magnetic field value. At strong magnetic fields, Fig. 8 (top), the theory exhibits the usual RG flow from the strongly coupled UV fixed point (with a Landau pole at the QCP: $g_c \rightarrow \infty$) to a free fermion (a noninteracting theory at $g \rightarrow 0$) at the IR fixed point, with no expectation value for the scalar operator O . At the QCP i.e. $h = h_c$, Fig. 8 (middle), the UV and IR fixed points merge and annihilate, leading to the BKT scaling [36]

$$\Lambda_{\text{IR}} \sim \mu \exp\left(-\frac{C}{\sqrt{h_c - h}}\right) \sim \mu \exp\left(-\frac{C'}{\sqrt{g - g_c}}\right), \quad (85)$$

which can be interpreted as a distance along the RG trajectory to get to the nontrivial IR fixed point with broken symmetry. In this case, the QPT is of infinite order and where the critical temperature T_c and the order parameter $\langle O \rangle$ are governed by the exponential BKT scaling of Eq. (85) as $T_c \sim \langle O \rangle \sim \Lambda_{\text{IR}}$. When the magnetic field h is further decreased, Fig. 8 (bottom), the theory becomes gapped leading to an apparent conformality loss [36] and the QPT is now of second order.

In this paper we use the Yukawa coupling (or four-fermion coupling) in the bulk. However, the results we obtain are in line with the theory having a double-trace deformation on the boundary as described by Fig. 8: we have observed the rise of a new critical point. Figure 3(b) in particular conveys the message: at some $h_* < h_c$ we observe a transition from the quasiparticle regime to an electron-hole condensate. Formally, it comes from the competition between the pairing channel and the particle-photon interaction, encoded by the bilinears K_1 and I_1 . Physically, it corresponds to the competition between the Fermi surface “order” and the pairing order. At $h = h_c$, it is the entrance into the non-Fermi liquid region ($\nu < 1/2$) that drives the transition. At very high G_{int} values, the pairing is again suppressed which we interpret as the consequence of the Fermi surface depletion. The number density near the Fermi momentum is given by the current J_0 . In Eq. (52), it is clear that the gauge field term, encoding for the chemical potential (and implicitly density), is competing with the term containing $\Delta(r)$, i.e. the term proportional to the coupling G_{int} . When the latter is dominant, the pairing is highly enhanced but only up to the point that all electrons are “used up,” and their total number density is small. Notice also how Δ drastically increases at nonzero G_{int} , growing by about an order of magnitude.

D. AdS₂ analysis of the critical exponents

Most of our conclusions so far were driven by numerical results, with some qualitative analytical insight. A somewhat more detailed analytical understanding of the model can be gained by considering the far IR region, corresponding to the AdS₂ throat of the RN black hole.

We will follow the arguments of Ref. [32], where it was shown by analyzing the AdS₂ region that a new IR scale Λ_{IR} is generated which leads to the scaling behavior for the critical temperature T_c and the condensate Δ vs a tuning parameter (the magnetic field in our case). The key point of this analysis is to show that an instability for a scalar field develops in a certain parameter range. In particular, for a neutral scalar field the mass should be lower than the AdS₂ BF bound, $m^2 R^2 < -\frac{3}{2}$ (where R is the AdS₄ radius), which corresponds to a point where the IR conformal dimension

becomes imaginary. For a charged scalar, the mass value can be slightly higher if the product of the charge and the chemical potential, μ_q is sufficiently large. We therefore consider a composite bosonic field, which can be constructed as a bilinear combination of ψ 's and in our case it is given by a bulk current.

Let us start by recalling that at $T = 0$, the redshift factor develops a double zero near the horizon: $f \approx 6z^2$. Adopting the rescaled coordinates ζ, τ instead of the dimensionless coordinates z, t

$$\frac{1}{z} - 1 = \frac{\omega}{6\zeta}, \quad t = \frac{\tau}{\omega}, \quad (86)$$

with $\omega \rightarrow 0$ and ζ, τ finite, the metric (2) becomes near the horizon

$$ds^2 = \frac{1}{6\zeta^2}(-d\tau^2 + d\zeta^2) + dx^2 + dy^2, \quad (87)$$

where the gauge field is

$$A_\tau = \frac{\mu}{6\zeta}. \quad (88)$$

In this metric, the currents defined in Eq. (41) become

$$\begin{aligned} J(E, p, z) &= (-i) \int d\omega \int d^2 k \bar{\psi}(\omega, k, z) \sigma^1 \psi(E - \omega, p - k, z), \\ I(E, p, z) &= (-i) \int d\omega \int d^2 k \bar{\psi}(\omega, k, z) \psi(E - \omega, p - k, z), \\ K(E, p, z) &= - \int d\omega \int d^2 k \bar{\psi}(\omega, k, z) \sigma^2 \psi(E - \omega, p - k, z), \end{aligned} \quad (89)$$

with $\bar{\psi} = i\psi^\dagger \sigma^1$. The Dirac equation at $\omega = k = 0$ assumes the form

$$\left(\partial_\zeta - i \frac{\mu_q}{\sqrt{6}e_\zeta} \sigma^2 + \frac{(m + \Delta)}{e_\zeta} \sigma^3 + \frac{\lambda}{e_\zeta} \sigma^1, \right) \psi = 0, \quad (90)$$

giving the following equations of motion for the currents:

$$\partial_\zeta J + \frac{2(m + \Delta)}{e_\zeta} K + \frac{2\lambda}{e_\zeta} I = 0, \quad (91)$$

$$\partial_\zeta I + 2 \frac{\mu_q}{\sqrt{6}e_\zeta} K + \frac{2\lambda}{e_\zeta} J = 0, \quad (92)$$

$$\partial_\zeta K - 2 \frac{\mu_q}{\sqrt{6}e_\zeta} I + \frac{2(m + \Delta)}{e_\zeta} J = 0 \quad (93)$$

where $e_\zeta = \sqrt{6}\zeta$, $\mu_q = \mu q$, $h_q = h q$, $\lambda = 2|h_q|l$, $l = 1, 2, \dots$ and $\Delta = -(I)$. Differentiating the second equation for I with respect to ζ and eliminating the derivatives of J

and K currents from the other two equations, we obtain the zero-energy Schrödinger equation:

$$\partial_{\tilde{\zeta}}^2 \tilde{I} - \frac{\nu_{\tilde{l}}^2 - 1/4}{\tilde{\zeta}^2} \tilde{I} = 0, \quad (94)$$

$$\nu_{\tilde{l}} = \sqrt{\frac{2\lambda^2}{3} - \frac{\mu_q^2}{9}}, \quad (95)$$

where $\tilde{I} = I\sqrt{\tilde{\zeta}}$. We assume that condensation occurs for the lowest (first) Landau level ($l = 1$) and it is caused by an instability when $\nu_{\tilde{l}}$ becomes imaginary. Therefore we can represent the conformal dimension as

$$\tilde{\nu}_{\tilde{l}} = \sqrt{\frac{4}{3}(h_q^c - h_q)}, \quad h_q^c = \frac{\mu_q^2}{12} \quad (96)$$

where $\nu_{\tilde{l}} \equiv i\tilde{\nu}_{\tilde{l}}$, and h_q^c is found from the condition $\nu_{\tilde{l}} = 0$. Generalizing for $m \neq 0$ we get

$$\nu_{\tilde{l}} = \sqrt{\frac{2}{3}(\lambda^2 + m^2) - \frac{\mu_q^2}{9}}, \quad (97)$$

$$h_q^c = -\frac{m^2}{2} + \frac{\mu_q^2}{12}, \quad (98)$$

in dimensionless units.

Now consider the scaling behavior near the quantum critical point, $h \approx h_c$ or $G \approx G_c$ (solid red line in the phase diagram Fig. 6). As in Ref. [32], imposing the Dirichlet boundary condition $\tilde{I}(\zeta = \zeta_{\text{IR}}) = 0$ gives an oscillatory solution of Eq. (94):

$$I(\zeta) = \sin\left(\tilde{\nu} \log \frac{\zeta}{\zeta_{\text{UV}}}\right), \quad (99)$$

where ζ_{UV} is the location of the boundary of the AdS₂ throat. In order to satisfy the boundary condition we should have

$$\tilde{\nu} \log \frac{\zeta_{\text{IR}}}{\zeta_{\text{UV}}} = \pi. \quad (100)$$

According to the discussion in Sec. IV of Ref. [32], this means that a new IR scale is generated

$$\Lambda_{\text{IR}} \sim \frac{1}{\zeta_h} \sim \mu \exp\left(-\frac{\pi}{\tilde{\nu}}\right), \quad (101)$$

where μ is the UV scale, that leads to the infinite-order BKT scaling behavior:

$$\begin{aligned} T_c &\sim \mu \exp\left(-\frac{C}{\sqrt{h_q^c - h_q}}\right), \\ \Delta &\sim \mu \exp\left(-\frac{C}{2\sqrt{h_q^c - h_q}}\right), \end{aligned} \quad (102)$$

with $C = \frac{\pi}{\sqrt{4/3}}$ and h_q^c given by Eq. (98). The factor of 2 in the exponent comes from the difference in operator dimensions in the intermediate conformal regime: the current I scales as a dimension-1/2 operator and the temperature scales with dimension 1. Equation (102) describes the behavior below the critical magnetic field $h < h_c$, which can be seen in Fig. 5. Since $h_q = hq$, increasing the charge q would produce higher curves.

Choosing the mass m as a tuning parameter, we obtain the infinite-order BKT scaling behavior from the condition $\nu_{\tilde{l}} = 0$ in Eq. (98):

$$\begin{aligned} T_c &\sim \mu \exp\left(-\frac{C'}{\sqrt{m_c^2 - m^2}}\right), \\ \Delta &\sim \mu \exp\left(-\frac{C'}{2\sqrt{m_c^2 - m^2}}\right), \end{aligned} \quad (103)$$

with $C' = \frac{\pi}{\sqrt{2/3}}$ and $m_c^2 = -2h_q + \mu_q^2/6$. The scaling behavior from Eqs. (102) and (103) describes the BKT regime found also for the condensation of a scalar field in Ref. [32], with the condensed phase for $h < h_c$ (or at $m^2 < m_c^2$) and the normal state with zero condensate at $h > h_c$ (or at $m^2 > m_c^2$).

While the above analysis fits well into the results we have found for the normal branch, the anomalous branch, where at high $h > h_c$ the magnetic field catalyzes and enhances the condensate is still to be explained. The scaling behavior in this region is given by

$$T_c \sim \Delta \sim |h - h_c|^\delta, \quad (104)$$

where $\delta > 1$. In Figs. 3(a) and 4(a), a sharp increase with h is found, which is in agreement with field theory calculations of magnetic catalysis [22] and experiments on graphite in strong magnetic fields [18]. We leave the explanation of this regime within the AdS₂ analysis for further work.

For $m = 0$, the equation of motion for I can be reduced to a Schrödinger-like equation also in the general AdS₄ case. This is what we will do in the next subsection.

E. The $m = 0$ formalism

As elucidated before in a slightly different context [14], nonzero contributions to the current (corresponding to the quasiparticles at the boundary) are quantified by counting the bound states at zero energy for the formal wave function I_- of the above equation. An important novel feature in our

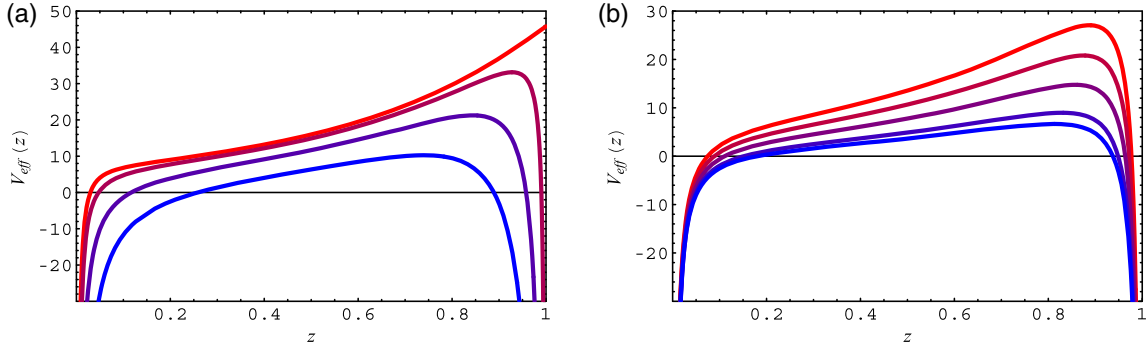


FIG. 9 (color online). Effective potential for the current \tilde{I}_- for $m = 0$, $q = 2$, $T = 0.001 \times 10^{-3}$ and $h = 0$, $G_{\text{int}} = 0, 1/3, 2/3, 1$ [red to blue, (a)] and $G_{\text{int}} = 0.2$, $h = 0, 0.50, 1.00, 1.50, 1.71$ [red to blue, (b)]. The pairing interaction opens the near-boundary gap (a), which gets wider but shallower as the magnetic field increases (b). The competition between the broadening and the shallowing effect gives rise to the transition between the normal and anomalous regime at $h = h_c$.

setup is that the momentum is quantized due to the magnetic field, and thus we cannot use the usual quasi-classical (WKB) formalism. Still, in the massless limit we will be able to gain some more insight by constructing an effective Schrödinger equation with a formal WKB momentum, that can be studied analytically.

Notice first that the RN geometry allows the spin connection term from Eq. (8) to be absorbed into the definition of the currents as it is a total derivative [14]:

$$\mathcal{A} = \partial_z(-gg^{zz})^{1/4}. \quad (105)$$

Upon implementing Eq. (105), the system (52) for $m = 0$ and in the static limit $\omega \rightarrow 0$ is simplified to

$$e_z \partial_z J_{\pm} + 2\Delta K_{\mp} + 2e_i \lambda I_{\pm} = 0, \quad (106a)$$

$$e_z \partial_z I_{\pm} + 2e_i \Phi K_{\pm} + 2\lambda e_i J_{\pm} = 0, \quad (106b)$$

$$e_z \partial_z K_{\pm} - 2e_i \Phi I_{\pm} + 2\Delta J_{\mp} = 0, \quad (106c)$$

where the vierbeine of the metric (2) are $e_z = (1-z)\sqrt{f}$, $e_i = (1-z)/\sqrt{f}$, $e_{\bar{i}} = (1-z)$, and the scalar potential is rescaled as $q\Phi \rightarrow \Phi$ to absorb q . As before, the magnetic field is implemented by rescaling the chemical potential and the fermion charge as given by Eq. (16), meaning that we can put $\lambda = 0$. The expectation values are given by the minus component, with only three coupled equations for J_- , K_- , I_- remaining to be solved. In order to understand the phenomenology of the bulk pair current, it is useful to eliminate J_- from Eq. (106). Rescaling I_- as

$$I_- \mapsto \tilde{I}_- \equiv I_- \frac{e_i \Phi}{e_z} \equiv I_- \tilde{\Phi} \quad (107)$$

we first easily eliminate J_- and differentiate Eq. (106b) with respect to z . The derivative $\partial_z K_-$ can be expressed from Eq. (106c) and K_- from Eq. (106b). In this way we arrive at the second-order equation involving I_- only and having the form of the Schrödinger equation for \tilde{I}_- :

$$\partial_{zz} \tilde{I}_- - \left[\frac{2\partial_z \tilde{\Phi}}{\tilde{\Phi}} + 4\tilde{\Phi}^2 - \Delta \partial_{zz} \log \tilde{\Phi} \right] \tilde{I}_- = 0. \quad (108)$$

Notice that the term containing the first derivative vanishes automatically due to the transform (107).

We are interested in the behavior of the current in the limit $z \rightarrow z_0 = 1$. While the Schrödinger formulation might in some cases be more convenient also for computational reasons, the real benefit is that we can use a formal WKB scheme to arrive at surprisingly accurate solutions without solving the differential equation. Equation (108) has the form $(\partial_{zz} - V_{\text{eff}}(z))\tilde{I}_- = 0$, where the effective potential obeys the inverse square law near the boundary [we also use the relation (69)]:

$$V_{\text{eff}}(z \rightarrow 1) = \delta^2(1-z) - \frac{8\Delta}{(1-z)^2} + \mu^2(1-z)^2 + O(1) \quad (109)$$

where $\Delta \equiv \Delta(z \rightarrow z_0) \approx \text{const}$; although, strictly speaking, one needs to compute Δ self-consistently given the value of G_{int} , for qualitative considerations we may assume a constant Δ proportional to G_{int} . The formal squared Dirac delta function is there to enforce the condition $J_{\pm}(z_0) = I_{\pm}(z_0) = K_{\pm}(z_0) = 0$. The typical appearance of the potential is given in Fig. 9. The development of the electron-hole condensate can be seen as the accumulation of bound states inside the potential well, analogously to the similar logic for electron states in Fermi and non-Fermi liquids, elucidated in Ref. [14] and applied in Ref. [37]. We can easily visualize our findings on the transition points $h = h_*$ and $h = h_c$ by looking at the potential (Fig. 9). In the figures, we have left out the Dirac-delta squared spike at the boundary, as it is completely localized and only ensures that the currents reach zero at $z = 1$, exerting no influence on the behavior at small but finite $1-z$ values. Importantly, the near-boundary gap opens with $\Delta > 0$, supporting the electron-hole pair

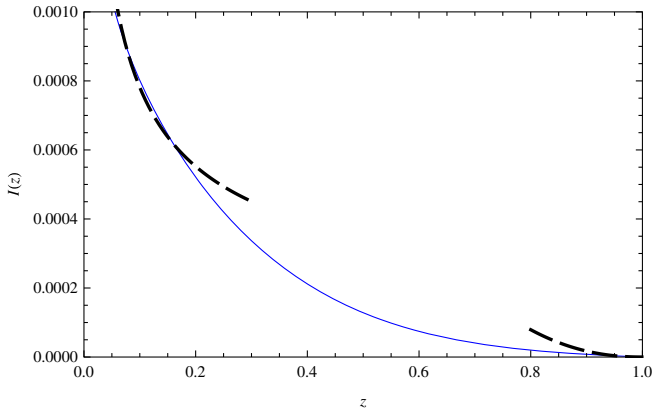


FIG. 10 (color online). Radial profile of the excitonic condensate (solid line) from the numerical solution of the effective Schrödinger equation. The transformation law between radial coordinates is $r = \frac{1}{1-z}$. The fits (dashed lines) are the asymptotic behaviors $(1-z)^3 \rightarrow \frac{1}{r^3}$ at $z \sim 1$ in the UV and $\frac{1}{z} \rightarrow \frac{1}{r-1}$ at $z \sim 0$ in the IR.

condensate near the boundary. The influence of the magnetic field through the relation $q \mapsto q\sqrt{1-H^2/(Q^2+H^2)}$ is subtler: it makes the potential well both broader and shallower. The former generally facilitates the formation of bound states, while the latter acts against it. It is this competition that gives rise to the transition from the normal toward the anomalous region at $h = h_c$.

Within the WKB approximation, the solution to Eq. (108) can be written as

$$\tilde{I}_-(z) = \frac{(1-z)^2}{\sqrt{V_{\text{eff}}(z)}} \left(\exp(-\sqrt{-V_{\text{eff}}(z)}) + \exp\left(\frac{3\pi}{4}i - \sqrt{V_{\text{eff}}(z)}\right) \right). \quad (110)$$

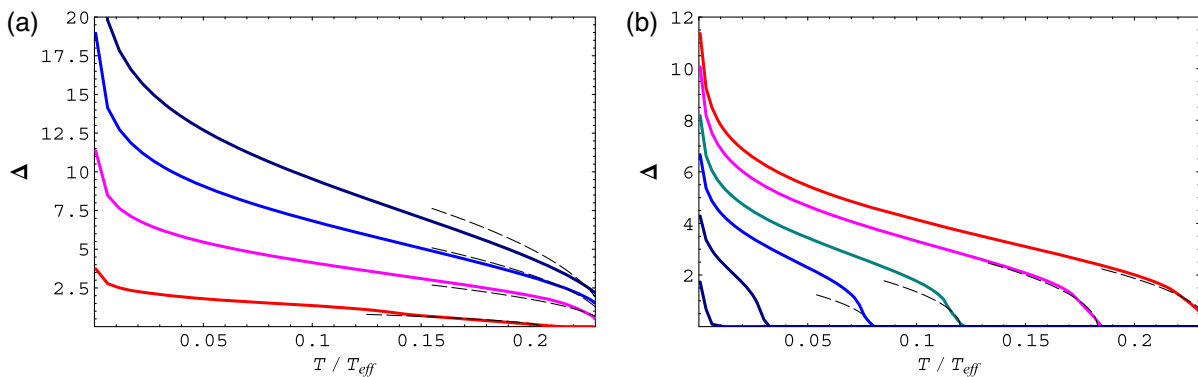


FIG. 11 (color online). Order parameter of the pair density Δ vs the temperature (all in dimensionless units) (a) for $h = 1$ and different values of the coupling strength $q = 1, 3, 5, 7$ (red, magenta, blue, black) and (b) for $q = 3$ and different values of the magnetic field $h = 0, 0.8, 1.2, 1.4, 1.6, 1.7$ (red to black). Pairing is favored in the overdamped phase, with stable quasiparticles for $q \gg 1$ and $\nu \sim 1$, and suppressed at very high magnetic fields when the effective chemical potential is lowered and thus only a small number of electrons is available for pairing.

We have constructed the solution by equating the WKB expansion with the near-boundary expansion [Eqs. (63) and (64)]. Notice that the phase shift is $3\pi/4$ instead of the usual $\pi/4$, as the boundary itself provides an additional $\pi/2$ shift due to the condition $I_-(z_0) \rightarrow 0$. The radial profile of the condensate is depicted in Fig. 10. It can be shown to have $\frac{1}{r^3}$ behavior at the UV boundary $r \rightarrow \infty$, and it diverges as $\frac{1}{r-1}$ at the horizon in the IR $r \rightarrow 1$. We obtain the same asymptotic behavior when $\Delta = 0$ in Eq. (109), but we impose the hard wall near the horizon in the IR, which brings us in agreement with the results of Ref. [30]. The UV behavior follows from the boundary condition on the fermion currents at the AdS boundary (putting the source term to zero) and the appearance of a fermion mass gap, to be discussed in more detail later.

Another advantage of the Schrödinger approach is that solving the Schrödinger equation numerically is easier than solving the current equations. In Figs. 11 and 12 we give the dependences $\Delta(h)$ and $\Delta(q)$, produced by solving the equation (108). Qualitatively similar behavior is seen in both cases. The WKB approach makes it feasible to study also the dependence on the fermion charge q . Figure 12 already shows that there is a critical value $q = q_c$ below which no pairing can occur at all. We conjecture that this value corresponds to $\nu < 1/2$, i.e. only stable quasiparticles can pair up. While plausible, this is not easy to see from the relations $\Delta(h)$ and $\Delta(T)$ that we obtained in the $m \neq 0$ case.

IV. SPECTRA AND THE PSEUDOGAP

In this section we will compute the spectra for the fermionic system with particle-hole pairs. We invoke again Eq. (15) to derive the equations of motion for the retarded propagator, which will directly give us the spectral function as $A(\omega, k) = \text{Im}G_R$.

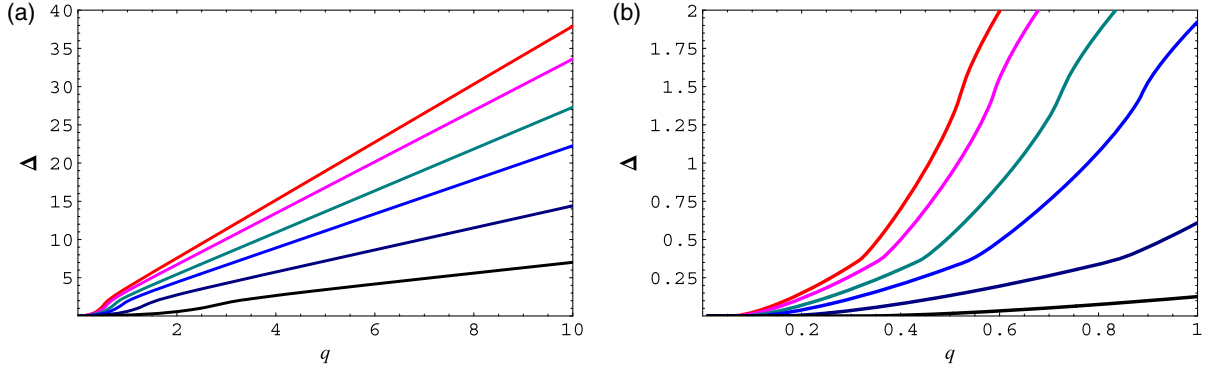


FIG. 12 (color online). (a) Order parameter of the pair density Δ vs the fermion charge q , for $T = 5.6 \times 10^{-4}$ and different values of the magnetic field $h = 0, 0.8, 1.2, 1.4, 1.6, 1.7$ (red to black). The critical value q_c is shifted again due to the shifting of the effective potential. (b) Zoom-in near $q = 0$ to better appreciate the transition.

Following Ref. [14], we can write a single nonlinear evolution equation for G_R . It will generically be a matrix equation, due to the additional, pairing channel. Of course, we can rewrite it as a system of four scalar equations for the four components of the bispinor. We adopt the basis given in Eq. (11) and the metric given by Eq. (2). Introducing the notation $\psi = (\psi_1, \psi_2)^T$ with $\psi_\alpha = (y_\alpha, z_\alpha)^T$ where $\alpha = 1, 2$, the resulting system reads

$$(\partial_z \mp m\sqrt{g_{zz}})y_{1;2} = \mp i\sqrt{\frac{g_{zz}}{g_{ii}}}(\lambda - u)z_{2;1} - \Delta\sqrt{g_{zz}}y_{1;2} = 0, \quad (111a)$$

$$(\partial_z \mp m\sqrt{g_{zz}})z_{1;2} = \pm i\sqrt{\frac{g_{zz}}{g_{ii}}}(\lambda + u)y_{2;1} + \Delta\sqrt{g_{zz}}z_{1;2} = 0, \quad (111b)$$

with

$$u = \sqrt{\frac{g_{ii}}{-g_{tt}}}(\omega + q\Phi(z)). \quad (112)$$

Introducing $\xi_\alpha = iy_\alpha/z_\alpha$ as in Ref. [14], where the boundary Green's function is found from the asymptotics of the solution at the boundary [Eq. (20)]

$$G_\alpha = \lim_{z \rightarrow 1} \left(\frac{1}{1-z} \right)^{2m} \xi_\alpha(z) = \lim_{\epsilon \rightarrow 0} \epsilon^{-2m} \xi_\alpha(1-z=\epsilon), \quad (113)$$

the equations of motion for ξ_α become

$$\begin{aligned} \partial_z \xi_{1;2} &= -2m\sqrt{g_{zz}}\xi_{1;2} - \sqrt{\frac{g_{zz}}{g_{ii}}}(\lambda - u) \\ &+ \sqrt{\frac{g_{zz}}{g_{ii}}}(\lambda + u)\xi_{1;2} \mp 2\Delta\sqrt{g_{zz}}\xi_{1;2}. \end{aligned} \quad (114)$$

The infalling boundary conditions at the horizon are imposed $\xi_\alpha = i$, while the amplitude of y_α remains free

(it cancels out in the propagator G_R) and can be chosen to be of order unity for convenience in the numerical integration.

With no pairing channel, the morphology of the spectra is well known and has been analyzed in detail in Refs. [14,15]: near $k = k_F$, gapless quasiparticle excitations appear, belying a Fermi surface. Let us now repeat the AdS_2 analysis of Ref. [14] for the equations with pairing. We will use the (ζ, τ) coordinates introduced in Eq. (86). The near-horizon equation of motion now assumes the following form:

$$\zeta \partial_\zeta \psi = \left(i\sigma^2 \frac{\mu_q}{6} - \sigma^3 \frac{(m+s\Delta)}{\sqrt{6}} - \sigma^1 \frac{k}{\sqrt{6}} \right) \psi, \quad (115)$$

where $s = \pm 1$, and in the presence of magnetic field the role of the momentum k is taken over by Landau levels $\lambda = \sqrt{2|qh|l}$. Near the AdS_2 boundary ($\zeta \rightarrow 0$), the equation can be solved analytically at the leading order:

$$\psi = A \left(\frac{m+s\Delta}{\sqrt{6}} + \nu \right) \zeta^{-\nu} + B \left(\frac{m+s\Delta}{\sqrt{6}} - \nu \right) \zeta^\nu \quad (116)$$

with

$$\nu = \frac{1}{6} \sqrt{\mu_q^2 - 6((m+s\Delta)^2 + k^2)}, \quad (117)$$

and the self-energy scales as

$$\text{Im}\Sigma \sim \omega^{2\nu}. \quad (118)$$

As usual, the Fermi surface is stable for $\nu^2 > 1/4$, unstable for $\nu^2 < 1/4$ and nonexistent for $\nu^2 < 0$.

In the bulk (and also as we move toward the boundary), the pairing term acts by shifting the mass as $m \mapsto m \pm \Delta$, meaning that the position of the quasiparticle pole is shifted, effectively modifying the k_F value, which removes

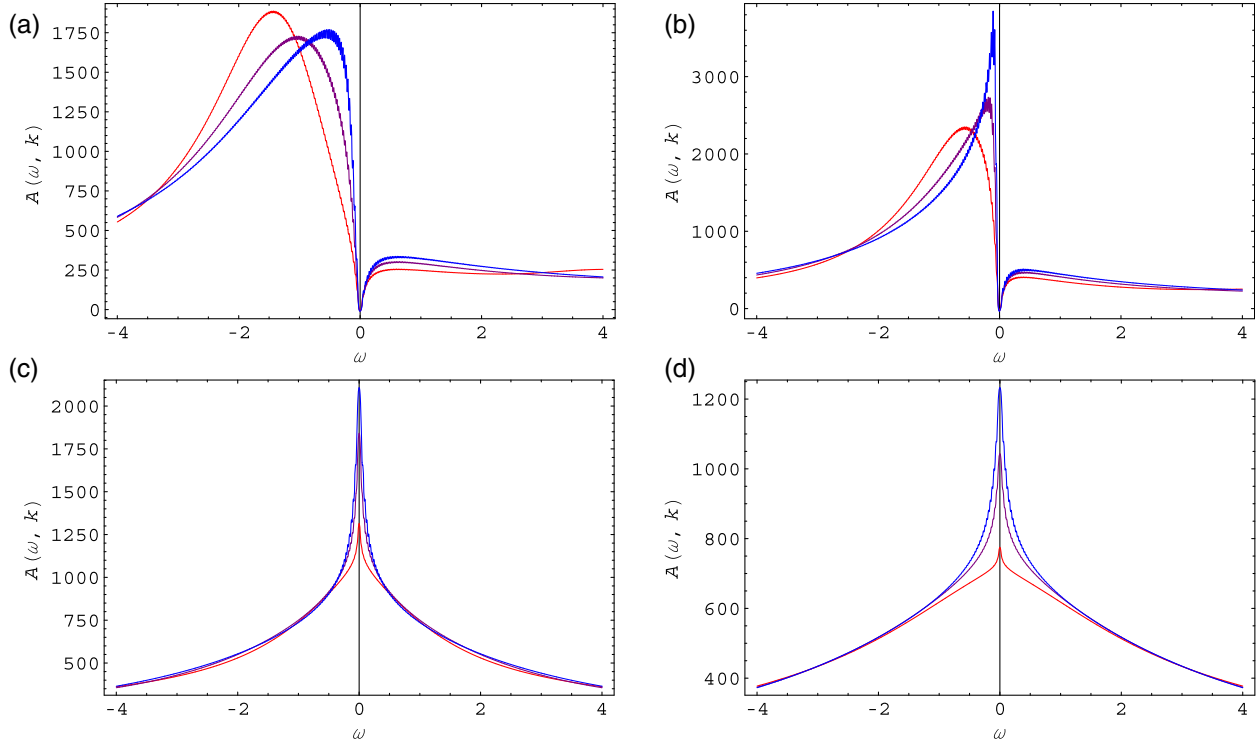


FIG. 13 (color online). The spectral function $A(\omega, \lambda)$ for $\Delta = 0.2$, $h = 0.9, 1.11, 1.3, 1.5$ [(a), (b), (c), (d)] and three momentum values around k_F^{eff} . At $h < h_*$ [(a), (b)] we see that $\nu^2 < 0$, corresponding to zero weight at $\omega \approx 0$, the phenomenon we have dubbed the pseudogap. For $h > h_*$ [(c), (d)] we enter the quasiconformal regime, with no Fermi surfaces left, the conformality being only slightly broken by nonzero Δ .

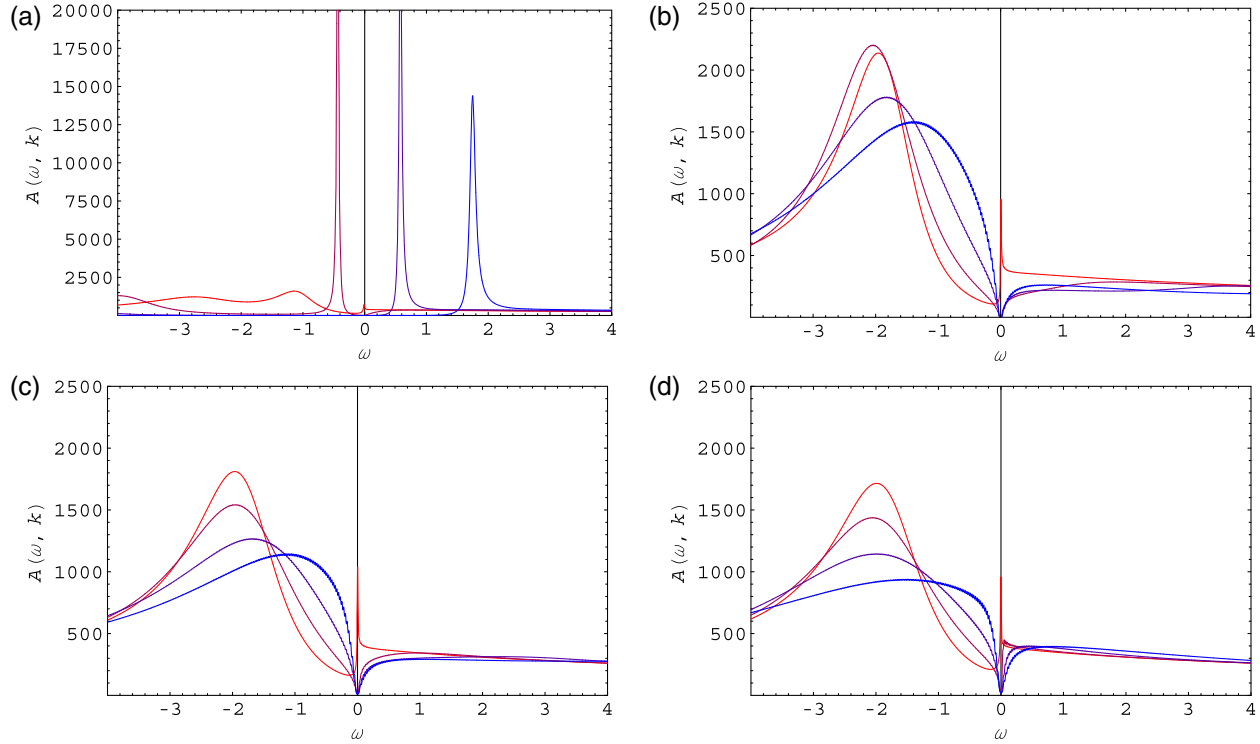


FIG. 14 (color online). The spectral function $A(\omega, \lambda)$ for $h = 0.2$, $\Delta = 0.9, 1.11, 1.3, 1.5$ [(a), (b), (c), (d)] and four momentum values around k_F^{eff} . At $\Delta < \Delta_c \approx 0.2$ (a), the quasiparticle peak survives; for higher Δ the influence of the exact value of the pairing term is negligible, and the spectrum always shows the pseudogap behavior.

the spectral weight from the vicinity of $\omega = 0$. It thus resembles a gap even though it is, strictly speaking, not a gap since the poles in ψ_1 and ψ_2 do not coincide (see also Ref. [29]). Nevertheless, we expect the size of the zero-weight region to be a useful benchmark for the degree to which the pairing eats up the (non-)Fermi liquid quasiparticles.

The typical appearance of the spectrum is given in Fig. 13, where we plot the spectra for $\Delta = 0.2$ and for increasing magnetic field values. Increasing the magnetic field leads to destabilization of the quasiparticle [panels (a) and (b)], leading to a gap-like behavior, and destabilization of the quasiparticle as seen from the asymmetry of the peak which loses its Fermi-liquid-like scaling. Eventually [panels (c) and (d)] the effective chemical potential is so low that we enter the “almost conformal” regime. Figure 14 shows the dependence on the pairing coupling: the peak at $\omega = 0$ turns into a dip, a “pseudogap” develops and we lose the quasiparticle.

V. DISCUSSION AND CONCLUSIONS

Before concluding the paper, we will discuss possible universal aspects of our findings, and show that the formation and enhancement of the particle-hole condensate in a strong magnetic field is a robust phenomenon seen in a number of distinct systems. We will limit ourselves to short remarks only, as more detailed comparisons with earlier work can be made by consulting the appropriate references.

We found the exciton instability using a Dirac hair or bilinear approach. A Dirac hair method uses bilinear combinations where a bilinear in a given channel develops an expectation value at the UV boundary provided a source is switched off. Dirac hair is equivalent to a Tamm-Dancoff approximation; planar diagrams of processes $2 \rightarrow 2$ are included with no bulk fermion loops. In this sense, Dirac hair is a quantum-mechanical treatment with one single classical wave function. It is quite remarkable to see that the condensate develops on a “classical” level due to a non-trivial nature of the curved space-time with the help of the AdS/CFT dictionary, a phenomenon that was first obtained as a holographic superconductor [5].

We have associated the rising critical temperature vs magnetic field with the magnetic catalysis (MC), and the decreasing T_c vs h with the inverse MC (anomalous and normal branches in Fig. 5 for $G_c^* < G < G_c^{**}$, respectively). We adopted the terminology from Ref. [34]. It corresponds to a double-valued regime in the phase diagram (Fig. 6). Similar behavior of increasing T_c vs the scalar mass m has been observed in Ref. [32] under the action of a double-trace deformation, for the alternative quantization starting at the critical mass $m^2 R^2 \geq -\frac{27}{16}$. There it was associated with the formation of a new condensed phase corresponding to the high-temperature regime. However, it was suggested that the high- T condensed phase is thermodynamically unstable [32].

Likewise, in Ref. [38], exploring the phase diagram for a nonrelativistic conformal field theory, the authors found the high-temperature condensate for $T \geq T_H$. The similarity of the dependences $\langle O \rangle(T)$ at different chemical potentials μ and $T_c(h)$ at different couplings G to our Fig. 5 is obvious. In that work, the high-temperature condensate was related to the high-temperature instability predicted by Cremonesi *et al.* [39], and it was found to be thermodynamically disfavored over the trivial vacuum by direct calculation of the difference in the free energies [38]. However, the particle-hole condensate found at high magnetic fields in our case is crucially different from the unstable high-temperature condensate in Refs. [32,38]. Though naively both the magnetic field h and the fermion mass m destroy the condensate, increasing m^2 (or h) drives the bulk system to the UV (or the IR). Indeed, from the radial profile of the wave functions at large m the system resides near the UV boundary and at strong h it resides near the RN black hole horizon in the IR (Fig. 5 in Ref. [15]). Therefore, from a holographic viewpoint large magnetic fields can lead to low-energy behavior and possible quantum critical phenomena, involving different ordering in the system. The main argument in favor of robustness and stability of our high- h condensate is provided by the magnetic catalysis effect. In strong magnetic fields only the lowest Landau level contributes significantly to the ground state. Therefore, the dynamics is effectively dimensionally reduced as $d \rightarrow d - 2$. In field theory this dimensional reduction leads to an increase in the density of states [40] or in QCD to one-gluon exchange with a linear binding potential [41], with both effects working towards pairing and enhancement of the condensate. In the AdS space, dimensional reduction leads to a Schwinger model showing an instability which is very similar to the Bardeen-Cooper-Schrieffer (BCS) pairing instability, where also the dynamics is effectively one dimensional at the Fermi surface. The exact mapping between the magnetic catalysis at $h \neq 0$ and the BCS Cooper pairing at $\mu \neq 0$ has been established in Ref. [40].

We obtained a nontrivial radial profile and a boundary VEV for the bulk excitonic condensate $\langle \bar{\psi} \Gamma \psi \rangle$ at vanishing source, with the relation

$$\begin{aligned} \langle \bar{\psi}_1 \psi_1 \rangle &= \frac{1}{2} \langle \bar{\psi} \psi \rangle - \frac{1}{2} \langle \bar{\psi} \Gamma \psi \rangle, \\ \langle \bar{\psi}_2 \psi_2 \rangle &= \frac{1}{2} \langle \bar{\psi} \psi \rangle + \frac{1}{2} \langle \bar{\psi} \Gamma \psi \rangle, \end{aligned} \quad (119)$$

where $\Gamma = i\Gamma^2\Gamma^5$ and $\psi_{1,2} = \frac{1}{2}(1 \mp \Gamma)\psi$ are the eigenvalues of the Dirac operator (13) [the projectors $\Pi_{1,2} = \frac{1}{2}(1 \mp \Gamma)$ are constructed out of gamma matrices which enter the Dirac operator only [14]]. We need to find the boundary condensate whose gravity dual is $\langle \bar{\psi} \Gamma \psi \rangle$ where the bulk Dirac field ψ corresponds to a fermionic operator Ψ , $\psi \rightarrow \Psi$. The AdS/CFT correspondence does not provide

a straightforward way to match a double-trace condensate to a boundary operator, though only gravity dual single-trace fields are easy to identify with the operators at the boundary. For example, in holographic superconductors a superconducting condensate is modeled by a charged scalar field $\langle\Phi\rangle$ (see e.g. Ref. [31]). As in Ref. [30], we find a boundary operator by matching discrete symmetries on the gravity and field theory sides and considering the asymptotic behavior of the gravity dual condensate at the boundary. As a result we associate a gravity dual excitonic order to some sort of a chiral condensate

$$\langle\bar{\psi}\Gamma\psi\rangle\leftrightarrow\bar{\Psi}\Psi\quad(120)$$

or some combination of condensates which break chiral symmetry. In Ref. [30], this strategy provided the correspondence $\langle\bar{\psi}\Gamma^5\psi\rangle\leftrightarrow\bar{\Psi}\Psi$. There an explicit use of the chiral basis $\psi_{L,R}=\frac{1}{2}(1\mp\Gamma^5)\psi$ and the relation $\bar{\psi}_L\psi_R=\frac{1}{2}\langle\bar{\psi}\psi\rangle+\frac{1}{2}\langle\bar{\psi}\Gamma^5\psi\rangle$ made the correspondence evident. Specifically, by matching symmetries with respect to the discrete transformations (39) we find that $\langle\bar{\psi}\Gamma\psi\rangle$ and $\langle\bar{\Psi}\Psi\rangle$ are pseudoscalars under parity and are unaffected by the charge conjugation; therefore they both spontaneously break the combination $\hat{C}\hat{P}$ symmetry. This finding is consistent with the existence of the parity-odd mass in graphene associated with the excitonic order parameter in the $2+1$ -dimensional effective field theory of graphene [22,42]. Also the asymptotic behavior of the bulk condensate at the boundary, which was found numerically (Fig. 10) to be $\langle\bar{\psi}\Gamma\psi\rangle\rightarrow C/r^3$ as $r\rightarrow\infty$, allows us to use a standard AdS/CFT dictionary to identify C as the response or VEV of the boundary operator. The third power in the decay exponent indicates an extra mass scale. Indeed provided the response $\langle\Phi\rangle\sim 1/r^3$, the gauge-gravity duality gives a strong coupling form of the magnetic catalysis in $2+1$ dimensions [30]:

$$\langle\bar{\Psi}\Psi\rangle\sim hM_F,\quad(121)$$

with the magnetic field h and mass gap M_F [30]. It can be compared to the weak coupling field theory result $\langle\bar{\Psi}\Psi\rangle\sim h$ (we absorbed dimensional electric charge in the definition of magnetic field h , i.e. in $2+1$ dimensions the operator dimension is given by $[e]=\frac{1}{2}$ and $[h]=\frac{3}{2}$ with $[eh]=2$ and therefore we substitute $|e|h\rightarrow h$) [22]. Strong coupling realization follows from the anomalous fermion dimension $[\Psi]=\frac{3}{2}$ compared to the weak coupling conformal dimension $[\Psi]=1$ (free value dimension) in $2+1$ -dimensional field theory. An extra fermion mass gap M_F appears as a consequence of the dimensional four-fermion coupling $G_{\text{int}}=1/M_F$ in the bulk or the introduction of the IR cutoff thought of as a hard wall at the radial slice $z_*=1/M$. The authors of Ref. [30] have used the hard wall construction to obtain the strong coupling realization of the magnetic catalysis (121). It is remarkable that the chiral condensate

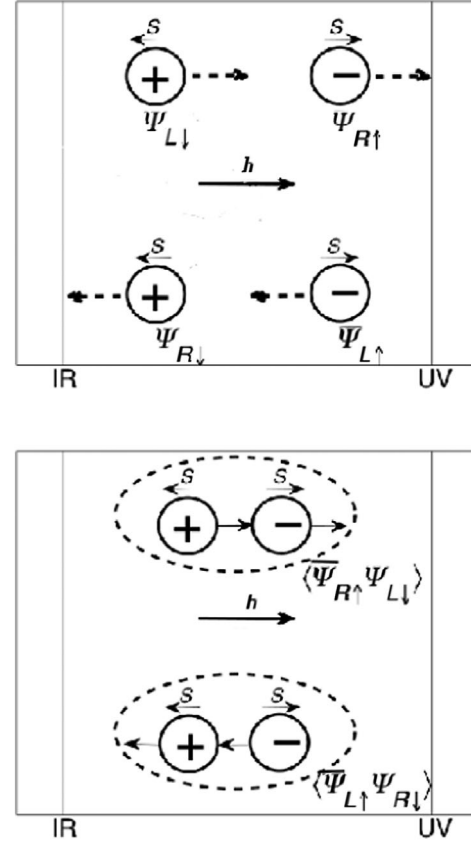


FIG. 15. Formation of the chiral-symmetry-breaking excitonic condensate in the AdS space-time. Individual “bouncing” events are shown schematically by the dashed lines. In an individual event, helicity flips while spin and charge are conserved.

is proportional to the magnetic field even at strong coupling, that manifests the essence of the magnetic catalysis.

Another aspect of the chiral condensate is related to the Callan-Rubakov effect. As found in the field theory and also shown in the context of the gauge-gravity duality [43], the chiral condensate can be spontaneously created in the field of a magnetic monopole. Due to the chiral anomaly $\partial j_5 = F\tilde{F}$, the chiral symmetry is spontaneously broken and the chiral condensate $\langle\bar{\psi}\psi\rangle\sim e^{i\theta}/r^3$ is generated in the field of a monopole. In AdS, a construction involving a monopole wall (more precisely, a dyonic wall) and light fermions in the bulk produces an analog of the Callan-Rubakov effect resulting in the formation of the chiral symmetry breaking (CSB) condensate: $\langle\bar{\psi}\psi\rangle\neq 0$ [43]. The scaling behavior of the condensate is, however, different in our setup: as pointed out before, due to the lowest Landau level (LLL), the dimensional reduction $3d\rightarrow 1d$ takes place in the bulk. This reduces the equation of motion to an effective Schrödinger equation for the condensate, given by Eq. (108) with the potential (109). Solving the equation, we have found the IR behavior of the condensate near the horizon of the RN black hole ($1/r$) to be less divergent than the one near the monopole $\frac{1}{r^3}$ or the monopole wall $\frac{1}{(r-r_w)^3}$ [43].

It turns out that the AdS space with two boundaries—the UV boundary and the IR hard wall—plays an additional role in stabilizing the chiral condensate [30,43]. It also provides an important hint for the interpretation of our current $\bar{\psi}\Gamma\psi$ in the boundary theory. In particular, for the lightest states to condense, we should take the LLL which only has one spin state available (instead of two states available for the higher LLs). This means that for a given charge, the spin direction is fixed. Therefore, fixing the direction of motion and the charge fixes also the helicity. Out of eight possibilities with a given charge, helicity and direction, only four are available for the LLL, as depicted in Fig. 15 (left). The charge \pm denotes e^\pm , positive/negative helicity is denoted by R/L, and S gives the spin orientation; lines with arrows show the momentum direction and h stands for the magnetic field. The following bilinear combinations are possible when only LLLs participate.

- (i) $\langle\bar{\psi}_{R\uparrow}\psi_{R\downarrow}\rangle, \langle\bar{\psi}_{L\uparrow}\psi_{L\downarrow}\rangle$ —(spin) scalar, charge neutral, momentum of the pair $\vec{P} = 0$, chiral symmetry (CS) is not broken.
- (ii) $\langle\bar{\psi}_{R\uparrow}\psi_{L\downarrow}\rangle, \langle\bar{\psi}_{L\uparrow}\psi_{R\downarrow}\rangle$ —(spin) scalar, charge neutral, momentum of the pair $\vec{P} \neq 0$, CS is broken.
- (iii) $\langle\bar{\psi}_{R\uparrow}\bar{\psi}_{L\uparrow}\rangle, \langle\psi_{L\downarrow}\psi_{R\downarrow}\rangle$ —(spin) vector triplet, charged, momentum of the pair $\vec{P} = 0$, CS is broken.

We will not consider the first combination because it does not break the CS, and in our case CS is broken otherwise there would be no preferred scale for the current I_- . As for the third combination, it has been considered in the context of nonzero-density QCD, where it describes the condensate of charged ρ^\pm vector mesons [41]. It cannot be our order parameter either, since our current is a spin singlet. It is tempting to regard the doublet $\Gamma^i\Gamma^5$, $i = 1, 2$ as a vector, and we leave it for a future work.

We are thus left with the second combination. One can think of this order parameter as a spin-density wave, or magnetization which precesses around the direction of the magnetic field. The analog of the second combination has been considered within the Sakai-Sugimoto model as a holographic top-down approach to QCD [34]. The setting of Ref. [34] is very different from ours: it identifies the embedding coordinate of a probe D-brane with a scalar field dual to a single-trace fermion bilinear operator; the magnetic catalysis is modeled as a bending of the probe brane under the influence of the magnetic field. There the anisotropic spatially modulated CSB condensate in the form of a single plane wave Larkin-Ovchinnikov-Fulde-Ferrell (LOFF) state has been found. To have a condensate in the form of the second combination, we need to introduce the $SU(2)$ spin symmetry as in Ref. [32]. We should note the difference with our case where the construction of the condensate is done in the bulk and there is a special effort involved to identify the boundary operator. Provided the condensate of the second form is realized, the AdS boundary and the IR hard wall play a stabilizing role in its formation [43]. As the pair $\langle\bar{\psi}_{R\uparrow}\psi_{L\downarrow}\rangle$ “bounces” from

either of the boundaries it converts into the pair $\langle\bar{\psi}_{L\uparrow}\psi_{R\downarrow}\rangle$ conserving the total charge. This process can be decomposed into elementary “bouncing” events.

- (i) $\bar{\psi}_{R\uparrow} \rightarrow \psi_{R\downarrow}, \psi_{L\downarrow} \rightarrow \bar{\psi}_{L\uparrow}$ —helicity is conserved, spin flips, mixing of charge occurs.
- (ii) $\bar{\psi}_{R\uparrow} \rightarrow \psi_{L\uparrow}, \psi_{L\downarrow} \rightarrow \bar{\psi}_{R\downarrow}$ —helicity flips, spin and charge are unaffected.

In the first case a particle deposits the charge at the boundary, which is picked up by the antiparticle, thus conserving the total charge of the particle-hole pair. The main difference between the two cases is either the “bouncing” event involves a spin flip or not, and therefore either helicity is conserved or broken, respectively. By imposing the AdS boundary condition which breaks CS, helicity gets inverted by the boundary and CS breaking propagates from the boundary into the bulk. Then CS breaking occurs due to the boundary condition before the chiral condensate forms, which affects the propagation of the fields in the bulk in accordance with the second case stabilizing the condensate [30].

Next we discuss an analogy between the MC and the BCS Cooper pairing, and mapping between the Gross-Neveu model (or the Nambu–Jona-Lasinio model) in the presence of the magnetic field and the BCS model at nonzero chemical potential. The reason this mapping works is that effectively the dynamics in both cases is one dimensional: in the strong magnetic field the motion is constrained to Larmor orbits and includes only states from the lowest Landau level, while in a high-density system only states at the Fermi surface contribute to the dynamics. We can draw the following analogy [44]:

MC	BCS
$(3+1)d \rightarrow (1+1)d$	$(1+1)d$
LLL and $\varepsilon=0$ surface	Fermi surface $\varepsilon=\mu$
$\varepsilon = \sqrt{k_z^2 + 2 eh n}$	$\varepsilon = k - k_F, k = \sqrt{k^2}$
excitonic: $\Delta \sim G\langle\bar{\psi}\psi\rangle$	SC: $\Delta \sim G\langle\psi\psi\rangle$
$\Delta \sim \sqrt{eh}\exp(-\frac{\text{const}}{G\nu_0})$	$\Delta \sim \mu\exp(-\frac{\text{const}}{G\nu_F})$
ν_0 is DOS at $\varepsilon=0$	ν_F is DOS at $\varepsilon=\mu$
h enhances, μ destroys Δ	μ enhances, h destroys Δ
$\delta\Omega \sim h\left(\mu^2 - \frac{\Delta^2}{2}\right)$	$\delta\Omega \sim \mu^2\left(\delta\mu^2 - \frac{\Delta^2}{2}\right)$
$h \gg \mu, \Delta$	$\mu \gg \delta\mu, \Delta$
it can have $\mu=0$	it can have $h=0$
T_c grows with h (MC)	T_c decreases with h
T_c decreases with μ	T_c grows with μ (SC)

(122)

Effectively one-dimensional dynamics in both cases leads to similarities in formulas for the pairing gap Δ and the gain in the thermodynamic potential $\delta\Omega$ as compared to the normal unpaired state. In the BCS, the density of states at the Fermi surface $\varepsilon = \mu$ defines the gap Δ , and there is an energy cost $\mu^2\delta\mu^2$ to bring two Fermi surfaces together to

pair in case of nonzero mismatch $\delta\mu$ between them. In MC, the density of states at the $\varepsilon = 0$ surface separating electrons and holes contributes to the gap, and a similar cost in energy $h\mu^2$ exists to involve both particles and holes to pair. The gain from the pairing is proportional to Δ^2 in both cases, and is linear in μ^2 for the BCS and in h for the MC, manifesting the essence of both phenomena. These simple formulas for $\delta\Omega$ can be obtained when there is a hierarchy of scales: the largest scale is μ in the BCS and it is h in the MC.

The comparison given in Eq. (122) provides the following mapping between parameters in the two systems at a nonzero density and at a nonzero magnetic field [40]:

$$\begin{aligned}
 & \text{MC} \longleftrightarrow \text{BCS} \\
 & \langle \bar{\psi}\psi \rangle \neq 0 \longleftrightarrow \langle \psi\psi \rangle \neq 0 \\
 & \text{finite } h \longleftrightarrow \text{finite } \mu \\
 & \text{small } \mu \longleftrightarrow \text{small } \delta\mu \\
 & h \gg \mu \longleftrightarrow \mu \gg \delta\mu
 \end{aligned} \tag{123}$$

where the last line expresses the hierarchy of scales. A similar mapping has been obtained in case of the Gross-Neveu and the BCS models, where the magnetic field h maps to the chemical potential mismatch $\delta\mu$ and is relevant for the inhomogeneous superconductors in the incommensurate phase [45]. Based on Fig. 5 and using the above-described mapping, we can speculate and draw an analogy between the condensed matter phase diagram in T_c vs h and the QCD phase diagram in T_c vs μ , as depicted in Fig. 16. The high-magnetic-field phase is mapped to the color superconductor state at very large densities [for example color-flavor-locked (CFL)] in QCD, while weak magnetic fields which do not destroy superconductivity are mapped to the chirality-broken phase in QCD. The robust feature of the phase diagram in Fig. 5 is the existence of two regions, with small and large h where the condensate is destroyed and enhanced, respectively, by the magnetic field. We found numerically that both branches are thermodynamically favored compared to the normal states, as can be seen in Fig. 1. In the Sakai-Sugimoto model [34], analytical formulas for the free energy difference between condensed and normal states have been obtained, proving the stability of both condensed states. The strong- h regime (“direct” magnetic catalyses) has a remarkably simple form [34]

$$\delta\Omega \sim -h \left(\frac{\Delta(h)^2}{2} - \mu^2 \right), \tag{124}$$

which is exactly the result obtained in the field theory (122); compare also with Fig. 1. The condition for a thermodynamically stable ordered phase with the excitonic condensate is given by

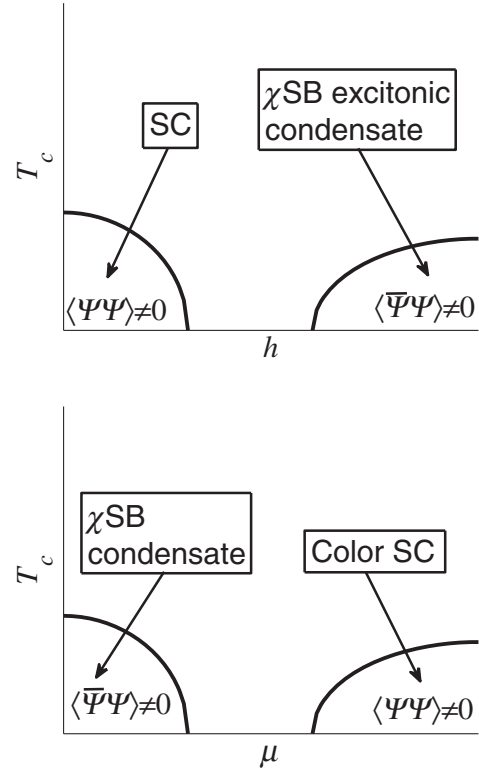


FIG. 16. Analogy between the phase diagram of a condensed matter system at nonzero magnetic field and the QCD phase diagram at nonzero density. In strong magnetic fields, the excitonic condensate is mapped to the asymptotic regime of high-chemical-potential QCD with the color superconductor phase.

$$\mu \leq \frac{\Delta(h)}{\sqrt{2}}, \tag{125}$$

which according to the mapping (123) coincides with the familiar Clogston limit in the SC: $\delta\mu \leq \frac{\Delta}{\sqrt{2}}$. However, there is an important difference between the formation of the excitonic and superconducting condensates. In MC the excitonic condensate $\Delta(h)$ is a growing function with h [Fig. 3(a)] which ensures that Eq. (124) is always satisfied at high enough magnetic fields. This finding is important, since it demonstrates the robustness of the chiral condensate.

Though MC and BCS both have one-dimensional dynamics, the mapping between the two models may come as a surprise. Indeed properties of both systems (one is a magnetic and the other is a dense medium) including the symmetry-breaking pattern when a condensate forms are quite different. However, we speculate that these two systems can be unified on the gravity side using the duality between electric and magnetic fields. In the gravity dual description the two phenomena can be represented as follows:

HolographicMC	HolographicSC
dyonic AdSRNBH, SchwarzschildBH $ H > Q $ it can be $Q=0$ Z_2 (chiral SB) broken magnetic field enhances it electric field destroys it	AdSRNBH $ Q > H $ it can be $H=0$ $U(1)$ broken magnetic field destroys it electric field enhances it
Callan – Rubakov effect	dual Callan – Rubakov effect

(126)

which shows the electromagnetic duality [the invariance under an interchange of the electric and magnetic charges of the black hole $(|Q|, |H|) \rightarrow (|H|, |Q|)$]. The motivation for this duality is a similarity in the expressions for the gap and the energy gain of the ordered phase between two systems as given by Eq. (122). Probably the underlying reason for the duality is a symmetry of how both charges of the black hole enter in the red shift factor. They always enter in combination $Q^2 + H^2$, which defines also the Hawking temperature of the black hole or the temperature of the system $T \sim r_0(1 - \frac{Q^2 + H^2}{3r_0^2})$ with r_0 is the radius of the horizon of the BH. Similarly, according to the Montonen-Olive conjecture, the spectrum in the Georgi-Glashow model is invariant under the electromagnetic Z_2 duality $(g, g) \rightarrow (g, -g)$ as a consequence of the fact that the Bogomol'nyi bound is invariant under electromagnetic duality (the Bogomol'nyi bound for the mass of the 't Hooft-Polyakov monopole is $M \geq a\sqrt{q^2 + g^2}$), and the spectrum of the Georgi-Glashow model saturates this bound [46]. Notably, the mass of the black hole

$$M = r_0^3 + \frac{Q^2 + H^2}{r_0} \quad (127)$$

is also invariant under the electromagnetic duality. The electromagnetic duality (126) holds on a classical level and is destroyed by quantum corrections. It stays intact for the supersymmetric theories though.

In this work a four-fermi interaction has been used as a control parameter to go from one regime mimicking the SC to the other one of MC. The robustness of both regimes can be seen in a symmetric form of the dependence T_c vs h (top of Fig. 16). In the application to nonzero-density QCD, this means that at strong enough magnetic fields the chiral symmetry is spontaneously broken by a chiral condensate. Moreover, due to a dimensional reduction QCD as well as plain QED are in the confined regime even on the perturbative level: they can be reduced to a Schwinger model where one-gluon (one-photon) exchange in one dimension leads to a linear rising potential in the configuration space (a similar argument provides confinement

along the boost direction for theories in the light-front quantization). Evidence of the QED confinement in a strong magnetic field can be provided by the existence of a $2e$ bound state which contributes to the fractional quantum Hall effect [47]. Summarizing, quark-gluon plasma (QGP) at strong magnetic fields is probably confined and has a broken chiral symmetry, as opposed to QGP at zero magnetic fields which is in a deconfined and chiral-symmetry-invariant phase. This finding might have some implications for the chiral magnetic effect in heavy-ion collisions at the RHIC [48].

A general note is that the low-energy behavior of the non-Fermi liquids is governed by a nontrivial IR fixed point which arises from the near-horizon region with AdS_2 geometry [14]. This IR fixed point arises as a consequence of the interplay between the emergent quantum critical bosonic modes and the fermions at finite density. In other words, the class of systems studied is both metallic and quantum critical at low energies. On the gravity side, this is reflected by the instability of the background (Reissner-Nordstrom black hole in the AdS space) unless order parameter fields are introduced to stabilize it [7].

We have explored the quantum critical aspects of the system by using the magnetic field as a knob to tune the system to a quantum critical point. Indeed, the magnetic field as an external parameter driving the system to quantum criticality is used in experiments on heavy fermions and graphene. We have shown that by increasing the magnetic field, the system evolves from the normal metallic to a quantum critical phase, where the stable quasiparticle is destroyed. The quantum critical point is controlled by the IR fixed point with the scaling dimension $\nu = \frac{1}{2}$, where the Fermi velocity vanishes $v_F = 0$ (see Fig. 10 in Ref. [15]) but the Fermi momentum stays finite $k_F \neq 0$ (see Fig. 9 in Ref. [15]). It is important that we are able to deduce the position of the quantum critical point from our calculations. The phase transition can be understood as the formation of a semiclassical condensate on the gravity side near the AdS_4 boundary. Using the bilinear formalism developed in Ref. [6], we have also calculated the thermodynamic parameters of both phases. We found that the particle-hole pairing instability arises for both $\nu > \frac{1}{2}$ corresponding to $h < h_c$ and $\nu < \frac{1}{2}$ corresponding to $h > h_c$. In a holographic superconductor, a superconducting instability has been shown to exist only for $\nu > \frac{1}{2}$ [27]. This shows the remarkable difference in nature between superconducting and excitonic instabilities: existence of excitonic condensate beyond the critical point $\nu = \frac{1}{2}$ is a quantum critical phenomenon. The magnetic field acts as a catalyzer of the particle-hole pairing because of the dimensional reduction $d \rightarrow d - 2$ in the magnetic field [22].

Other thermodynamic and transport quantities including the heat capacity and DC conductivity are calculated for both normal- and anomalous-paired phases in Appendix B.

The results support our findings obtained from the bilinear holographic approach on the nature and scaling behavior of the two phases.

The critical temperature of the normal-paired phase transition follows the expected behavior for $h < h_c$: the critical temperature T_c decreases with increasing h , with the scaling $T_c \propto \mu \exp(-C/\sqrt{q(h_c - h)})$. At $h > h_c$, however, we find anomalous behavior: T_c grows with increasing h . To the best of our knowledge, this is the first example of non-mean field scaling from an AdS₄ holographic model. Mathematically, it follows from the fact that, for $\nu < \frac{1}{2}$, we have the scaling $T_c \sim \delta^{2\nu-1}$ with δ small and decreasing. Physically, such behavior is consistent with the fact that the system is driven through the quantum critical point at h_c where $T_c = 0$, and beyond the quantum critical point at $h > h_c$ it can be characterized as a quantum critical metal possessing new properties. In the existing literature, a novel antiferromagnetic behavior has been predicted for heavy fermions driven through the quantum critical point [3]. Such an anomalous behavior for T_c vs h has been seen in experiments on highly oriented pyrolytic graphite at strong magnetic fields $h > h_c$ [21]. Furthermore, the anomalous branch matches the properties of excitons in bilayer interfaces and cold atom realizations [49], and can further be related to the behavior of chiral condensates in holographic QCD models, signaling the universal significance of the twofold normal-anomalous regime in the phase diagram.

ACKNOWLEDGMENTS

We thank Gerald Dunne, Tom Faulkner, Daniel Fernandez-Fraile, Tom Hartman, Sean Hartnoll, Nabil Iqbal, Dima Kharzeev, Alex Kovner, Hong Liu, John McGreevy, Mark Mezei, Piero Nicolini, Andrei Parnachev, Rob Pisarski, Andreas Schmitt and Igor Shovkovy for helpful inputs and discussions. We also thank Dirk Rischke and Francesco Giacosa for reading the manuscript and valuable corrections and suggestions. As our paper was close to completion, we learned of a similar work done by Stefano Bolognesi and David Tong, which is now published in Ref. [30]: we are very grateful to the authors for sharing their results and illuminating discussions. The work was supported in part by the Alliance program of the Helmholtz Association, Contract No. HA216/EMMI ‘‘Extremes of Density and Temperature: Cosmic Matter in the Laboratory’’ and by ITP of Goethe University, Frankfurt (E. G.).

APPENDIX A: BULK GREEN’S FUNCTION AND ZERO MODES

We express the bulk Green’s function through the boundary one as in Ref. [27]. The bulk Green’s function is a solution of the free Dirac equation,

$$\hat{D}(\Omega, k_l) \mathcal{G}^R(z, z', \Omega, k_l) = \frac{1}{\sqrt{-g}} i\delta(z, z'), \quad (\text{A1})$$

with the free radial Dirac operator $\hat{D}(\Omega, k) = \Gamma^i D_i$, which includes the mass term, chemical potential and the magnetic field but has zero gap, $\Delta = 0$, i.e. the equation (15). The bulk Green’s function is constructed from the modes $\psi(z)$ which are solutions of the free Dirac equation

$$\hat{D}(\Omega, k_l) \psi_{\text{radial}}(z) = 0. \quad (\text{A2})$$

Due to the choice of the Dirac matrices in Eq. (11), ψ decouples into two-component spinors, $\psi_{\text{radial}} = (\psi_1, \psi_2)^T$. Therefore the bulk retarded Green’s function has a block-diagonal form:

$$\mathcal{G}^R(z, z', \Omega, k_l) = \begin{pmatrix} \mathcal{G}_1^R & 0 \\ 0 & \mathcal{G}_2^R \end{pmatrix}, \quad (\text{A3})$$

where the components \mathcal{G}_α , $\alpha = 1, 2$ are constructed from the solutions to the Dirac equation [27]

$$\mathcal{G}_\alpha^R(z, z', \Omega, k_l) = \frac{i}{W(\psi_\alpha^{\text{in}}, \psi_\alpha^{\text{bdy}})} \times \begin{cases} \psi_\alpha^{\text{in}}(z) \bar{\psi}_\alpha^{\text{bdy}}(z') z < z', \\ \psi_\alpha^{\text{bdy}}(z) \bar{\psi}_\alpha^{\text{in}}(z') z > z', \end{cases} \quad (\text{A4})$$

with $\bar{\psi}_\alpha = i\psi_\alpha^\dagger \sigma^1$ and W_α are the components of the Wronskian

$$W(\psi_\alpha^{\text{in}}, \psi_\alpha^{\text{bdy}}) = -\frac{\sqrt{-g}}{2\sqrt{g_{zz}}} (\bar{\psi}_\alpha^{\text{bdy}} \sigma^3 \psi_\alpha^{\text{in}} - \bar{\psi}_\alpha^{\text{in}} \sigma^3 \psi_\alpha^{\text{bdy}}). \quad (\text{A5})$$

The retarded Green’s function (A4) must satisfy the following two conditions. At the boundary ($z, z' \rightarrow 1$) where $\psi_\alpha^{\text{radial}} \sim a_\alpha(1-z)^{3-\Delta_\psi} + b_\alpha(1-z)^{\Delta_\psi} + \dots$ with $\Delta_\psi = \frac{3}{2} + m$ it must be the normalizable solution, i.e. $\psi_\alpha^{\text{bdy}} = b_\alpha(1-z)^{\Delta_\psi} + \dots$. At the horizon ($z, z' \rightarrow 0$) where $\psi_{\text{radial}} \sim A_\alpha z^{-i\omega/4\pi T} + B_\alpha z^{i\omega/4\pi T}$, the retarded propagator corresponds to the ingoing solution $\psi_\alpha^{\text{in}} = z^{-i\omega/4\pi T} A_\alpha$. This infalling solution behaves near the boundary as

$$\psi_\alpha^{\text{in}} \sim a_\alpha(1-z)^{3-\Delta_\psi} + b_\alpha(1-z)^{\Delta_\psi} + \dots \quad (\text{A6})$$

In principle, the coefficients in ψ^{bdy} and ψ^{in} are different, i.e. b^{bdy} and b^{in} (we omit the difference for simplicity). This determines the z -independent Wronskian $W_\alpha = -i\text{Re}(b_\alpha^{\text{bdy}\dagger} \sigma_1 \sigma_3 a_\alpha^{\text{in}})$ after substituting the asymptotic behavior near the AdS boundary. The Wronskian is directly proportional to the spectral function of the dual CFT. The two spinor components of each spinor a_α and b_α are not independent, but are related by the Dirac equation [12,26,50]. Defining up/down spin eigenstates with respect to $\gamma^z = -\sigma^3$,

$$a_\alpha \equiv \begin{pmatrix} a_\uparrow \\ a_\downarrow \end{pmatrix} = \begin{pmatrix} 1 \\ 0 \end{pmatrix}, \quad b_\alpha \equiv \begin{pmatrix} b_\uparrow \\ b_\downarrow \end{pmatrix} = \begin{pmatrix} 0 \\ 1 \end{pmatrix}. \quad (\text{A7})$$

Substituting this into the Wronskian

$$W = -ib_{\alpha\downarrow}^\dagger a_{\alpha\uparrow} \quad (\text{A8})$$

and recalling the expression for the boundary propagator,

$$G_\alpha = \frac{b_{\alpha\downarrow}}{a_{\alpha\uparrow}} \quad (\text{A9})$$

one finds that

$$W(\psi_\alpha^{\text{in}}, \psi_\alpha^{\text{bdy}}) = -i|b_{\alpha\downarrow}|^2 G_\alpha^{-1} = -\frac{i}{G_\alpha}. \quad (\text{A10})$$

The result is similar to the one for fermion transport in Ref. [33].

This expression for the bulk propagator in terms of boundary spectral functions shows us that the contribution to the effective action is dominated by the poles of the boundary Green's function. These poles precisely correspond to the values where $\psi^{\text{in}} \propto \psi^{\text{bdy}} \equiv \psi^0$ is the zero mode with $a_\alpha = 0$.

APPENDIX B: THERMODYNAMICS AND TRANSPORT AT ZERO MAGNETIC FIELD

Quantum critical behavior is associated, among other things, with unusual scaling exponents of the heat capacity and the resistivity with temperature. In this section, we obtain an equation of state and find the scaling behavior of the specific heat and the DC conductivity with temperature. Following a prescription worked out in detail for conductivity [33], we bypass the bulk calculations and do our calculations directly in the boundary field theory making use of the gravity-“dressed” fermion propagators [14]. Since the two-point Green's function is obtained from the AdS/CFT correspondence, it is “exact” in terms of gauge coupling corrections, and the lowest-order diagrams on the field theory side should suffice. However, we lack the knowledge of the gravity-“dressed” gauge-fermion vertex. Nevertheless, for the quantities considered below, the scaling behavior should not change when vertex corrections are taken into account.

1. Single-particle spectral functions and dispersion relations

Using AdS/CFT, one finds that, close to the Fermi surface ($\omega/\mu \ll 1$) and at low temperatures ($T/\omega \ll 1$), the retarded fermion Green's function is given by [14]

$$G_R(\omega, \vec{k}) = \frac{h_1 v_F}{v_F k_\perp - \omega + v_F h_2 e^{i\theta - i\pi\nu_{k_F}} \omega^{2\nu_{k_F}}} + O\left(\frac{\omega}{\mu}\right). \quad (\text{B1})$$

Here $k_\perp = k - k_F$, the last term in the denominator defines the self-energy Σ , h_1 and v_F are real constants obtained from the UV (bulk) physics, h_2 is positive with contributions from both the UV and IR regions, the phase θ is such that the poles of Eq. (B1) are in the bottom frequency half-plane corresponding to stable quasiparticle poles and ν_{k_F} is the IR conformal dimension at the Fermi momentum. At $T = 0$, it is given by (in dimensionless units)

$$\nu_{k_F} = \frac{1}{6} \sqrt{6(m^2 + k_F^2) - \mu_q^2}, \quad (\text{B2})$$

with $\mu_q = \mu q$. The IR conformal dimension ν_{k_F} defines the quasiparticle dispersion. Writing the Green's function pole in Eq. (B1) as $\omega_c(k) = \omega_*(k) - i\Gamma(k)$, at leading order $\omega \sim 0$ we get the following dispersion relations:

$$\omega_* \sim \begin{cases} v_F k_\perp, & \nu_{k_F} > \frac{1}{2}, \\ k_\perp / \ln k_\perp, & \nu_{k_F} = \frac{1}{2}, \\ k_\perp^{1/2\nu_{k_F}}, & \nu_{k_F} < \frac{1}{2}. \end{cases} \quad (\text{B3})$$

For $\nu_{k_F} = 1/2$, the leading-order coefficients in front of ω and $\omega^{2\nu_{k_F}}$ diverge and cancel exactly, leaving the subleading logarithmic dependence $\tilde{c}_1 \omega \ln \omega$ where \tilde{c}_1 is a real constant.⁶ As ν_{k_F} is decreased we move from a metal (Fermi liquid) at $\nu > 1/2$ to a marginal metal at $\nu = 1/2$ to a quantum critical metal (non-Fermi liquid) at $\nu_{k_F} < 1/2$, and the dispersion Eq. (B3) becomes softer. This has consequences for the behavior of thermodynamic properties, e.g. the heat capacity.

The imaginary part of the self-energy $\Sigma \sim \omega^{2\nu_{k_F}}$ gives rise to the following width of the quasiparticle dispersion:

$$\Gamma \sim \begin{cases} k_\perp^{2\nu_{k_F}}, & \nu_{k_F} > \frac{1}{2}, \\ k_\perp / \ln k_\perp, & \nu_{k_F} = \frac{1}{2}, \\ k_\perp^{1/2\nu_{k_F}}, & \nu_{k_F} < \frac{1}{2}. \end{cases} \quad (\text{B4})$$

Comparing Eqs. (B3) and (B4), we see that the pole represents a stable quasiparticle only for $\nu_{k_F} > 1/2$ when the width is much smaller than the real part: $\Gamma/\omega_* \ll 1$, while a coherent quasiparticle is replaced by an unstable pole for $\nu_{k_F} \leq 1/2$ where $\Gamma/\omega_* = \text{const}$. The imaginary part of the self-energy becomes important for the behavior of transport coefficients, e.g. conductivity, where the dissipation processes play the key role.

⁶The logarithmic dependence for the real part of the self-energy defines the dispersion for $\nu_{k_F} = \frac{n}{2}$, $n \in \mathbb{Z}_+$. Therefore, the linear spectrum is valid for $\nu_{k_F} \neq \frac{n}{2}$.

We rewrite Eq. (B1) as

$$G_R(\omega, \vec{k}) = \frac{h_1 v_F}{v_F k_\perp - \omega + \Sigma(\omega, k_F)}, \quad (\text{B5})$$

with the self-energy $\Sigma = \Sigma_1 + i\Sigma_2$. Therefore the spectral function defined as $A(\omega, \vec{k}) = \frac{1}{\pi} \text{Im}G_R(\omega, \vec{k})$ is given by

$$A(\omega, \vec{k}) = \frac{1}{\pi} \frac{h_1 v_F \Sigma_2(\omega, k_F)}{(\omega - v_F k_\perp + \Sigma_1(\omega, k_F))^2 + \Sigma_2(\omega, k_F)^2}. \quad (\text{B6})$$

From the above form we can directly read off the structure: a sharp quasiparticle near $k = k_F$ and $\omega = 0$ goes through the infrared scaling region for $\omega/T < 1$ and eventually asymptotes to the universal conformal scaling in the UV, i.e. for $\omega, k \gg 1$.

2. Equation of state and specific heat

Having established the formal structure of the single-particle propagator, we can use it to construct the Landau-Ginzburg action for our system. An effective potential in the CJT formalism is given by [51]

$$\Gamma_{\text{eff}} = \frac{1}{2} \text{Tr} \ln S^{-1} + \frac{1}{2} \text{Tr}(S_0^{-1} S - 1) + \Gamma_2[S], \quad (\text{B7})$$

where S is a dressed fermion propagator, Γ_2 is the sum of all two-particle irreducible diagrams, and the trace Tr involves also the summation over the Matsubara frequencies and the integration $\int d^2x$. The last two terms can be simplified with the help of the Dyson-Schwinger equation, to give

$$\Gamma_{\text{eff}} = \frac{1}{2} \text{Tr} \ln S^{-1} - \frac{1}{4} \text{Tr}(\Sigma S), \quad (\text{B8})$$

where the self-energy is $\Sigma = S^{-1} - S_0^{-1}$.

The fact that we have a finite quasiparticle width, encoding for inelastic/dissipative processes, allows us to calculate the transport coefficients, which would otherwise be infinite. However, the imaginary part of the self-energy gives rise to a branch cut in the fermion propagator along $\text{Im}\omega = 0$ in a complex ω plane [52–55]. In the calculation of the Matsubara sum we should take into account the contributions from poles and from the discontinuities along the branch cuts [54,55]:

$$T \sum_{\text{odd } m} F(i\omega_m) = \sum_{\text{poles}} n(z_i) \text{Res}(F, z = z_i) - \sum_{\text{cuts}} \int_{-\infty}^{\infty} \frac{d\zeta}{2\pi i} n(\zeta) \text{Disc } F, \quad (\text{B9})$$

with the analytical continuation $i\omega_m \rightarrow z$, and the Fermi distribution function $n(x)$. In the contour integral one can

use either $n(x) \equiv n(\frac{x}{T})$ or $\tanh(\frac{x}{2T})$ functions with prefactors $(-\frac{1}{2\pi i})$ and $(-\frac{1}{4\pi i})$ respectively, as both give the same result for the observables. The calculation of Matsubara sums using a perturbative expansion in the imaginary part of the self-energy has been developed in Ref. [56].

For simplicity we will take $h_1 v_F \rightarrow -1$ which will not change our results qualitatively. Using the retarded fermion propagator, an effective potential is found to be

$$\Gamma_{\text{eff}} \rightarrow -\frac{1}{4\pi i} \frac{V_2}{T} \int \frac{d^2k}{(2\pi)^2} \int_C dz \tanh \frac{z}{2T} \times T \left(\frac{1}{2} \ln \frac{z - v_F k_\perp + \Sigma(z, k_F)}{T} - \frac{1}{4z - v_F k_\perp + \Sigma(z, k_F)} \right), \quad (\text{B10})$$

where we have substituted the Matsubara sum by the contour integral. The original contour C_0 going around the poles along the imaginary z axis was deformed into the contour C going along the real z axis and then along the arcs at infinity with vanishing contribution, denoted by Γ [54]. In the case of a pure real self-energy the result for the contour integration is (see Ref. [52])

$$\Gamma_{\text{eff}} \rightarrow \frac{V_2}{T} \int \frac{d^2k}{(2\pi)^2} \sum_{z_*} \left(\frac{1}{2} T \ln \left(2 \cosh \frac{z_*}{2T} \right) + \frac{1}{4} \Sigma(z_*) \tanh \frac{z_*}{2T} \right), \quad (\text{B11})$$

where z_* are the poles of the retarded propagator, and the sum over all allowed poles is taken. As was shown in Ref. [52], when the self-energy and hence the poles include an imaginary part, the following substitution of hyperbolic functions with Γ functions should be made [57]:

$$\left| \Gamma \left(\frac{1}{2} + iz \right) \right|^2 = \frac{\pi}{\cosh(\pi z)}, \quad |\Gamma(iz)|^2 = \frac{\pi}{z \sinh(\pi z)}. \quad (\text{B12})$$

We can now use Γ_{eff} to compute all thermodynamic quantities, using the relations

$$p = \frac{T}{V_2} \Gamma_{\text{eff}}, \quad s = \frac{\partial p}{\partial T}, \quad c = T \frac{\partial s}{\partial T}, \quad n = \frac{\partial p}{\partial \mu}, \quad (\text{B13})$$

where the role of μ is played by k_F , and we get the equation of state

$$p = \int \frac{d^2k}{(2\pi)^2} \sum_{z_*} \left(-\frac{1}{2} T \ln \left(\frac{1}{2\pi} \left| \Gamma \left(\frac{iz_*}{2\pi T} + \frac{1}{2} \right) \right|^2 \right) \right. \\ \left. + \frac{1}{4} \frac{\Sigma(z_*) \left| \Gamma \left(\frac{iz_*}{2\pi T} + \frac{1}{2} \right) \right|^2}{\frac{|z_*|}{2\pi T} \left| \Gamma \left(\frac{iz_*}{2\pi T} \right) \right|^2} \right), \quad (\text{B14})$$

where the summation over complex poles z_* is performed. We only take into account the contribution of the pole closest to $\omega = 0$, with the imaginary part of the self-energy scaling as $\Sigma(z) \sim z^{2\nu}$. Near the Fermi surface, the one-loop contribution dominates over the self-energy term for Fermi liquids $\nu > \frac{1}{2}$, while the self-energy becomes leading for non-Fermi liquids $\nu < \frac{1}{2}$.

What we are truly interested in are the temperature scaling relations for these quantities, in particular for the specific heat c . The first term in Eq. (B14) gives the following contributions to c :

$$\sim \frac{1}{T^2} \int \frac{d^2k}{(2\pi)^2} \text{Re} \left(z_*^2 \Psi' \left(\frac{iz_*}{2\pi T} + \frac{1}{2} \right) + z_*^2 \Psi' \left(-\frac{iz_*^*}{2\pi T} + \frac{1}{2} \right) \right), \\ \times \frac{1}{T^2} \int \frac{d^2k}{(2\pi)^2} \text{Re} \left(\sim z_* T \Psi \left(\frac{iz_*}{2\pi T} + \frac{1}{2} \right); \right. \\ \left. \sim z_*^* T \Psi \left(\frac{-iz_*^*}{2\pi T} + \frac{1}{2} \right) \right) \quad (\text{B15})$$

where $\Psi'(x) = \frac{d\Psi}{dx} = \frac{d^2 \ln \Gamma}{dx^2}$. The second term gives the following contribution:

$$\frac{1}{T^2} \int \frac{d^2k}{(2\pi)^2} \text{Re} \left(\sim T \Sigma(z_*) F[\Gamma]; \right. \\ \left. \sim z_* \Sigma(z_*) F[\Gamma]; \sim \frac{z_*^2 \Sigma(z_*)}{T} F[\Gamma] \right), \quad (\text{B16})$$

where $F[\Gamma]$ denotes a combination of Γ functions and their first and second derivatives. Here, the momentum integration is performed around the Fermi surface, $d^2k \rightarrow k_F dk_\perp$ with $k_\perp = k - k_F$, the poles $z_* = \omega_c - i\Gamma$ are given by Eqs. (B3) and (B4) for the three cases of interest, and $\Sigma(z) \sim z^{2\nu}$.

For a Fermi liquid, one has $\nu > \frac{1}{2}$ and $z_\perp \sim k_\perp$ (the real part is dominant). The first term then gives $\frac{1}{T^2} \int dk_\perp z_*^2 \rightarrow T$ and the same behavior from the other combination, while in the second term we have $\Sigma \sim k_\perp^{2\nu}$. Therefore, the second term gives $\frac{1}{T^2} \int dk_\perp \Sigma(z_*) z_* \rightarrow T^{2\nu}$ and the same behavior for the other two combinations.⁷ Thus for a Fermi liquid at low temperatures we have

$$c \sim T. \quad (\text{B17})$$

⁷This is related to the fact that in Eq. (B14) for the effective action the one-loop term dominates over the self-energy for $\nu > \frac{1}{2}$.

We thus reproduce the linear temperature dependence of the heat capacity known for Fermi liquids.

For a non-Fermi liquid, we have instead $\nu < \frac{1}{2}$ and $z_\perp \sim k_\perp^{\frac{1}{2\nu}}$ (for both real and imaginary parts). The first term gives $\frac{1}{T^2} \int dk_\perp k_\perp^{\frac{1}{2\nu}} \rightarrow T^{\frac{1}{2\nu}-1}$ and $\frac{1}{T^2} \int dk_\perp k_\perp^{\frac{1}{2\nu}} T \rightarrow T^{\frac{1}{2\nu}}$. The second term gives $\frac{1}{T^2} \int dk_\perp \Sigma(z_*) T \rightarrow T^{2\nu}$ and subleading behavior for the other two combinations. For $\nu < \frac{1}{2}$, the self-energy dominates over the one-loop contributions in the pressure and at low temperatures we have

$$c \sim T^{2\nu}. \quad (\text{B18})$$

This result for the heat capacity reflects the scaling behavior of the self-energy. Finally, for $\nu = \frac{1}{2}$, all the terms are $\sim T$, so for the marginal liquids we have $c \sim T$. One can understand it physically from the dispersion relation (B3). As the dispersion becomes softer, the number of states per energy interval increases, and thus the heat capacity increases as well:

$$c_{\text{qcm}} > c_{\text{m}}, \quad (\text{B19})$$

where ‘‘m’’ stands for the normal metal and ‘‘qcm’’ for the quantum critical metal.

It is illustrative to repeat the derivation of the equation of state using the spectral function as given in Eq. (B6). The density of states can be written through a spectral function as follows:

$$n = T \sum_m \int \frac{d^2k}{(2\pi)^2} A(i\omega_m, \vec{k}) \\ \rightarrow -\frac{1}{4\pi i} \int \frac{d^2k}{(2\pi)^2} \int_C dz A(z, \vec{k}) f(z), \quad (\text{B20})$$

where $f(z) = \tanh(\frac{z}{2T})$. One can also use the Fermi distribution function $f(z) = n(z)$ with a prefactor $(-\frac{1}{2\pi i})$, which gives the same result for the observables. The pressure is given by

$$p = \int_{-\infty}^{\mu} d\mu' n, \quad (\text{B21})$$

where in our case $\mu \equiv k_F$. For simplicity we again take $h_1 v_F \rightarrow 1$. We expand the spectral function with respect to the imaginary part of the self-energy, which we treat as a small parameter in this calculation [56]:

$$A(z, \vec{k}) \approx 2\pi \delta(z - z_*) - \Sigma_2(z, k_F) \mathcal{P}' \frac{1}{z - z_*}, \\ \mathcal{P}' \frac{1}{z - z_*} \equiv \frac{\partial}{\partial z} \left(\mathcal{P} \frac{1}{z - z_*} \right). \quad (\text{B22})$$

The pole of the propagator z_* is a solution of the equation $z - v_F k_\perp - \Sigma_1(z, k_F) = 0$ which does not contain the

imaginary part of the self-energy Σ_2 . Substituting this representation into the equation for the pressure, we have

$$p = -\frac{1}{4\pi i} \int \frac{d^2 k}{(2\pi)^2} \int_{-\infty}^{k_F} dk'_F \int_{-\infty}^{\infty} dz \left(2\pi \delta(z - z_*) \right. \\ \left. + \Sigma_2(z) \mathcal{P}' \frac{1}{z_* - z} \right) f(z). \quad (\text{B23})$$

The frequency integral in the first term gives the familiar expression for the number density

$$n = \int \frac{d^2 k}{(2\pi)^2} f(z_*), \quad (\text{B24})$$

where usually f is a Fermi distribution function, and the dispersion relation is given by z_* (in standard notation $z_* \rightarrow \varepsilon_k$). Here we have $f(x) = \tanh(\frac{x}{2})$, and therefore integrating over k_F gives $\int dk'_F \tanh \frac{z_*}{2} \rightarrow \ln(2 \cosh \frac{z_*}{2})$ where, at the leading order $z_* \sim (k - k_F)$. In the second term we exchange the order of integrations in z and k_F . Therefore, $\int_{-\infty}^{k_F} dk'_F \mathcal{P}' \frac{1}{z_*(k'_F) - z} \rightarrow -\frac{1}{z_*(k_F) - z}$, and there is no k_F dependence in $\Sigma_2(z) \sim z^{2\nu}$ at the leading order. The second integral is $\frac{1}{2\pi i} \int_{-\infty}^{\infty} dz \Sigma_2(z, k_F) f(z) \frac{1}{z_* - z} \rightarrow \Sigma_2(z_*) f(z_*)$. Combining all terms together we have

$$p = \int \frac{d^2 k}{(2\pi)^2} \sum_{z_*} \left(\frac{1}{2} T \ln \left(2 \cosh \frac{z_*}{2T} \right) + \frac{1}{4} \Sigma_2(z_*) \tanh \frac{z_*}{2T} \right), \quad (\text{B25})$$

which is exactly Eq. (B11). Here, z_* is the pole of the fermion propagator without the imaginary part Σ_2 , and summing over the poles is understood. If we take z_* to be the pole of the full propagator, z_* becomes imaginary and a generalization of hyperbolic functions to the Γ functions is necessary as in Eq. (B12). Then we arrive at Eq. (B14) for the pressure of the system.

3. DC conductivity from the Kubo formula

We calculate the DC conductivity in the boundary theory using the gravity-“dressed” retarded/advanced fermion propagators. Strictly speaking, we need also the “dressed” vertex, to satisfy the Ward identities. As argued in Ref. [33] however, the boundary vertex which is obtained from the bulk one can be approximated by a constant in the low-temperature limit. Also, according to Ref. [54], the vertex only carries the singularities of the product of the Green’s functions. Therefore, dressing the vertex will not change the temperature dependence of the DC conductivity at low ω [54].

We can start from the Kubo formula for conductivity:

$$\sigma = -\frac{\partial}{\partial \omega} \text{Im} \Pi_{AA}(\omega, \vec{k} = 0) |_{\omega=0}. \quad (\text{B26})$$

The polarization operator Π_{AA} is given by

$$\Pi_{AA}(i\nu_n, 0) = \int \frac{d^2 k}{(2\pi)^2} T \sum_{\omega_m} G(i\omega_m + i\nu_n, \vec{k}) \Lambda_A \\ \times (i\omega_m + i\nu_n, i\omega_m, \vec{k}) G(i\omega_m, \vec{k}) \Lambda_A^{(0)}(\vec{k}), \quad (\text{B27})$$

where the fermion frequency is $\omega_m = (2m + 1)\pi T$, and the boson frequency is $\nu_n = 2n\pi T$, and in the low-temperature limit $\Lambda_A(i\omega_m + i\nu_n, i\omega_m, \vec{k}) = \Lambda_A^{(0)}(\vec{k})$. Usually the most difficult step is to take the Matsubara sum. Here we can do it in two ways. The first way consists of analytically continuing in the complex plane $i\omega_m \rightarrow z$ and replacing the Matsubara sum by a contour integral with the Fermi distribution function $n(x) = \frac{1}{e^x + 1}$ whose poles sit at the Matsubara frequencies along the imaginary axis. The second way is to use the spectral representation. In both cases we follow Ref. [54], where transport coefficients were calculated with propagators including their imaginary parts.

Taking the first way, we have for the fermion Matsubara sum

$$H(i\nu_n, \vec{k}) = T \sum_{\omega_m} G(i\omega_m + i\nu_n, \vec{k}) G(i\omega_m, \vec{k}) \\ \rightarrow -\frac{1}{2\pi i} \int_C dz G(z + i\nu_n, \vec{k}) G(z, \vec{k}) n(z), \quad (\text{B28})$$

where the contour along the imaginary z axis can be deformed to the contour C which goes along two branch cuts, $\text{Im}z = 0$ and $\text{Im}z = -\nu_n$, and the large arcs Γ with vanishing contribution [54]. The fermion propagator has a branch cut along $\text{Im}z = 0$ [54,55]. Therefore we can rewrite

$$H(i\nu_n) = -\frac{1}{2\pi i} \int_{-\infty}^{\infty} d\zeta n(\zeta) G(i\nu_n + \zeta) (G_R(\zeta) - G_A(\zeta)) \\ -\frac{1}{2\pi i} \int_{-\infty}^{\infty} d\zeta n(\zeta) G(-i\nu_n + \zeta) (G_R(\zeta) - G_A(\zeta)), \quad (\text{B29})$$

where the difference of the retarded and advanced functions in the first bracket is due to the discontinuity along $\text{Im}z = 0$ and in the second bracket it is due to the discontinuity along $\text{Im}z = -\nu_n$. This contribution corresponds to the second term in Eq. (B28), and there are no pole contributions [54]. We use the usual prescription for retarded and advanced Green’s functions, $G_R = G(\omega + i0^+)$ and $G_A = G(\omega - i0^+)$ and suppress the momentum indices. Taking $i\nu_n \rightarrow \omega + i0^+$, we have

$$\begin{aligned}
H(\omega) = & -\frac{1}{2\pi i} \int_{-\infty}^{\infty} d\zeta n(\zeta) G_R(\omega + \zeta) (G_R(\zeta) - G_A(\zeta)) \\
& -\frac{1}{2\pi i} \int_{-\infty}^{\infty} d\zeta n(\zeta + \omega) G_A(\omega + \zeta) \\
& \times (G_R(\zeta + \omega) - G_A(\zeta + \omega)), \quad (\text{B30})
\end{aligned}$$

where we changed the integration variable in the second integral $\zeta - \omega \rightarrow \zeta$. In the limit $\omega \rightarrow 0$, the dominant contribution comes from the pair $G_R G_A$, and it is inversely proportional to the distance between the poles given by the imaginary part Σ_2 . The combinations $G_R G_R$ and $G_A G_A$ with the poles on one side of the real axis make a much smaller contribution due to the cancellation between the residues at the poles. Therefore, as $\omega \sim 0$, we have

$$\begin{aligned}
H(\omega, \vec{k}) \rightarrow & -\frac{1}{2\pi i} \int_{-\infty}^{\infty} d\zeta (n(\zeta + \omega) \\
& - n(\zeta)) G_R(\zeta + \omega) G_A(\zeta), \quad (\text{B31})
\end{aligned}$$

and

$$\begin{aligned}
\text{Im}\Pi_{AA}(\omega, 0) = & \frac{1}{2\pi} \int \frac{d^2 k}{(2\pi)^2} \Lambda_A^{(0)}(\vec{k}) \int_{-\infty}^{\infty} \frac{d\zeta}{2\pi} (n(\zeta + \omega) \\
& - n(\zeta)) G_R(\zeta + \omega, \vec{k}) \\
& \times \Lambda_A(\zeta + \omega + i0^+, \zeta - i0^-, \vec{k}) G_A(\zeta, \vec{k}). \quad (\text{B32})
\end{aligned}$$

In the small- T limit the vertex is a constant. We integrate around the Fermi surface, and therefore the momentum integral is $\int \frac{d^2 k}{(2\pi)^2} \rightarrow \frac{k_F dk_{\perp}}{(2\pi)^2}$ with $k_{\perp} = k - k_F$. We exchange the order of integration and perform first the momentum integration [27,33]. For $\omega \sim 0$, we have

$$\int_{-\infty}^{\infty} \frac{dk_{\perp}}{2\pi} \frac{1}{\left(\frac{\zeta}{\nu_F} - k_{\perp} + \Sigma(\zeta, k_F) + i0^+\right) \left(\frac{\zeta}{\nu_F} - k_{\perp} + \Sigma^*(\zeta, k_F) - i0^+\right)} = \frac{i}{\Sigma(\zeta, k_F) - \Sigma^*(\zeta, k_F)} = \frac{1}{2\text{Im}\Sigma(\zeta, k_F)}. \quad (\text{B33})$$

Writing $n'(\zeta) = -\beta n(\zeta)(1 - n(\zeta))$, we have for $\omega \sim 0$

$$\sigma \rightarrow \Lambda^{(0)2} k_F h_1^2 \int_{-\infty}^{\infty} \frac{\beta d\zeta n(\zeta)(1 - n(\zeta))}{2\pi \text{Im}\Sigma(\zeta, k_F)}, \quad (\text{B34})$$

where we have dropped constant terms. Note that we get the same result for the conductivity also if we use $\tanh \frac{x}{2}$ in the contour integral (B28) since $n'(x) = -2 \tanh'(\frac{x}{2})$. For the Landau Fermi liquid $\Sigma(\omega) \sim \omega^2$ at small T [33,58]. We get

$$\sigma \sim T^{-2}, \quad (\text{B35})$$

meaning that we recover the standard result for the resistivity of the Fermi liquid: $\rho \sim T^2$.

In our case, $\Sigma(\omega) \sim \omega^{2\nu_{k_F}}$, which produces

$$\sigma \sim T^{-2\nu_{k_F}}. \quad (\text{B36})$$

This result agrees with the DC conductivity obtained in Ref. [33]. For the marginal liquid, $\nu_{k_F} = \frac{1}{2}$, we recover the resistivity $\rho \sim T$, which is empirically found in the strange metal phase.

(i) It is interesting that the scaling behavior of the DC conductivity is the same as the single-particle scattering rate. On the gravity side it is explained by the fact that the dissipative part of the current-current correlator is controlled by the rate of the bulk fermion falling in the horizon, given by the single-particle scattering rate. Comparing the resistivity in

the quantum critical metal “qcm” to the one in the normal metal “m,”

$$\rho_{\text{qcm}} > \rho_{\text{m}}, \quad (\text{B37})$$

which indicates that the quantum critical metal becomes increasingly insulating as ν_{k_F} is decreased. This suggests that there is some sort of ordering in the system, not necessarily associated with a gap.

To check our calculation, we get the DC conductivity using the spectral representation

$$G(i\omega_m, \vec{k}) = \int \frac{dk_0}{2\pi} \frac{A(k_0, \vec{k})}{k_0 - i\omega_m}, \quad (\text{B38})$$

where the spectral function $A(k_0, \vec{k})$ is given by Eq. (B6). For the product of the Green functions we use the following formula:

$$T \sum_m \frac{1}{i\omega_m - \omega_1} \frac{1}{i\omega_m + i\nu_n - \omega_2} = \frac{n(\omega_1) - n(\omega_2)}{i\nu_n + \omega_1 - \omega_2}. \quad (\text{B39})$$

Taking $i\nu_n \rightarrow \omega + i0^+$, the polarization operator is given by

$$\begin{aligned}
\Pi_{AA}(\omega, 0) = & \int \frac{d^2 k}{(2\pi)^2} \frac{d\omega_1}{2\pi} \frac{d\omega_2}{2\pi} \frac{n(\omega_1) - n(\omega_2)}{\omega + \omega_1 - \omega_2} \\
& \times \Lambda_A^{(0)2} A(\omega_1, k_{\perp}) A(\omega_2, k_{\perp}). \quad (\text{B40})
\end{aligned}$$

Performing the integration over ω_2 , we have

$$\begin{aligned} \text{Im}\Pi_{AA}(\omega, 0) = & \int \frac{d^2k}{(2\pi)^2} \frac{d\omega_1}{2\pi} (n(\omega_1) \\ & - n(\omega_2)) \Lambda_A^{(0)2} A(\omega_1, k_\perp) A(\omega_1 + \omega, k_\perp). \end{aligned} \quad (\text{B41})$$

In the limit $\omega \sim 0$, the momentum integration proceeds as

$$\int \frac{d^2k}{(2\pi)^2} A^2(\omega_1, k_\perp) \rightarrow k_F \int \frac{dk_\perp}{2\pi} A^2(\omega_1, k_\perp) \rightarrow \frac{k_F h_1^2}{\Sigma_2(\omega_1, k_F)}, \quad (\text{B42})$$

with $\Sigma_2 = \text{Im}\Sigma$. Therefore, the DC conductivity given by Eq. (B26) is

$$\sigma \rightarrow \Lambda_A^{(0)2} k_F h_1^2 \int \frac{\beta d\omega_1}{2\pi} \frac{n(\omega_1)(1-n(\omega_1))}{\text{Im}\Sigma(\omega_1, k_F)} \quad (\text{B43})$$

which is the same as Eq. (B34) obtained by the contour integration.

-
- [1] S. S. Lee, A non-Fermi liquid from a charged black hole: a critical Fermi ball, *Phys. Rev. D* **79**, 086006 (2009).
- [2] D. F. Mross, J. McGreevy, H. Liu, and T. Senthil, A controlled expansion for certain non-Fermi liquid metals, *Phys. Rev. B* **82**, 045121 (2010).
- [3] P. Coleman and A. J. Schofield, Quantum criticality, *Nature (London)* **433**, 226 (2005).
- [4] C. M. Varma, P. B. Littlewood, S. Schmitt-Rink, E. Abrahams, and A. E. Ruckenstein, Phenomenology of the normal state of Cu-O high-temperature superconductors, *Phys. Rev. Lett.* **63**, 1996 (1989).
- [5] S. A. Hartnoll, J. Polchinski, E. Silverstein, and D. Tong, Towards strange metallic holography, *J. High Energy Phys.* **04** (2010) 120.
- [6] M. Čubrović, J. Zaanen, and K. Schalm, Constructing the AdS dual of a Fermi liquid: AdS black holes with Dirac hair, *J. High Energy Phys.* **10** (2011) 017.
- [7] S. A. Hartnoll and A. Tavanfar, Electron stars for holographic metallic criticality, *Phys. Rev. D* **83**, 046003 (2011).
- [8] S. A. Hartnoll, D. M. Hofman, and A. Tavanfar, Holographically smeared Fermi surface: quantum oscillations and Luttinger count in electron stars, *Europhys. Lett.* **95**, 31002 (2011).
- [9] S. Sachdev, A model of a Fermi liquid using gauge-gravity duality, *Phys. Rev. D* **84**, 066009 (2011).
- [10] L. Huijse and S. Sachdev, Fermi surfaces and gauge-gravity duality, *Phys. Rev. D* **84**, 026001 (2011).
- [11] S. Sachdev, Holographic metals and the fractionalized Fermi liquid, *Phys. Rev. Lett.* **105**, 151602 (2010).
- [12] M. Čubrović, J. Zaanen, and K. Schalm, String theory, quantum phase transitions and the emergent Fermi-liquid, *Science* **325**, 439 (2009).
- [13] H. Liu, J. McGreevy, and D. Vegh, Non-Fermi liquids from holography, *Phys. Rev. D* **83**, 065029 (2011).
- [14] T. Faulkner, H. Liu, J. McGreevy, and D. Vegh, Emergent quantum criticality, Fermi surfaces, and AdS2, *Phys. Rev. D* **83**, 125002 (2011).
- [15] E. Gubankova, J. Brill, M. Čubrović, K. Schalm, P. Schijven, and J. Zaanen, Holographic fermions in external magnetic fields, *Phys. Rev. D* **84**, 106003 (2011).
- [16] T. Faulkner, G. T. Horowitz, and M. M. Roberts, Holographic quantum criticality from multi-trace deformations, *J. High Energy Phys.* **04** (2011) 051.
- [17] A. H. Castro Neto, F. Guinea, N. M. R. Peres, K. S. Novoselov, and A. K. Geim, The electronic properties of graphene, *Rev. Mod. Phys.* **81**, 109 (2009).
- [18] J. G. Checkelsky, L. Li, and N. P. Ong, Divergent resistance at the Dirac point in graphene: evidence for a transition in a high magnetic field, *Phys. Rev. B* **79**, 115434 (2009); The zero-energy state in graphene in a high magnetic field, *Phys. Rev. Lett.* **100**, 206801 (2008).
- [19] Y. Zhao, P. Cadden-Zimansky, Z. Jiang, and P. Kim, Symmetry breaking of the zero energy Landau level in bilayer graphene, *Phys. Rev. Lett.* **104**, 066801 (2010).
- [20] A. J. M. Giesbers, L. A. Ponomarenko, K. S. Novoselov, A. K. Geim, M. I. Katsnelson, J. C. Maan, and U. Zeitler, Gap opening in the zeroth Landau level of graphene, *Phys. Rev. B* **80**, 201430(R) (2009).
- [21] Y. Kopelevich, V. V. Lemanov, S. Moehlecke, and J. H. S. Torres, Landau level quantization and possible superconducting instabilities in highly oriented pyrolytic graphite, *Phys. Solid State* **41**, 1959 (1999); H. Kempa, Y. Kopelevich, F. Mrowka, A. Setzer, J. H. S. Torres, R. Hhne, and P. Esquinazi, Magnetic-field-driven superconductor-insulator-type transition in graphite, [arXiv:cond-mat/0005439](https://arxiv.org/abs/cond-mat/0005439).
- [22] E. V. Gorbar, V. P. Gusynin, V. A. Miransky, and I. A. Shovkovy, Dynamics in the quantum Hall effect and the phase diagram of graphene, *Phys. Rev. B* **78**, 085437 (2008); Coulomb interaction and magnetic catalysis in the quantum Hall effect in graphene, *Phys. Scr. T* **146**, 014018 (2012); E. V. Gorbar, V. P. Gusynin, and V. A. Miransky, Toward theory of quantum Hall effect in graphene, *Low Temp. Phys.* **34**, 790 (2008).
- [23] T. Faulkner and J. Polchinski, Semi-holographic Fermi liquids, *J. High Energy Phys.* **06** (2011) 012.
- [24] T. Albash and C. V. Johnson, Holographic aspects of Fermi liquids in a background magnetic field, *J. Phys. A* **43**, 345405 (2010).

- [25] T. Albash and C. V. Johnson, Landau levels, magnetic fields and holographic Fermi liquids, *J. Phys. A* **43**, 345404 (2010).
- [26] H. Liu, J. McGreevy, and D. Vegh, Non-Fermi liquids from holography, *Phys. Rev. D* **83**, 065029 (2011).
- [27] T. Hartman and S. A. Hartnoll, Cooper pairing near charged black holes, *J. High Energy Phys.* **06** (2010) 005.
- [28] L. D. Landau and E. M. Lifshitz, *Statistical Physics Part 2* (Elsevier, New York, 1980), Chap. 41.
- [29] T. Faulkner, G. T. Horowitz, J. McGreevy, M. M. Roberts, and D. Vegh, Photoemission “experiments” on holographic superconductors, *J. High Energy Phys.* **03** (2010) 121.
- [30] S. Bolognesi and D. Tong, Magnetic catalysis in AdS4, *Classical Quantum Gravity* **29**, 194003 (2012).
- [31] G. T. Horowitz and M. M. Roberts, Zero temperature limit of holographic superconductors, *J. High Energy Phys.* **11** (2009) 015.
- [32] N. Iqbal, H. Liu, M. Mezei, and Q. Si, Quantum phase transitions in holographic models of magnetism and superconductors, *Phys. Rev. D* **82**, 045002 (2010).
- [33] T. Faulkner, N. Iqbal, H. Liu, J. McGreevy, and D. Vegh, Strange metal transport realized by gauge/gravity duality, *Science* **329**, 1043 (2010).
- [34] F. Preis, A. Rebhan, and A. Schmitt, Inverse magnetic catalysis in dense holographic matter, *J. High Energy Phys.* **03** (2011) 033.
- [35] S. S. Gubser and I. R. Klebanov, A universal result on central charges in the presence of double-trace deformations, *Nucl. Phys.* **B656**, 23 (2003).
- [36] D. B. Kaplan, J.-W. Lee, D. T. Son, and M. A. Stephanov, Conformality lost, *Phys. Rev. D* **80**, 125005 (2009).
- [37] M. Čubrović, Y. Liu, K. Schalm, Y.-W. Sun, and J. Zaanen, Spectral probes of the holographic Fermi ground state: dialing between the electron star and AdS Dirac hair, *Phys. Rev. D* **84**, 086002 (2011).
- [38] A. Adams and J. Wang, Towards a non-relativistic holographic superfluid, *New J. Phys.* **13**, 115008 (2011).
- [39] S. Cremonesi, D. Melnikov, and Y. Oz, Stability of asymptotically Schwarzschild RN black hole and superconductivity, *J. High Energy Phys.* **04** (2010) 048.
- [40] V. Gusynin, V. Miransky, and I. Shovkovy, Catalysis of dynamical flavor symmetry breaking by a magnetic field in $2 + 1$ dimensions, *Phys. Rev. Lett.* **73**, 3499 (1994); Dynamical flavor symmetry breaking by a magnetic field in $2 + 1$ dimensions, *Phys. Rev. D* **52**, 4718 (1995); Dimensional reduction and dynamical chiral symmetry breaking by a magnetic field in $3 + 1$ dimensions, *Phys. Lett. B* **349**, 477 (1995); Dynamical chiral symmetry breaking by a magnetic field in QED, *Phys. Rev. D* **52**, 4747 (1995).
- [41] M. Chernodub, Can nothing be a superconductor and a superfluid?, [arXiv:1104.4404](https://arxiv.org/abs/1104.4404); Superconductivity of QCD vacuum in strong magnetic field, *Phys. Rev. D* **82**, 085011 (2010).
- [42] G. W. Semenoff, Chiral symmetry breaking in graphene, *Phys. Scr. T* **T146**, 014016 (2012).
- [43] S. Bolognesi, Monopoles and holography, in *Proceedings of Continuous Advances in QCD, Minneapolis, MN, May 12–15, 2011* (to be published), <http://www.ftpi.umn.edu/workshops/>.
- [44] A. Schmitt, *Inverse magnetic catalysis in dense holographic matter, CSC seminar at Goethe University, Frankfurt*, 2012, <http://hep.itp.tuwien.ac.at/~aschmitt/frankfurt.pdf>.
- [45] M. Thies, From relativistic quantum fields to condensed matter and back again: updating the Gross-Neveu phase diagram, *J. Phys. A* **39**, 12707 (2006); J. Hofmann, Dimensional reduction in quantum field theories at finite temperature and density, *Phys. Rev. D* **82**, 125027 (2010).
- [46] J. Figueroa-O’Farrill, Electromagnetic duality for children, <http://www.maths.ed.ac.uk/jmf/Teaching/Lectures/EDC.pdf>.
- [47] B. I. Halperin, *Helv. Phys. Acta* **56**, 75 (1983); Y. Kopelevich, B. Raquet, M. Goiran, W. Escoffier, R. R. da Silva, J. C. Medina Pantoja, I. A. Lukyanchuk, A. Sinchenko, and P. Monceau, Searching for the Fractional Quantum Hall Effect in Graphite, *Phys. Rev. Lett.* **103**, 116802 (2009).
- [48] D. E. Kharzeev and H. J. Warringa, Chiral magnetic conductivity, *Phys. Rev. D* **80**, 034028 (2009); K. Fukushima, D. E. Kharzeev, and H. J. Warringa, Electric-current susceptibility and the chiral magnetic effect, *Nucl. Phys.* **A836**, 311 (2010); Real-time dynamics of the chiral magnetic effect, *Phys. Rev. Lett.* **104**, 212001 (2010).
- [49] J. P. Eisenstein and A. P. MacDonald, Bose-Einstein condensation of excitons in bilayer electron system, *Nature (London)* **432**, 691 (2004).
- [50] R. Contino and A. Pomarol, Holography for fermions, *J. High Energy Phys.* **11** (2004) 058.
- [51] S. B. Ruster, I. A. Shovkovy, and D. H. Rischke, Phase diagram of dense neutral three-flavor quark matter, *Nucl. Phys.* **A743**, 127 (2004); S. B. Ruster and D. H. Rischke, Effect of color superconductivity on the mass and radius of a quark star, *Phys. Rev. D* **69**, 045011 (2004).
- [52] F. Denef, S. A. Hartnoll, and S. Sachdev, Quantum oscillations and black hole ringing, *Phys. Rev. D* **80**, 126016 (2009).
- [53] F. Denef, S. A. Hartnoll, and S. Sachdev, Black hole determinants and quasinormal modes, *Classical Quantum Gravity* **27**, 125001 (2010).
- [54] M. A. V. Basagoiti, Transport coefficients and ladder summation in hot gauge theories, *Phys. Rev. D* **66**, 045005 (2002); J. M. M. Resco and M. A. V. Basagoiti, Color conductivity and ladder summation in hot QCD, *Phys. Rev. D* **63**, 056008 (2001).
- [55] T. Koide, notes on a branch cut in the integrals $\ln z = \int_1^z \frac{d\zeta'}{\zeta'}$ where z is imaginary (unpublished).
- [56] A. Sedrakian and G. Röpke, A quantum kinetic equation for Fermi-systems including three-body correlations, *Ann. Phys. (N.Y.)* **266**, 524 (1998).
- [57] I. S. Gradshteyn and I. W. Ryzhik, *Tables of Integrals, Series, and Products* (Academic Press, New York, 1965).
- [58] L. D. Landau and E. M. Lifshitz, *Physical Kinetics* (Elsevier, New York, 1981), Chap. 76.